



UNIVERSITY OF LEEDS

This is a repository copy of *The contribution of global aviation to anthropogenic climate forcing for 2000 to 2018*.

White Rose Research Online URL for this paper:
<https://eprints.whiterose.ac.uk/165692/>

Version: Accepted Version

Article:

Lee, DS, Fahey, DW, Skowron, A et al. (18 more authors) (2021) The contribution of global aviation to anthropogenic climate forcing for 2000 to 2018. *Atmospheric Environment*, 244. 117834. ISSN 1352-2310

<https://doi.org/10.1016/j.atmosenv.2020.117834>

© 2020, Elsevier. This manuscript version is made available under the CC-BY-NC-ND 4.0 license <http://creativecommons.org/licenses/by-nc-nd/4.0/>.

Reuse

This article is distributed under the terms of the Creative Commons Attribution-NonCommercial-NoDerivs (CC BY-NC-ND) licence. This licence only allows you to download this work and share it with others as long as you credit the authors, but you can't change the article in any way or use it commercially. More information and the full terms of the licence here: <https://creativecommons.org/licenses/>

Takedown

If you consider content in White Rose Research Online to be in breach of UK law, please notify us by emailing eprints@whiterose.ac.uk including the URL of the record and the reason for the withdrawal request.



eprints@whiterose.ac.uk
<https://eprints.whiterose.ac.uk/>

1 The contribution of global aviation to anthropogenic climate forcing for 2000 to
2 2018

3
4 D. S. Lee^{a, 1}, D. W. Fahey^b, A. Skowron^a, M. R. Allen^{c, n}, U. Burkhardt^d, Q. Chen^e, S. J. Doherty^f, S.
5 Freeman^a, P.M. Forster^g, J. Fuglested^h, A. Gettelmanⁱ, R. R. De León^a, L. L. Lim^a, M. T. Lund^h, R. J.
6 Millar^{c, o}, B. Owen^a, J. E. Penner^j, G. Pitari^l, M. J. Prather^k, R. Sausen^d, L. J. Wilcox^m

7
8 ^a Faculty of Science and Engineering, Manchester Metropolitan University, John Dalton Building, Chester Street,
9 Manchester M1 5GD, United Kingdom;

10 ^b NOAA Chemical Sciences Laboratory (CSL), Boulder, CO USA;

11 ^c School of Geography and the Environment, University of Oxford, Oxford, UK;

12 ^d Deutsches Zentrum für Luft- und Raumfahrt (DLR), Institut für Physik der Atmosphäre, Oberpfaffenhofen,
13 Germany;

14 ^e State Key Joint Laboratory of Environmental Simulation and Pollution Control, College of Environmental Sciences
15 and Engineering, Peking University, Beijing 100871, China;

16 ^f Cooperative Institute for Research in Environmental Sciences (CIRES), University of Colorado, Boulder, CO,
17 USA;

18 ^g School of Earth and Environment, University of Leeds, Leeds LS2 9JT, United Kingdom;

19 ^h CICERO—Center for International Climate Research—Oslo, PO Box 1129, Blindern, 0318 Oslo, Norway;

20 ⁱ National Center for Atmospheric Research, Boulder, CO, USA;

21 ^j Department of Climate and Space Sciences and Engineering, University of Michigan, 2455 Hayward St., Ann
22 Arbor, MI 48109-2143, USA;

23 ^k Department of Earth System Science, University of California, Irvine, 3329 Croul Hall, CA 92697-3100, USA;

24 ^l Department of Physical and Chemical Sciences, Università dell'Aquila, Via Vetoio, 67100 L'Aquila, Italy;

25 ^m National Centre for Atmospheric Science, Department of Meteorology, University of Reading, Earley Gate,
26 Reading RG6 6BB, UK;

27 ⁿ also at the Department of Physics, University of Oxford, Oxford, UK;

28 ^o also at the Committee on Climate Change, 151 Buckingham Palace Road, London, SW1W 9SZ, UK.

29

30 ¹To whom correspondence should be addressed. Email: d.s.lee@mmu.ac.uk Tel: +44 161 247 3663

31

32 Highlights

- 33 • Global aviation warms Earth's surface through both CO₂ and net non-CO₂ contributions.
- 34 • Global aviation contributes a few percent to anthropogenic radiative forcing.
- 35 • Non-CO₂ impacts comprise about 2/3 of the net radiative forcing.
- 36 • Comprehensive and quantitative calculations of aviation effects are presented.
- 37 • Data are made available to analyze past, present and future aviation climate forcing.

39 Abstract

40 Global aviation operations contribute to anthropogenic climate change via a complex set of processes that
 41 lead to a net surface warming. Of importance are aviation emissions of carbon dioxide (CO₂), nitrogen
 42 oxides (NO_x), water vapor, soot and sulfate aerosols, and increased cloudiness due to contrail formation.
 43 Aviation grew strongly over the past decades (1960–2018) in terms of activity, with revenue passenger
 44 kilometers increasing from 109 to 8269 billion km yr⁻¹, and in terms of climate change impacts, with CO₂
 45 emissions increasing by a factor of 6.8 to 1034 Tg CO₂ yr⁻¹. Over the period 2013–2018, the growth rates
 46 in both terms show a marked increase. Here, we present a new comprehensive and quantitative approach
 47 for evaluating aviation climate forcing terms. Both radiative forcing (RF) and effective radiative forcing
 48 (ERF) terms and their sums are calculated for the years 2000–2018. Contrail cirrus, consisting of linear
 49 contrails and the cirrus cloudiness arising from them, yields the largest positive net (warming) ERF term
 50 followed by CO₂ and NO_x emissions. The formation and emission of sulfate aerosol yields a negative
 51 (cooling) term. The mean contrail cirrus ERF/RF ratio of 0.42 indicates that contrail cirrus is less
 52 effective in surface warming than other terms. For 2018 the net aviation ERF is +100.9 milliwatts (mW)
 53 m⁻² (5–95% likelihood range of (55, 145)) with major contributions from contrail cirrus (57.4 mW m⁻²),
 54 CO₂ (34.3 mW m⁻²), and NO_x (17.5 mW m⁻²). Non-CO₂ terms sum to yield a net positive (warming) ERF
 55 that accounts for more than half (66%) of the aviation net ERF in 2018. Using normalization to aviation
 56 fuel use, the contribution of global aviation in 2011 was calculated to be 3.5 (4.0, 3.4) % of the net
 57 anthropogenic ERF of 2290 (1130, 3330) mW m⁻². Uncertainty distributions (5%, 95%) show that non-
 58 CO₂ forcing terms contribute about 8 times more than CO₂ to the uncertainty in the aviation net ERF in
 59 2018. The best estimates of the ERFs from aviation aerosol-cloud interactions for soot and sulfate remain
 60 undetermined. CO₂-warming-equivalent emissions based on global warming potentials (GWP* method)
 61 indicate that aviation emissions are currently warming the climate at approximately three times the rate of
 62 that associated with aviation CO₂ emissions alone. CO₂ and NO_x aviation emissions and cloud effects
 63 remain a continued focus of anthropogenic climate change research and policy discussions.

64 **Key words:** | aviation | contrail cirrus | climate | radiative forcing | CO₂ | NO_x |

65 **Dedication:** This paper is dedicated to the memory of Professor Ivar S. A. Isaksen of the University of
 66 Oslo, whose scientific excellence, friendship, and mentorship is sorely missed.

67

68 1. Introduction

69 Aviation is one of the most important global economic activities in the modern world. Aviation emissions
 70 of CO₂ and non-CO₂ aviation effects result in changes to the climate system (**Figure 1**). Both aviation
 71 CO₂ and the sum of quantified non-CO₂ contributions lead to surface warming. The largest contribution to
 72 anthropogenic climate change across all economic sectors comes from the increase in CO₂ concentration,
 73 which is the primary cause of observed global warming in recent decades (IPCC, 2013; 2018). Aviation
 74 contributions involve a range of atmospheric physical processes, including plume dynamics, chemical
 75 transformations, microphysics, radiation, and transport. Aggregating these processes to calculate changes
 76 in a greenhouse gas component or a cloud radiative effect is a complex challenge for contemporary

77 atmospheric modeling systems. Given the dependence of aviation on burning fossil fuel, its significant
78 CO₂ and non-CO₂ effects, and the projected fleet growth, it is vital to understand the scale of aviation's
79 impact on present-day climate forcing.

80 Historically, estimating aviation non-CO₂ effects has been particularly challenging. The primary
81 (quantified) non-CO₂ effects result from the emissions of NO_x, along with water vapor and soot that can
82 result in contrail formation. Aviation aerosols are small particles composed of soot (black and organic
83 carbon (BC/OC)) and sulfur (S) and nitrogen (N) compounds. The largest positive (warming) climate
84 forcings adding to that of CO₂ are those from contrail cirrus and from NO_x-driven changes in the chemical
85 composition of the atmosphere (Lee et al., 2009 (L09)). L09 estimated that in 2005, aviation CO₂
86 radiative forcing (RF (Wm⁻²)) was 1.59% of total anthropogenic CO₂ RF and that the sum of aviation CO₂
87 and non-CO₂ effects contributed about 5% of the overall net anthropogenic forcing.

88 Understanding of aviation's impacts on the climate system has improved over the decade since the last
89 comprehensive evaluation (L09), but remains incomplete. Published studies of aviation contributions to
90 climate change generally focus on one or a few ERF terms. For example, about 20 studies are cited here
91 that quantify the contribution from global NO_x emissions. In contrast, only a few studies have addressed
92 the net RF from global aviation (IPCC, 1999; Sausen et al., 2005; L09). A more recent study updated
93 some aviation terms without providing a net RF (Brasseur et al., 2016). Here, a comprehensive analysis of
94 individual aviation ERFs is undertaken in order to provide an overall ERF for global aviation, along with
95 the associated uncertainties, which is an analysis unavailable elsewhere. This step updates and improves
96 the analysis of L09. Best estimates of individual aviation ERF terms are derived here for the first time and
97 combined to provide a net ERF for global aviation. Quantifying the terms required new analyses of CO₂
98 and NO_x ERFs and recalibration of other individual ERFs accounting for factors not previously applied in
99 a common framework.

100 In L09, the net RF was calculated with and without the full contrail cirrus term but including an estimate
101 for linear contrails. The exclusion was based on the lack of a best estimate derived from existing studies.
102 At that time radiative forcing estimates were limited to linear or line-shaped contrails since the modelling
103 approaches required scaling contrail formation frequency to observed coverage and only satellite
104 observations of linear contrails existed (Burkhardt et al., 2010). The contrail cirrus term requires the
105 simulation of the whole contrail cirrus life cycle, starting from persistent linear contrails which spread and
106 often become later indistinguishable from natural cirrus. Persistent contrail formation requires ice-
107 supersaturated conditions along a flight track, which are variable in space and time in the troposphere and
108 tropopause region (Irvine et al., 2013). Estimating the RF from contrail cirrus requires knowledge of
109 complex microphysical processes, radiative transfer, and the interaction with background cloudiness
110 (Burkhardt et al., 2010). Contrail cirrus forcing dominates that of persistent linear contrails with the latter
111 on the order of 10% of the combined forcing (Burkhardt and Kärcher, 2011). In the present study, we
112 present a best estimate and uncertainty based on the results from global climate models employing
113 process-based contrail cirrus parameterizations.

114 Emissions of NO_x from aviation lead to photochemical changes that increase global ozone (O₃) formation
115 while decreasing the lifetime and abundance of methane (CH₄). The changes result in positive and
116 negative (cooling) RF contributions, respectively. Since L09, improved understanding and modeling
117 capabilities have emerged, as well as additional RF terms in response to NO_x emissions, namely a longer-
118 term decrease in background O₃ and a reduction in H₂O in the stratosphere in response to decreased CH₄.
119 Here, model results are used to calculate the additional RF terms, and to incorporate the updated CH₄
120 forcing as assessed by Etminan et al. (2016) and the equilibrium-to-transient corrections for the CH₄ term
121 (see Appendix D. Finally, aviation-specific efficacies (Appendix C) of the individual NO_x components
122 are used to estimate a net NO_x ERF for the first time.

123 L09 includes best estimates for the RFs resulting from the aerosol-radiation interactions (previously
 124 called direct effects) of soot and sulfate aerosols from aviation. However, no best estimates of RFs from
 125 aerosol-cloud interactions (previously called indirect effects) were available in 2009. Subsequent studies
 126 discussed here have yet to provide a basis for best estimates of ERFs from aviation aerosol-cloud
 127 interactions that may be significant.

128 The primary motivations for the present study are to provide an updated, comprehensive evaluation of
 129 aviation climate forcings in terms of RF and ERF based on new calculations and the normalization of
 130 values from published modeling studies, and to combine the resulting best estimates via a Monte-Carlo
 131 analysis to yield a best estimate for the net ERF for global aviation for the years 2000 to 2018. The three
 132 years 2018, 2011, and 2005 are notable because the year 2018 is the latest year for which air traffic and
 133 fuel use datasets are available, 2011 is the most recent year evaluated for net anthropogenic climate
 134 forcing by the IPCC (IPCC, 2013), and 2005 is the year evaluated in the latest comprehensive aviation
 135 and climate evaluation (L09). By normalizing the calculations across these years, more specific and self-
 136 consistent comparisons can be made of the changes in aviation contributions over time. The normalization
 137 step requires addressing in each study, for example, the choice of air traffic inventory, the integration of
 138 emissions along flight tracks, and the assumed jet-engine emission indices. The new best estimates of
 139 aviation ERF, for example, show that the 2018 value is about 48% larger than the updated 2005 value.

140 In general, previous global aviation climate assessments have made different assumptions concerning
 141 emissions, cloudiness effects, and aviation operations (e.g., IPCC, 1999). Here, our self-consistent set of
 142 component and net aviation ERFs for 2000 to 2018 allows historical and scenario projections of aviation
 143 climate impacts to be assessed in context with other sectors, such as maritime shipping, ground
 144 transportation and energy generation. This updated understanding is especially important given the
 145 potential role of international aviation in meeting the goals of the Paris Agreement (Section 2) on limiting
 146 future temperature increases.

147 The remaining sections address global aviation growth statistics (Section 2); a brief summary of methods
 148 used in the analysis (Section 3); results for the ERF estimates of CO₂, NO_x, water vapor, contrail cirrus,
 149 and aerosol-radiation and aerosol-cloud interactions with soot and sulfate (Section 4); results for the net
 150 ERF of global aviation (Section 5); emission metrics (Section 6); and aviation CO₂ vs non-CO₂ forcings
 151 (Section 7). The appendices contain additional detailed information on trends in aviation emissions (App.
 152 A); aviation CO₂ radiative forcing calculations (App. B); radiative forcing, efficacy and ERF definitions
 153 (App. C); aviation NO_x RF calculations (App. D); contrail cirrus RF scaling factors and uncertainty (App.
 154 E); and emission equivalency metric calculations (App. F). A Supplemental Data (SD) file is provided
 155 containing the interactive spreadsheet used to calculate RFs and ERFs for each aviation term.

156 2. Global aviation growth

157 Global aviation fuel use and CO₂ emissions have increased in the last four decades with large growth
 158 occurring in Asia and other developing regions due to the rapid expansion of civil aviation (**Figure 2** and
 159 Appendix A). Looking forward, this pattern of growth is expected to be maintained—for example, of the
 160 1229 orders of Airbus and 1031 orders of Boeing in 2017, 20.3% and 37.5%, respectively, are for airlines
 161 in the Asia region (Airbus, 2017; Boeing, 2018). Airbus projects 41% of orders over the next two decades
 162 to be from the Asia-Pacific region (Airbus, 2017). The uncertainty in this expectation has increased due to
 163 the slowdown in aviation operations in the early months of 2020 due to the COVID-19 pandemic (Le
 164 Quéré et al., 2020). Annual aviation emissions in 2020 are now expected to be below recent projections
 165 that are based on historical growth.

166 A striking feature of **Figure 2a** is the sustained multi-decade growth in CO₂ emissions; the average rate
 167 for the period 1960–2018 is 15 Tg CO₂ yr⁻¹. The growth rate for 2013 through 2018 is much larger (44 Tg
 168 CO₂ yr⁻¹). The annually averaged growth rate over the period 1970 to 2012 is 2.2% yr⁻¹ and for 2013 to
 169 2018 is 5% yr⁻¹ (increase of 27%). In 2018, global aviation CO₂ emissions exceeded 1000 million tonnes

170 per year for the first time (see methodology for scaling 2016 IEA data in Appendix A). The cumulative
 171 emissions of global aviation (1940 to 2018) are 32.6 billion (10^9) tonnes of CO₂, of which approximately
 172 50% were emitted in the last 20 years. Current (2018) CO₂ emissions from aviation represent
 173 approximately 2.4% of anthropogenic emissions of CO₂ (including land use change) (**Figure 2c**).

174 Aviation has grown strongly over time (**Figure 2b**) in terms of available seat kilometers (ASK, a measure
 175 of capacity) and revenue passenger kilometers (RPK, a measure of transport work). Fuel usage and hence
 176 CO₂ emissions have grown at a lesser rate than RPK, reflecting increases in aircraft efficiency derived
 177 from changes in technology, larger average aircraft sizes and increased passenger load factor. Aviation
 178 transport efficiency has improved by approximately eightfold since 1960, to 125 gCO₂ (RPK)⁻¹.

179 At present and for some considerable time into the future, aviation growth is likely to be largely
 180 dependent upon the combustion of kerosene fossil fuel (Jet A-1/A) (OECD, 2012), resulting in emission
 181 of CO₂. Renewable biofuels partially offset fossil fuel emissions but these have yet to be produced in
 182 sufficient quantities to offset growth of fossil fuel use. Furthermore, considerable uncertainties remain
 183 regarding the life-cycle emissions of biofuels, which determine the reductions in net CO₂ emissions (e.g.,
 184 Hari et al., 2015). There are current regulations regarding aviation emissions of CO₂, NO_x, and soot mass
 185 and number based on decisions by the International Civil Aviation Organization (ICAO). Under the 2016
 186 Paris climate agreement, nations are committing to limiting future increases in global temperatures with
 187 Nationally Determined Contributions (NDCs) (UNFCCC). Whereas domestic aviation CO₂ emissions are
 188 included in the NDCs, CO₂ emissions from international aviation are not mentioned in the agreement. It
 189 remains open as to whether emissions from international aviation or global emissions beyond greenhouse
 190 gases (e.g., short-lived (non-CO₂) climate forcers) will be included in future international agreements.

191 **3. Methods**

192 The methodologies used to calculate ERF and RF for individual aviation terms are described in this
 193 section, and results of these calculations are given in Section 4. Common to the methodologies is a
 194 comprehensive multi-page spreadsheet (see SD) that begins with a user's guide. The spreadsheet pages
 195 include those for contrail cirrus, CO₂, NO_x, H₂O, and sulfate and soot aerosol, along with CO₂-equivalent
 196 metrics, ERF probability distributions, ERF time series, and estimates of forcings from aerosol-cloud
 197 effects. The spreadsheet displays the results of aviation forcings provided by individual published studies.
 198 ERF and RF values were calculated for 2018 and other years based on the normalized values of ERF or
 199 RF per unit emission or distance, choice of appropriate emission indices, and times series data on fuel use
 200 and distance travelled. In the case of the contrail cirrus forcing, the flight-track distance was chosen as the
 201 proxy over fuel usage. Annual global emissions are derived from fuel burn by multiplying by the average
 202 emission indices (**Table 1**). The combined and normalized results are used to create sets of RF and ERF
 203 aviation terms for the years 2000 to 2018. In addition to facilitating the present study, the spreadsheet also
 204 provides a quantitative framework for follow-on analyses.

205 Calculations of radiative forcing are expanded here beyond the approach in L09 to include ERF values in
 206 addition to the traditional RF values (**Tables 2 and 3 and Figure 3**). The distinction between ERF and
 207 RF is presented in Appendix C. ERF is the preferred metric for comparing the expected impacts of
 208 climate forcing terms (Myhre et al., 2013). Its use derives from the stronger correlation between ERF and
 209 the change in the equilibrium global-mean surface temperature for some forcing agents than for the
 210 corresponding RF. ERF is calculated as the change in net top-of-the-atmosphere (TOA) downward
 211 radiative flux after allowing for rapid adjustments in atmospheric temperatures, water vapor and clouds
 212 with globally-averaged sea surface and/or land surface temperatures unchanged. ERF is preferred over RF
 213 estimates because the imposed forcing and rapid responses to the forcing cannot always be separately
 214 evaluated, especially for aerosols. In general, the largest differences between ERF and RF are expected
 215 for aerosol-cloud interactions and contrail cirrus (Myhre et al., 2013; Boucher et al., 2013). In calculating
 216 ERF values for 2000-2018, the ERF/RF ratio is assumed to be constant with time.

217 Most of the results for the non-CO₂ terms have associated statistics from which the median was chosen as
 218 the best estimate, including the net aviation ERF and RF, and the net non-CO₂ ERF and RF. For CO₂ and
 219 contrail cirrus, for which the sample sizes are small (3, in both cases), the mean was used as the best
 220 estimate. The best estimates of the non-CO₂ terms except contrail cirrus have associated uncertainties
 221 expressed as 5% and 95% confidence intervals calculated from 5, 95% percentile statistics. The
 222 uncertainty distributions for all forcing terms other than CO₂ and contrail cirrus are lognormal and that for
 223 net NO_x has a discrete probability distribution function (PDF). The uncertainties for the ERF and RF of
 224 CO₂ were taken from IPCC (2013) and fitted with a Monte Carlo analysis with a normal distribution (see
 225 Section 5). The uncertainties for contrail cirrus were estimated partly from expert judgement of the
 226 underlying processes, as described in Appendix E, again fitted with a Monte Carlo analysis with a normal
 227 distribution.

228 4. Calculations of ERFs for aviation terms

229 4.1. CO₂.

230 The time series of aviation CO₂ emissions is shown in **Figure 2** as derived from combined kerosene and
 231 avgas usage (UKDS, 2016). Calculating CO₂ concentrations from emissions requires use of a global
 232 carbon-cycle model, which has a range of complexity from a comprehensive Earth system model (ESM)
 233 to a simple climate model (SCM), with the latter being based on a box model or impulse response
 234 function (IRF) model. Three SCMs were used here: LinClim, an IRF model based on Sausen and
 235 Schumann (2000) (Appendix B); the Finite-amplitude Impulse Response (FaIR) model (Millar et al.,
 236 2017); and the CICERO-SCM (Fuglestedt and Berntsen, 1999; Skeie et al., 2017). The performance of
 237 LinClim and CICERO-SCM with respect to aviation emissions is documented in the multi-model
 238 comparison of Khodayari et al. (2013). The CO₂ concentrations attributable to aviation in 2018 based on
 239 LinClim, CICERO-SCM and FaIR are 2.9, 2.4 and 2.4 ppm, respectively, with concentrations nearly
 240 doubling in the last 20 years (see SD spreadsheet). The ERF/RF ratio for CO₂ is assumed to be unity. The
 241 resulting CO₂ ERFs, as derived from global concentrations using standard IPCC expressions (IPCC,
 242 2001), are 38.6, 32.0 and 32.4 mW m⁻², respectively. With only three model estimates, the average of 34.3
 243 mW m⁻² (5 and 95% percentiles of 29 and 40 mW m⁻²), is chosen be the CO₂ RF best estimate.

244 4.2. NO_x

245 The photochemical effects of aviation NO_x emissions on the atmospheric abundances of O₃, CH₄, carbon
 246 monoxide (CO) and reactive hydrogen (HO_x) are well established (Fuglestedt et al., 1999). Earlier
 247 studies assessed the short-term increase of O₃ and the longer-term reduction in CH₄ lifetime and
 248 abundance, which yield positive and negative RFs, respectively (IPCC, 1999; Sausen et al., 2005). L09
 249 introduced the concept of the ‘net NO_x’ effect by combining the two components, extending and updating
 250 the study of Sausen et al. (2005). Later studies expanded the analysis of NO_x effects to include the long-
 251 term decreases in both O₃ and stratospheric water vapor (SWV) resulting from the CH₄ reduction. Both
 252 effects yield negative RFs (Holmes et al., 2011; Myhre et al., 2011). In the present study, an ensemble of
 253 20 NO_x studies is assessed to provide NO_x forcing best estimates based on a wide range of global
 254 atmospheric chemistry/climate models and a broad range of present-day aviation emission inventories
 255 (details in Appendix D and SD spreadsheet). Results from 6 of the studies were adopted from Holmes et
 256 al. (2011).

257 The study ensemble represents various model methodologies in calculating and treating both the short-
 258 term and the long-term NO_x components. In order to avoid gaps and additional uncertainties, standardized
 259 ERFs were developed that estimated disparate elements (e.g., CH₄ mediated decreases in SWV and long-
 260 term O₃). Moreover, most of the studies were based upon a parameterization of the CH₄ response that
 261 assumed a full equilibrium response. In order to calculate the transient response for a specific year more
 262 accurately, a correction factor is needed (Myhre et al., 2011). Here, the CH₄ responses for individual
 263 years were calculated (see Appendix D) using the difference between two simulations with differing

264 aviation NO_x emissions. A number of transient and equilibrium simulations were conducted with a 2D
 265 chemical-transport model to find that the requirement for a correction factor is well supported and that the
 266 2018 value is 0.79 (see Transient vs. equilibrium in Appendix D and Appendix **Table D.2**). In addition, a
 267 scaling factor (1.23) is applied to derived CH_4 ERF numbers to account for the effect of shortwave CH_4
 268 forcing, following Etminan et al. (2016) (see Appendix D). The existence and nature of correlations
 269 between the NO_x RF components were also explored (see Correlations in Appendix D and Appendix
 270 Figure D.1) since the degree of correlation between short-term O_3 and CH_4 terms was a source of
 271 uncertainty in the calculation of the net- NO_x forcing in L09. The work of Holmes et al. (2011) supports
 272 the prior assumption of correlation, which is greatly expanded here. Regardless of inter-model
 273 differences, significant correlations are observed; for example, a significant negative correlation ($\rho = -0.7$)
 274 exists between the short-term and the long-term NO_x RF components.

275 The normalized sensitivity results for net NO_x in units of $\text{mW m}^{-2} (\text{Tg (N) yr}^{-1})^{-1}$ for the individual
 276 modeling studies are shown in **Figure 4** along with statistical parameters (see Ensemble values in
 277 Appendix D). Given the diversity of studies conducted over nearly two decades, the standard deviations
 278 of the distributions are reasonably small. In contrast, the sign of the net- NO_x RF obtained from summing
 279 over the 4 component values varies from positive to negative. The spread in NO_x RF values is caused by
 280 various factors (e.g., emissions inventories, experimental design or inter-model differences) and is
 281 particularly sensitive to the NO_x distribution in the model background troposphere (Holmes et al., 2011).
 282 The NO_x efficacies are 1.37 for the short-term ozone increases and 1.18 for methane decreases (Ponater et
 283 al., 2006). The efficacies do not equal the ERF/RF ratios, in general (Ponater et al., 2020; Appendix C);
 284 nonetheless, in the present study, we assume the efficacies and the ERF/RF ratios are equal, in the
 285 absence of better information. The factor of 1.18 was similarly adopted for the CH_4 -mediated decreases in
 286 long-term ozone and SWV. It is noted that these ratios are from one study and that, in general, the ratio of
 287 ERF to RF for CH_4 and tropospheric O_3 are currently the subject of some debate (Smith et al., 2018; Xie
 288 et al., 2016; Richardson et al., 2019). Given the strength of the net effect of the ERF adjustment on the net
 289 NO_x forcing (more than doubling over its stratosphere-adjusted RF), these ratios warrant further study.

290 The net- NO_x ERF sensitivity of $5.5 \pm 8.1 \text{ mW m}^{-2} (\text{Tg (N) yr}^{-1})^{-1}$ yields a 2018 best estimate of 17.5 (0.6,
 291 28.5) mW m^{-2} . This best estimate includes the correction factor for non-steady state conditions as well as
 292 the revised formulation of CH_4 RF (Appendix D).

293 Other potential short-term effects from NO_x emissions involve the direct formation of nitrate aerosol and
 294 indirect enhancement of sulfate aerosol. These effects, addressed in a few modelling studies, are
 295 associated with large uncertainties (Righi et al., 2013; Pitari et al., 2017; Unger, 2011). The effects of
 296 NO_x on aerosol abundances are not further considered here owing to the limited number of studies and the
 297 large associated uncertainties.

298 *4.3. Water vapor emissions.*

299 A large fraction of annual aircraft emissions from the global fleet occurs in the stratosphere, primarily in
 300 the northern hemisphere (Forster et al., 2003). The accumulation of water vapor emissions perturbs the
 301 low background humidity in the lower stratosphere and changes the water vapor radiative balance.
 302 Calculating the water vapor RF is complicated by the sensitivity to the vertical and horizontal distribution
 303 of emissions, seasonal changes in tropopause heights, and short stratospheric residence times. Some
 304 earlier studies do not include the water vapor effect.

305 The water vapor effects were explored in detail (see SD) using results from nine studies: IPCC (1999),
 306 Marquart et al. 2001, Gauss et al. (2003), Ponater et al. (2006), Frömming et al. (2012), Wilcox et al.
 307 (2012), Lim et al. (2015), Pitari et al. (2015) and Brasseur et al. (2016). The reported RFs from these
 308 studies vary from 0.4 mW m^{-2} (Wilcox et al., 2012) through 1.5 mW m^{-2} (Frömming et al. 2012, Lim et
 309 al., 2015) to 3.0 mW m^{-2} (IPCC, 1999). The differences are attributed to the different transport models
 310 used, with some contribution from the different meteorologies in different studies. Normalizing to the

311 same emissions and averaging these reported estimates yields a water vapor sensitivity of $0.0052 \pm$
 312 $0.0026 \text{ mW m}^{-2} (\text{Tg} (\text{H}_2\text{O}) \text{ yr}^{-1})^{-1}$. Scaling this value linearly to emissions of 382 Tg H₂O yields an ERF
 313 best estimate of 2.0 (0.8, 3.2) mW m^{-2} for 2018, which is well within the uncertainty range of the 2005
 314 L09 value of 2.8 (0.39, 20.3) mW m^{-2} . The ERF/RF ratio for stratospheric water increases is assumed to
 315 be unity. We have greater confidence in the new estimate and its smaller uncertainty since it is based on
 316 detailed physical studies, rather than a scaling of the earlier IPCC (1999) estimate. The new best estimate
 317 is also in good agreement with the earlier results of Gauss et al. (2003) and Ponater et al. (2006), after
 318 scaling their results to account for emissions differences.

319 4.4. Contrail cirrus.

320 The aviation fleet increases global cloudiness through the formation of persistent contrails when the
 321 ambient atmosphere is supersaturated with respect to ice (IPCC, 1999). Contrail cirrus, consisting of
 322 linear contrails and the cirrus cloudiness arising from them, have cooling (short-wave) and warming
 323 (long-wave) effects, with the effect at night being exclusively warming. In past assessments (e.g., IPCC,
 324 1999; L09), a best estimate was only available for the RF of linear persistent contrails, in part because of
 325 the difficulty of quantifying the cloudiness contribution of aging and spreading contrails (Minnis et al.,
 326 2013). The ERF of contrail cirrus was estimated for 2011 as 50 (20, 150) mW m^{-2} by Boucher et al.
 327 (2013). Results of a recent assessment of contrail cirrus and other aviation effects are included here,
 328 although the study did not propose new best estimates (Brasseur et al., 2016).

329 A persistent contrail requires ice-supersaturated conditions along the flight track. Contrail cirrus life
 330 cycles are dependent on the temporal and spatial scales of the ice supersaturated areas, which are highly
 331 variable in the troposphere and tropopause region (e.g., Lamquin et al., 2012; Irvine et al., 2013; Bier et
 332 al., 2017). Estimating the impact of contrail cirrus on upper tropospheric cloudiness requires the
 333 simulation of complex microphysical processes, contrail spreading, overlap with natural clouds, radiative
 334 transfer, and the interaction with background cloudiness (Burkhardt et al., 2010). We present new best
 335 estimates based on the results of global climate models employing process-based contrail cirrus
 336 parameterizations (Appendix E). Due to the small number of independent estimates the uncertainty must
 337 be estimated from the sensitivities of the respective processes and the uncertainty in the underlying
 338 parameters and fields.

339 Here, we consider RF and ERF estimates from global climate models (Burkhardt and Kärcher, 2011;
 340 Bock and Burkhardt, 2016; Chen and Gettelman, 2013; Schumann et al., 2015; Bickel et al., 2019) to
 341 ultimately produce an ERF best estimate. For the present study, the Chen and Gettelman study was
 342 repeated with lower prescribed initial ice-crystal diameters, thereby bringing assumptions in line with
 343 measurements (e.g., Schumann et al., 2017). Since the RF estimates differ regarding the air traffic
 344 inventory, the measure of air traffic distance (i.e., taking only surface-projected or overall flight distances
 345 into account) and the temporal resolution of the air traffic data, the estimates were homogenized using
 346 known sensitivities (Bock and Burkhardt, 2016) (see Appendix E). Furthermore, the estimates were
 347 corrected to account for the underestimation of the contrail cirrus RF, as calculated by climate models that
 348 use frequency bands, relative to more detailed line-by-line radiative transfer calculations (Myhre et al.,
 349 2009). The Chen and Gettelman (2013) study is closer to a calculation of an ERF, since it accounts for
 350 fast feedbacks on natural clouds, which Bickel et al. (2019) show in their model explains most of the
 351 differences between an ERF and an RF calculation. Bickel et al. (2019) presents an explicit calculation of
 352 the contrail cirrus ERF and uses the same basic model formulation of Bock and Burkhardt, so the ERF
 353 calculation was not used here directly but rather the estimation of the ERF/RF ratio was used.

354 The RF best estimate for 2011 was calculated here for comparison to the most recent IPCC estimate
 355 (Boucher et al., 2013). With each study weighted equally, the resulting 2011 RF best estimate for contrail
 356 cirrus (excluding any adjustments) is approximately 86 (25, 146) mW m^{-2} (see **Table 3**). The IPCC best
 357 estimate of 50 (20, 150) mW m^{-2} (including the natural cloud feedback) was derived from scaling and

358 averaging two studies. IPCC assigned a large uncertainty and low confidence to reflect important aspects
359 with incomplete knowledge (e.g., spreading rate, optical depth, and radiative transfer). The RF best
360 estimate derived here for 2018 is 111 (33, 189) mW m⁻². The uncertainties in the present study are
361 reduced due to the development of process-based approaches simulating contrail cirrus in recent years.
362 The uncertainty in the new RF estimate, excluding the uncertainty in the ERF/RF scaling of individual RF
363 values, is $\pm 70\%$, a value substantially lower than the factor of three stated in IPCC.

364 The $\pm 70\%$ uncertainty was derived differently than for the NO_x forcing due to the smaller number of
365 available studies. Instead, the uncertainty was derived from the combined uncertainties associated with
366 the processes involved (see Appendix E). The processes fall into two groups: those connected with the
367 upper tropospheric water budget and the contrail cirrus scheme itself, and those associated with the
368 change in radiative transfer due to the presence of contrail cirrus. We considered uncertainty in upper
369 tropospheric ice-supersaturation frequencies and their simulation in global models and the uncertainty of
370 ice-crystal numbers due to uncertainty in soot-number emissions, ice nucleation within the plume, and
371 loss processes in the contrail's vortex phase. Finally, an important uncertainty comes from the adjustment
372 of natural clouds (Burkhardt and Kärcher, 2011). There is also a small uncertainty associated with the
373 contrail cirrus life cycle, which affects the difference in nighttime and daytime contrail cirrus cover
374 (Stuber et al., 2006) based on work analyzing the diurnal cycle (Chen and Gettelman, 2013; Newinger
375 and Burkhardt, 2012).

376 Uncertainty connected with the radiative response to contrail cirrus is largely due to the differences in the
377 radiation schemes across climate models and the approximations made therein (Myhre et al., 2009;
378 Gounou and Hogan, 2007); the background cloud field and its vertical overlap with contrail cirrus; and
379 assumptions about the homogeneity of the contrail cirrus field. Furthermore, the presence of very small
380 ice crystals ($< 5\mu\text{m}$) (Bock and Burkhardt, 2016) and unknown ice-crystal habits (Markowicz and Witek,
381 2011) add to the uncertainty.

382 Our best estimate of the contrail cirrus uncertainty does not include the impact of contrails forming within
383 natural clouds, which was recently shown to be observable from space (Tesche et al., 2016), or the change
384 in radiative transfer due to soot cores in contrail cirrus ice crystals (Liou et al., 2013), which decreases the
385 albedo at solar wavelengths and increases the top of atmosphere net RF. Both effects are very likely to
386 lead on average to an increase in contrail cirrus RF, causing our best estimate to be conservative. The
387 estimated uncertainty relates to the average contrail cirrus RF. In specific synoptic situations,
388 uncertainties may be much larger and correlated with each other.

389 In contrast to other aviation forcing terms, the average ERF/RF ratio for contrail cirrus is estimated to be
390 0.42, much less than unity. The associated uncertainty is thought to be very large and dependent on
391 prevailing aviation traffic and its geographic distribution. The low ERF/RF value is largely due to the
392 reduction in natural cloudiness caused by increased contrail cirrus similar to the reduction in natural cirrus
393 cloudiness as reported by Burkhardt and Kärcher (2011). The ERF/RF value is the average of three global
394 climate model studies: two that estimated climate efficacies of 31% and 59% (Ponater et al., 2005; Rap et
395 al., 2010) and a third that gave a direct estimate of the ERF of contrail cirrus that is 35% of the
396 corresponding RF (Bickel et al., 2019). These studies conclude that efficacies equal to that of CO₂
397 overstate the role of cirrus changes due to aviation on global mean surface temperatures. The average
398 ERF/RF ratio was applied to the homogenized estimates of RF, while the RF of Chen and Gettelman
399 (2013) was interpreted as an ERF (see above). Weighting each study equally, the resulting ERF for
400 contrail cirrus is 57 (17, 98) mW m⁻² for 2018. It is important to note that the uncertainty does not include
401 any contribution coming from the ERF/RF estimate. Despite the large ERF/RF adjustment, this ERF term
402 is the largest for global aviation in 2018 and is comparable in magnitude to the CO₂ term in the
403 normalized results for 2000 to 2018 (**Figure 6**). While comparable in magnitude, these ERFs have
404 different implications for future climate change (Section 6).

405 4.5. Aerosol-radiation interaction.

406 Aircraft engines directly emit soot, defined as mixture of BC and OC, and precursors for sulfate (SO_4^{2-})
 407 and nitrate (NO_3^-) aerosol along flight tracks. Soot aerosol is formed from the condensation of unburnt
 408 aromatic compounds in the combustor (e.g. Ebbinghaus and Wiesen, 2001) and sulfate aerosol from the
 409 oxidation of sulfur in the fuel (Dstan 91-91, 2015). Most of the sulfur is emitted as SO_2 , whilst a small
 410 fraction (~3%) is emitted as oxidized H_2SO_4 (Petzold et al., 2005). Most of the sulfate aerosol is produced
 411 after emission from sulfur precursor compounds by oxidation in the ambient atmosphere. Both aerosol
 412 types create RFs from aerosol-radiation interactions: soot absorbs short-wave radiation leading to net
 413 warming and sulfate aerosol scatters incoming short-wave radiation leading to net cooling (IPCC, 1999).
 414 As figures of merit, year 2000 global aviation emissions increase aerosol mass for both soot and sulfate
 415 by a few percent and aerosol number by 10–30% near air traffic flight corridors in the northern
 416 extratropics (Righi et al., 2013).

417 Past calculations of aerosol-radiation RF values using a variety of global aerosol models have yielded
 418 values of a few mW m^{-2} and with large uncertainties (e.g., Righi et al., 2013; Gettelman and Chen, 2013;
 419 L09). In the present study, 10 estimates across 8 models were used to evaluate soot and sulfate aerosol
 420 normalized RFs (IPCC, 1999; Sausen et al., 2005; Fuglestedt et al., 2008; Balkanski et al., 2010;
 421 Gettelmann and Chen, 2013; Unger et al., 2013; Pitari et al., 2015; Brasseur et al., 2016) (see SD
 422 spreadsheet). Averaging the normalized values yields a 2018 best estimate of the soot aerosol-radiation
 423 RF of 0.9 (0.1, 4.0) mW m^{-2} for 0.0093 Tg soot emitted. The corresponding best estimate for sulfate
 424 aerosol is -7.4 (-19, -3) mW m^{-2} for 0.37 Tg SO_2 emitted. The uncertainties are derived from the standard
 425 deviation of the model values. The ERF/RF ratios for soot and sulfate are assumed to be unity in the
 426 absence of any estimates of this ratio.

427 4.6 Aerosol-cloud interaction.

428 Aerosol-cloud interactions are those processes by which aerosols influence cloud formation. For example,
 429 cloud droplets and ice crystals nucleate on aerosol particles. Thus, aerosol-cloud interactions involving
 430 aviation aerosol potentially result in an ERF. Aviation soot and sulfate particles are the predominant
 431 primary and secondary aerosol from aircraft. The uncertainties in evaluating the aerosol-cloud
 432 interactions of aviation soot and sulfate preclude best estimates of ERF contributions. Given the potential
 433 importance of these ERF terms, placeholders are included in **Figure 3**. Furthermore, to promote progress
 434 towards future best estimates, the results of relevant modeling studies were compiled and normalized to
 435 global aviation fuel usages in 2005, 2011, 2018, to a soot emission index, and to a fuel S content of 600
 436 pm (except in the cases of low fuel-S content tests) (see **Figure 5** and spreadsheet). As noted in the
 437 caption of **Figure 5**, some earlier wide-ranging values for the soot aerosol-cloud interaction have been
 438 superseded by a more recent study (Penner et al., 2018).

439 4.6.1 Sulfate aerosol.

440 Aviation sulfate aerosol primarily affects liquid clouds in the background atmosphere. Sulfate aerosol is
 441 very efficient as a cloud condensation nuclei (CCN) for liquid clouds, and for promoting homogeneous
 442 freezing of solution particles at cold temperatures, thus nucleating ice clouds. Two integrated model
 443 simulations (Kapadia et al., 2016; Gettelman and Chen, 2013) found large impacts on liquid clouds from
 444 aviation sulfate aerosol that is transported to liquid clouds at lower altitudes over oceans, which have low
 445 albedo. The reported RF values in these studies, when scaled appropriately, are -37 to -76 mW m^{-2} in
 446 2018, excluding a low fuel-sulfur case. Note that the study of Righi et al. (2013) that yields an RF of -213
 447 mW m^{-2} in 2018 includes sulfate aerosol-cloud interactions but cannot be directly compared with Kapadia
 448 et al. (2016) and Gettelman and Chen (2013), since the former treats the combined effects of sulfate,
 449 nitrate and particulate organic matter (POM) rather than isolating the effects of sulfate as done in the
 450 latter studies. While these RF estimates do not support a best estimate at present, they do suggest that the
 451 sign of the sulfate aerosol-cloud effect on low-level clouds is likely to be negative (i.e., a cooling), similar

452 to the ERF for the aerosol-cloud interactions of other anthropogenic sources of sulfate aerosol (IPCC,
453 2013).

454 Sulfate aerosol-cloud interaction forcing estimates are highly dependent on the sensitivity (or
455 susceptibility) of the cloud radiative field to aerosol perturbations, which is dependent on uncertain model
456 processes and the model background aerosol state. Clouds that form with small CCN number
457 concentrations in the background atmosphere are more sensitive to CCN perturbations. Forcing by these
458 cloud effects are largely concentrated near flight corridors over oceans because the high albedo contrast
459 between the ocean surface and clouds increases forcing sensitivity to CCN perturbations.

460 A large uncertainty was also reported for the magnitude of the aerosol-cloud ERF from all anthropogenic
461 activities, estimated for 2011 to be -450 (-1200 , 0.0) mW m^{-2} (Myhre et al., 2013). A more recent estimate
462 of the aerosol-cloud RF from all anthropogenic activities has a 68% confidence interval of -650 to -1600
463 mW m^{-2} (Bellouin et al., 2019). In general, aerosol-cloud interactions contribute the largest uncertainty in
464 calculations of anthropogenic ERF (IPCC, 2013).

465 4.6.2 Soot.

466 The magnitude and the sign of the global RF from aviation soot effects on background cloudiness remain
467 highly uncertain. The uncertainties center on the difficulties in accurately simulating homogeneous and
468 heterogeneous ice nucleation in the background atmosphere, variations in the treatment of updraft
469 velocities during cirrus formation, and the lack of knowledge of the ice nucleating (IN) ability of aviation
470 soot particles during their atmospheric lifetime (Zhou and Penner, 2014; Penner et al., 2018).

471 Two studies find moderate effects of soot aerosol on ice clouds, depending on the ice nucleating
472 efficiency and the size distribution. RF values of about 11 – 13 mW m^{-2} (normalized to 2018 emissions)
473 are calculated in some studies for moderate ice-nucleating efficiencies (Pitari et al., 2015, Gettelman and
474 Chen, 2013).

475 In sensitivity tests, if soot processed within contrails is assumed to be an efficient IN particle, then the RF
476 may be negative by up to -330 mW m^{-2} due to reductions in ice crystal number in regions dominated by
477 homogeneous freezing (Penner et al., 2018; see Figure 5). The RF could be significantly smaller (less
478 negative) if additional ice-forming particles, such as secondary organic aerosol (SOA), are already present
479 in the background atmosphere (Penner et al., 2018; Gettelman and Chen, 2013). In addition, increases in
480 ice crystal numbers occur when the background atmosphere has much lower sulfate or haze-forming
481 aerosol number concentrations and is dominated by heterogeneous freezing, causing forcings near zero or
482 even positive (Zhou and Penner, 2014). Other studies predict decreases in cirrus number for smaller
483 numbers of larger soot particles (Hendricks et al., 2011), resulting in a slight warming (Gettelman and
484 Chen, 2013).

485 A dominant uncertainty for the aerosol-cloud effect from soot is the IN properties of aviation soot aerosol.
486 Some laboratory studies indicate soot particles are not efficient ice nuclei (DeMott et al., 1999), while
487 other studies indicate higher efficiencies (Möhler et al., 2005; Hoose and Möhler, 2012). The possibility
488 that contrail-processed soot particles would show enhanced IN activity after sublimation in the
489 background atmosphere was addressed in the laboratory (Mahrt et al., 2020). The effect was limited to
490 large soot particles, suggesting that the impact of aviation soot on cloudiness may be overestimated in
491 previous studies that assume soot processed through contrails and not covered by a sulfate coating is an
492 efficient IN (Penner et al., 2018).

493 Another source of uncertainty is soot number concentrations. For individual engines, the soot number can
494 vary by two orders of magnitude (Agarwal et al., 2019). Soot number concentrations from aviation vary
495 with the assumed size of the particles emitted as well as the mass emissions. Soot emissions from aircraft
496 are set as a regulatory parameter for the landing/take-off (LTO) cycle by ICAO and are measured in terms
497 of mass. Robust conversion factors from mass to number have recently been developed for the ICAO-

498 LTO cycle (Agarwal et al., 2019) but have not yet been made for cruise, although other methodologies
 499 exist (Teoh et al., 2019).

500 **5. Calculated net aviation ERF and RF values**

501 ERF and RF values for the terms associated with global aviation emissions and cloudiness are given in
 502 **Tables 2 and 3**, respectively, for the years 2018, 2011, and 2005, along with uncertainties, sensitivities to
 503 emissions and the ERF/RF ratio for selected terms. ERF values are shown for all years in **Figure 6**. All
 504 ERF and RF values are available in the analysis spreadsheet (SD). Through normalization and scaling, all
 505 2000 to 2018 values are self-consistent. The sensitivity of each term to emission magnitudes or flight
 506 track distances is derived in the normalization process. ERF best estimates and uncertainties (95%
 507 confidence limits) are highlighted for year 2018 in **Figure 3** along with their assessed confidence levels.
 508 No best estimates are included for sulfate and soot aerosol-cloud interactions because of the substantial
 509 uncertainties noted above. However, placeholder spaces are included in both the **Tables 2 and 3** and
 510 **Figure 3** to indicate the potential importance of these terms and to flag the associated knowledge gaps for
 511 consideration in future research and assessment activities. The confidence levels and their justifications
 512 shown in **Figure 3** are obtained by employing the methodology of Mastrandrea et al. (2011), which is
 513 based on evidence and agreement in accordance with IPCC guidance (**Table 4**).

514 In **Figure 3**, contrail cirrus formation yields the largest positive (warming) ERF term, followed by CO₂
 515 and NO_x emissions. For the 1940 to 2018 period, the net aviation ERF is +100.9 mW m⁻² (5–95%
 516 likelihood range of (55, 145)) with major contributions from contrail cirrus (57.4 mW m⁻²), CO₂ (34.3
 517 mW m⁻²), and NO_x (17.5 mW m⁻²). The aerosol and water vapor terms represent minor contributions. The
 518 formation and emission of sulfate aerosol yields the only significant negative (cooling) term. Non-CO₂
 519 terms sum to yield a positive (warming) ERF that accounts for 66% of the aviation net ERF in 2018 (66.6
 520 (21, 111) mW m⁻²). The application of ERF/RF ratios more than halves the RF value of contrail cirrus
 521 while approximately doubling the NO_x value. ERF/RF ratios were not included in the L09 analysis.
 522 Uncertainty distributions (5%, 95%) show that non-CO₂ forcing terms contribute about 8 times more than
 523 CO₂ to the uncertainty in the aviation net ERF in 2018. The best estimates of the ERFs from aviation
 524 aerosol-cloud interactions remain undetermined.

525 The time series of ERF values for individual terms is shown in **Figure 6** for the 2000–2018 period.
 526 Through normalization and scaling the terms are self-consistent over this period. The increase in all of the
 527 terms with time is consistent with the growth of aviation fuel burn and CO₂ emissions over the same
 528 period (**Figure 2**). Note that net ERF values shown for each year are not linear sums over the component
 529 terms due to the separate probability distributions associated with each component term in the sum, and
 530 instead are calculated with a Monte Carlo sampling method described below.

531 A comparison of updated RF estimates with L09 values for 2005 is given in **Table 3**. The large increase
 532 in the contrail cirrus RF between 2005 and 2018 results in part because the 2005 value only includes
 533 linear contrails. In L09, only an estimate of 2005 contrail cirrus was provided rather than a best estimate.
 534 The present study now includes a process-based model estimate of the contrail cirrus term (Section 4.4).
 535 The NO_x treatment in L09 did not include the negative forcing contributions of the long-term O₃ decrease
 536 or the SWV decrease, the updated treatment of CH₄ of Etminan et al. (2016), nor an equilibrium-to-
 537 transient correction. As a result, the updated RF values for NO_x are approximately a factor of 2 smaller.
 538 Incorporating all the updated information in the RF calculations of the NO_x and contrail cirrus terms
 539 yields an approximately 30% increase in the net aviation RF for 2005, from 78.0 to 95.2 mW m⁻². In the
 540 ERF evaluation for 2005 the net aviation forcing is reduced from 95.2 to 66.9 mW m⁻² because the
 541 ERF/RF ratios for NO_x and contrail cirrus are different than unity.

542 In seeking comparison of net aviation ERF with net anthropogenic ERF, we note that IPCC (Myhre et al.,
 543 2013) provides a value for 1750–2011 of 2290 (1130, 3330) mW m⁻². The percentage contributions of
 544 aviation to the net ERF in 2011 are 3.5% (4.0, 3.4%) and 1.59% (1.65, 1.56%) for the sum of all terms

545 and the CO₂ term alone, respectively. The 2005 and 2018 percentages are likely the same because the
 546 fraction of aviation CO₂ emissions of total anthropogenic CO₂ emissions has averaged 2.1% (± 0.15) for
 547 the last two decades (see **Figure 2**). Normalized relative probabilities of CO₂ and non-CO₂ ERFs for 2018
 548 as derived from the Monte Carlo simulations show that non-CO₂ uncertainties are the predominant
 549 contribution to the uncertainty in the aviation net ERF (**Figure 7**). IPCC also separately estimated the
 550 contrail cirrus term for 2011 as 50 (20, 150) mW m⁻² as discussed above, which compares well with the
 551 updated value of 44.1 (13, 75) mW m⁻².

552 The determination of net aviation ERFs and their uncertainties shown in **Figure 3** and accompanying
 553 tables required a Monte Carlo approach to summing over terms with discrete probability distributions. A
 554 similar method was employed in L09. PDFs of each term were constructed from the respective individual
 555 studies as normal, lognormal or discrete distributions (see SD spreadsheet). Monte Carlo samplings (one
 556 million random points) of the individual forcing PDFs were then used to combine terms to yield net ERFs
 557 and the uncertainties (95% likelihood range) for the sum of all terms and for only non-CO₂ terms (**Figure**
 558 **7**). The forcing terms are generally assumed to be independent (uncorrelated) with the notable exception
 559 of the NO_x component terms which have strong paired correlations as shown in Appendix Figure D.1.
 560 Only the short-term O₃ and CH₄ terms were included in L09 and a 100% correlation was assumed, in part,
 561 because the assumption of uncorrelated effects was deemed less acceptable. A subsequent study showed
 562 that these terms are indeed strongly correlated ($R^2 = 0.79$) (Holmes et al., 2011), similar to the present
 563 results in Appendix Figure D.1. The Holmes et al. (2011) study further concluded that the assumption of
 564 100% correlation in this case would lead to an underestimate of uncertainty in the NO_x RF. Another
 565 correlation of forcing terms not considered here may be the dependence of the soot direct effect and
 566 contrail properties on the soot number index since ice nucleation at the time of contrail formation depends
 567 on the soot number index (e.g., Kärcher, 2018).

568 **6. Emission equivalency metrics**

569 Using the best estimate ERFs, we calculate updated aviation-specific Global Warming Potential (GWP)
 570 and Global Temperature change Potential (GTP) values, presented for 20-, 50-, and 100-year time
 571 horizons in **Table 5**. These metrics assign so-called ‘CO₂-emission equivalences’ for non-CO₂ emissions
 572 via ratios of time-integrated ERF and changes in future temperatures, respectively. The choice of metric
 573 depends upon the particular underlying application (Fuglestedt et al., 2010) such that there is no
 574 uniquely ‘correct’ metric or time horizon, and alternative metrics are available. GWP and GTP are the
 575 most commonly applied metrics and the values calculated here allow a comparison with previous
 576 estimations (e.g., Lee et al., 2010; Lund et al. 2017). In calculating the GWPs and GTPs, the CO₂ IRF
 577 from Joos et al. (2013) is used and the climate response IRF from Boucher and Reddy (2008) for the
 578 GTPs (see Appendix F for further details about the metrics calculations).

579 GWPs and GTPs for contrail cirrus and for water vapor reported here are similar to, albeit slightly smaller
 580 than, corresponding results previously reported, while soot and sulfate numbers are larger in magnitude
 581 (positive and negative) than previous estimates (Fuglestedt et al. 2010; Lund et al. 2017). The
 582 Fuglestedt et al. (2010) estimates for soot are based on RF due to soot emissions from all sources, not
 583 just aviation, which yields a lower radiative efficiency (i.e., forcing per unit emission) than in the present
 584 study. Also given in **Table 5** are CO₂-equivalent aviation emissions, along with ratios of total CO₂-
 585 equivalent emissions to CO₂ emissions. Such ratios are sometimes used as ‘multipliers’ to illustrate the
 586 additional climate impact from aviation non-CO₂ terms over those from CO₂ emissions alone. Here,
 587 estimated multipliers for 2018 range from 1.0 to 4.0 depending on the choice of time horizon and
 588 emission metric. This is broadly consistent with what has been reported and used previously (Lee et al.,
 589 2010). The broad range emphasizes the challenges associated with developing comparisons of emission
 590 equivalences for short- and long-lived climate forcers within a common framework and how such
 591 considerations strongly depend on the chosen perspective.

592 One of the significant uncertainties in calculating GWPs and GTPs is the treatment of climate-carbon (C-
 593 cycle) feedbacks in the modeling framework. The efficiency of carbon sinks reduces with increasing
 594 warming (Ciais et al., 2013) and this climate feedback is implicitly included in the Absolute GWP of CO₂
 595 through the IRF used (Joos et al., 2013). However, Myhre et al. (2013) highlighted that this introduces an
 596 inconsistency since the numerators for the GWP and GTP do not include such a climate carbon feedback.
 597 One of the studies that have proposed ways of addressing this inconsistency is Gasser et al. (2017). They
 598 show that when the C-cycle feedback is consistently accounted for, the non-CO₂ emission metrics
 599 increase, but less so than initially suggested by Myhre et al. (2013). They also find that removing the C-
 600 cycle feedback from both numerator and denominator give similar metric values as including it in both
 601 places. Using the CO₂ IRF without the C-cycle feedback provided by Gasser et al. (2017), we calculate a
 602 second set of aviation emission metrics (Table F.1), showing that the changes to the GWP100 and
 603 GTP100 values from those given in Table 5 are rather small.

604 In response to the challenges related to comparing short-lived and long-lived forcing components, a
 605 number of new ‘flow-based’ methods have been introduced representing both short-lived and long-lived
 606 climate forcings explicitly as ‘warming-equivalent’ emissions that have approximately the same impact on
 607 the global average surface temperature over multi-decade to century timescales (Lauder et al., 2012; Allen
 608 et al., 2016; 2018; Cain et al., 2019; Collins et al., 2019). A simple version of these methods, known as
 609 GWP*, defines the average annual rate of CO₂-warming-equivalent emissions ($E_{CO_2e}^*$) over a period of Δt
 610 years arising from a particular component of RF or ERF by (Cain et al., 2019):

$$611 \quad E_{CO_2e}^* = [(1 - \alpha)H/AGWP_H] \Delta F / \Delta t + [\alpha/AGWP_H] \bar{F}, \quad (1)$$

612 where ΔF is the ERF change and \bar{F} the average ERF arising from that component over that period,
 613 $AGWP_H$ is the Absolute GWP of CO₂ (Wm⁻² kg⁻¹ year) over time-horizon H and α is a small coefficient
 614 depending on the previous history of that RF component. This equation gives the rate of CO₂ emission
 615 that would, alone, create the same rate of global temperature increase as the combined effect of aviation
 616 climate forcings. For historically small and/or rapidly changing RF components, α may be neglected, and
 617 hence to a good approximation, total CO₂-warming-equivalent emissions over this period ($\Delta t E_{CO_2e}^*$) are
 618 approximated by an increase in forcing, ΔF , multiplied by $H/AGWP_H$ (see Appendix F), which is about
 619 1000 GtCO₂ per W/m² for H in the range 20 to 100 years (Myhre et al, 2013; IPCC, 2018, Figure SPM.1,
 620 caption). This result follows from the definition of AGWP: since all GWP calculations assume a
 621 linearization, the $AGWP_H$ is equivalent to the forcing change resulting from the emission of H tonnes of
 622 CO₂ spread over H years (Shine et al, 2005), so $AGWP_H/H$ is the forcing change per tonne of CO₂. Under
 623 the historical profile of increasing global annual aviation-related emissions and associated ERFs, CO₂-
 624 warming-equivalent emissions based on GWP* indicate that aviation emissions are currently warming the
 625 climate around three times faster than that associated with aviation CO₂ emissions alone (**Table 5**).

626 It is important to note that, unlike the conventional GWP and GTP metrics given in **Table 5**, the ratio
 627 between total CO₂-warming-equivalent emissions from all forcing agents and those from CO₂ alone will
 628 change substantially if future aviation emissions deviate from their current growth trajectory (calculated
 629 here over the period 2000–2018). If annual global aviation emissions were to stabilize, this ratio declines
 630 towards unity, as $\Delta F/\Delta t$ would decline to zero. This does not indicate, however, that the non-CO₂ effects
 631 do not have a warming affect. This human-induced warming still represents a mitigation potential.
 632 Warming-equivalent emissions capture the fact that constant emission of short-lived climate forcings
 633 maintain an approximately constant level of warming, whilst constant emissions of long-lived climate
 634 forcings, such as CO₂, continue to accumulate in the atmosphere resulting in a constantly increasing level
 635 of associated warming. Hence warming-equivalent emissions show that the widely-used assumption of a
 636 constant ‘multiplier’, assuming that net warming due to aviation is a constant ratio of warming due to
 637 aviation CO₂ emissions alone, only applies in a situation in which aviation emissions are rising
 638 exponentially such that the rate of change of non-CO₂ RF is approximately proportional to the rate of CO₂
 639 emissions (assuming non-CO₂ RF is proportional to CO₂ emissions, and noting that the rate of change any

640 quantity is proportional to that quantity only when both are growing exponentially). In contrast, under a
 641 future hypothetical trajectory of decreasing aviation emissions, this GWP* based multiplier could fall
 642 below unity, as a steadily falling rate of emission of (positive) short-lived climate forcers has the same
 643 effect on global temperature as active removal of CO₂ from the atmosphere. The GWP* based ‘multiplier’
 644 calculated here (which depends on the ratio of the increase in net aviation warming to the increase in
 645 warming due to aviation CO₂ emissions alone over the recent past), should not be applied to future
 646 scenarios that deviate substantially from the current trend of increasing aviation-related emissions. The
 647 broad range of values for a ‘multiplier’ presented here is an illustration of the limitations of using a
 648 constant multiplier in the assessment of climate impacts of aviation, and a reminder that the choice of
 649 metric for such a multiplier involves subjective choices.

650 7. Aviation CO₂ vs non-CO₂ forcings

651 Since IPCC (1999), the comparison of aviation CO₂ RF with the non-CO₂ RFs has been a major scientific
 652 topic, as well as a discussion point amongst policy makers and civil society (ICAO, 2019). Aviation as a
 653 sector is not unique in having significant non-CO₂ forcings; the same is true of agriculture with significant
 654 CH₄ and N₂O emissions, or maritime shipping with net-negative current-day RF despite CO₂ emissions of
 655 a similar magnitude to those from aviation (Fuglesvedt et al., 2009). However, unlike direct emissions of
 656 the greenhouse gases N₂O and CH₄ from the agricultural sector, aviation non-CO₂ forcings are not
 657 covered by the former Kyoto Protocol. It is unclear whether future developments of the Paris Agreement
 658 or ICAO negotiations to mitigate climate change, in general, will include short-lived indirect greenhouse
 659 gases like NO_x and CO, aerosol-cloud effects, or other aviation non-CO₂ effects. Aviation is not
 660 mentioned explicitly in the text of the Paris Agreement, but according to its Article 4, total global
 661 greenhouse-gas emissions need to be reduced rapidly to achieve a balance between anthropogenic
 662 emissions by sources and removals by sinks of greenhouse gases in the second half of this century.

663 The IPCC concludes: “*Reaching and sustaining net-zero global anthropogenic CO₂ emissions and*
 664 *declining net non-CO₂ radiative forcing would halt anthropogenic global warming on multi-decadal time*
 665 *scales.*” (IPCC, 2018, bullet A2.2, SPM). Crucially, both conditions would need to be met to halt global
 666 warming. Hence, to halt aviation’s contribution to global warming, the aviation sector would need to
 667 achieve net-zero CO₂ emissions and declining non-CO₂ radiative forcing (unless balanced by net negative
 668 emissions from another sector): neither condition is sufficient alone. Some combination of reductions in
 669 CO₂ emissions and non-CO₂ forcings might halt further warming temporarily, but only for a few years: it
 670 would not be possible to offset continued warming from CO₂ by varying non-CO₂ radiative forcing, or
 671 *vice versa*, over multi-decade timescales.

672 That aviation’s non-CO₂ forcings are not included in global climate policy has resulted in studies as to
 673 whether they could be incorporated into existing policies, such as the European Emissions Trading
 674 Scheme, using an appropriate overall emissions ‘multiplier’; however, scientific uncertainty has so far
 675 precluded this (Faber et al., 2008). In addition, as noted above, the multiplier is highly dependent on the
 676 future emissions scenario (Section 6). Alternatively, proposals have been made to reduce aviation’s non-
 677 CO₂ forcings by, for example, avoiding contrail formation by re-routing aircraft (Matthes et al., 2017), or
 678 optimizing flight times to avoid the more positive (warming) fractional forcings (e.g., by avoiding night
 679 flights, Stuber et al., 2006). There is a developing body of literature on this topic (e.g., Newinger and
 680 Burkhardt, 2012; Yin et al., 2018). Similarly, studies have assessed whether changes in cruise altitudes
 681 could mitigate NO_x impacts (e.g. Frömming et al., 2012). The potential impacts of changes in technology
 682 have also been examined to reduce the non-CO₂ forcings such as lowering the emission index for NO_x
 683 (Freeman et al., 2018) or soot particle number emissions (Moore et al., 2017) to reduce net NO_x and
 684 contrail cirrus forcings, respectively (Burkhardt et al., 2018).

685 Avoidance of contrail formation through re-routing can incur a fuel penalty and therefore additional CO₂
 686 emissions during a flight, and changes in combustor technology to minimize NO_x generally increases

687 marginal fuel burn and CO₂ emission. Both methods invoke the usage of climate metrics such as those
 688 calculated and presented in Section 6 to evaluate whether there is a net climate benefit or disbenefit over
 689 a defined period. In examining such mitigation scenarios involving tradeoffs (e.g. Teoh et al., 2020), the
 690 perceived success or otherwise of the outcome will be a function of the user's choice of metric and time
 691 horizon. A limitation noted for the GWP is that it has an 'artificial memory' over longer time horizons,
 692 since the integrated-RF nature of the metric accumulates 'signal' over time that the climate system has
 693 'forgotten' (Fuglestedt et al., 2010). The GTP, being an 'end point' metric that captures the temperature
 694 response, overcomes this limitation of the GWP but is not yet in usage within current climate policy.

695 Changes to aviation operations or technology that result in a reduction of a non-CO₂ forcing with the
 696 added consequence of increased CO₂ emissions can result in net reductions of forcing on short timescales
 697 while increasing the net forcing on longer timescales (e.g., Freeman et al., 2018). In a case study of
 698 contrail avoidance through routing changes, Teoh et al. (2019) found that the resultant small increase in
 699 CO₂ emissions still reduces the net forcing over a timescale of 100 years. In such 'tradeoff cases' the
 700 balance between non-CO₂ and CO₂ forcings have to be weighted carefully, since CO₂ accumulates in the
 701 atmosphere and a fraction has millennial timescales (Archer and Brovkin, 2008; IPCC, 2007). Prior to the
 702 COVID-19 pandemic, global aviation traffic and emissions were projected to grow to 2050 (Fleming and
 703 Lepinay, 2019). As the COVID-19 pandemic diminishes, aviation traffic is likely to recover to meet
 704 projected rates on varying timescales (IATA, 2020), with continued growth further increasing CO₂
 705 emissions. Thus, reducing CO₂ aviation emissions will remain a continued focus in reducing future
 706 anthropogenic climate change, along with aviation non-CO₂ forcings. The latter increase the current-day
 707 impact on global average temperatures by a factor of around 3 (using GWP*) above that due to CO₂
 708 alone.

709 **Author Contributions**

710 **D. S. Lee, D. W. Fahey**

711 Role: Investigation, Methodology, Writing–review & editing, Data curation; Formal analysis, Project
 712 administration, Supervision

713 **A. Skowron**

714 Role: Investigation, Methodology, Writing–review & editing, Data curation, Formal analysis;
 715 Software

716 **M. R. Allen, U. Burkhardt, Q. Chen, S. J. Doherty, S. Freeman, P.M. Forster, J. Fuglestedt, A.
 717 Gettelman, R. R. De León, L. L. Lim, M. T. Lund, R. J. Millar, B. Owen, J. E. Penner, G. Pitari,
 718 M. J. Prather, R. Sausen, L. J. Wilcox**

719 Role: Writing–review & editing, Investigation, Methodology, Writing–original draft, Data curation;
 720 Formal analysis;

721 **Declaration of competing interest**

722 The authors declare that they have no known competing financial interests or personal relationships that
 723 could have appeared to influence the work reported in this paper.

724 **Acknowledgements**

725 We gratefully acknowledge discussions with many colleagues during the preparation of this paper, in
 726 particular Andreas Bier and Bernd Kärcher. We acknowledge help with graphical displays from Beth
 727 Tully (Figure 1) and Chelsea R. Thompson (Figures 5, 6 and 7).

728 **Funding**

729 DSL, AS, RRdL, LL, BO acknowledge support from the UK Department for Transport. PMF
 730 acknowledges support of the European Union’s Horizon 2020 Research and Innovation Programme under
 731 grant agreement number 820829 (CONSTRAIN) by the UK National Environment Research Council
 732 (NERC) SMURPHS project (NE/N006038/1). MRA acknowledges support from the EU H2020 grant
 733 agreement number 821205 (FORCeS) and the Oxford Martin Programme on Climate Pollutants. MTL
 734 and JSF acknowledges support from the Norwegian Research Council (RCN) grant number 300718
 735 (AVIATE), for which DSL and RS have a collaboration agreement. JEP acknowledges support from the
 736 National Science Foundation (NSF 1540954).

737 **Data Availability**

738 Supplementary data to this article is a spreadsheet that can be found online at: <https://doi.org/xxxxx>.

739

740 **References**

- 741 Airbus, Global Market Forecast 2017–2036 (Airbus, France 2017).
- 742 Allen, M. R. J. S. Fuglestedt, K. P. Shine, A. Reisinger, R. T. Pierrehumbert, and P. M. Forster, New use
 743 of global warming potentials to compare cumulative and short-lived climate pollutants. *Nature Climate*
 744 *Change* 6 (8), 773–776, <https://doi.org/10.1038/nclimate2998> (2016).
- 745 Allen, M. R. K. P. Shine, J. S. Fuglestedt, R. J. Millar, M. Cain, D. J. Frame, A. H. Macey, A solution to
 746 the misrepresentations of CO₂-equivalent emissions of short-lived climate pollutants under ambitious
 747 mitigation. *npj Climate and Atmospheric Science* 1:16; <https://doi.org/10.1038/s41612-018-0026-8>
 748 (2018).
- 749 Agarwal, A., R. L. Speth, T. M. Fritz, S. D. Jacob, T. Rindlisbacher, R. Iovinelli, B. Owen, R. C. Miake-
 750 Lye, J. S. Sabnis, S. R. H. Barrett, SCOPE11 method for estimating aircraft black carbon mass and
 751 particle number emissions. *Environmental Science and Technology* 53, 1364–1373,
 752 <https://doi.org/10.1021/acs.est.8b04060>, (2019).
- 753 Alfsen, K. H. and T. Berntsen, T., An Efficient and Accurate Carbon Cycle Model for Use in Simple
 754 Climate Models. CICERO, Oslo, Norway, <https://core.ac.uk/reader/52082516>
- 755 Archer, D. and V. Brovkin, The millennial atmospheric lifetime of anthropogenic CO₂. *Climatic Change*
 756 90, 283–297, <https://doi.org/10.1007/s10584-008-9413-1> (2008).
- 757 Balkanski, Y., G. Myhre, M. Gauss, G. Rädcl, E. J. Highwood, K. P. Shine, Direct radiative effect of
 758 aerosols emitted by transport: from road, shipping and aviation. *Atmospheric Chemistry and Physics*
 759 10(10), 4477–4489, <https://doi.org/10.5194/acp-10-4477-2010> (2010).
- 760 Barrett, S., M. Prather, J. Penner, H. Selkirk, S. Balasubramanian, A. Doppelheuer, G. Fleming, M. Gupta,
 761 R. Halthore, J. Hileman, M. Jacobson, S. Kuhn, S. Lukachko, R. Miake-Lye, A. Petzold, C. Roof, M.
 762 Schaefer, U. Schumann, I. Waitz, R. Wayson R., Guidance on the use of AEDT gridded aircraft emissions
 763 in atmospheric models. Massachusetts Institute for Technology, Laboratory for Aviation and the
 764 Environment, LAE-2010-008-N. (2010)
 765 <http://citeseerx.ist.psu.edu/viewdoc/download?doi=10.1.1.719.2090&rep=rep1&type=pdf>
- 766 Bellouin, N., J. Quaas, E. Gryspeerdt, S. Kinne, P. Stier, D. Watson-Parris, O. Boucher, K.S. Carslaw, M.
 767 Christensen, A.-L. Daniau, J.-L. Dufresne, G. Feingold, Bounding global aerosol radiative forcing of
 768 climate change. *Reviews of Geophysics* 58, e2019RG000660, <https://doi.org/10.1029/2019RG000660>
 769 (2019).
- 770 Bickel, M., M. Ponater, L. Bock, U. Burkhardt, S Reineke, Estimating the effective radiative forcing of
 771 contrail cirrus, *Journal of Climate*, 33, 1991-2005, <https://doi.org/10.1175/JCLI-D-19-0467.1> (2020).

- 772 Bier, A., U. Burkhardt, L. Bock, Synoptic control of contrail cirrus life cycles and their modification due
773 to reduced soot number emissions. *Journal of Geophysical Research Atmospheres* 122 (21), 11,584-
774 11,603 <https://doi.org/10.1002/2017JD027011> (2017).
- 775 Bier, A. and A. U. Burkhardt, Variability in contrail ice nucleation and its dependence on soot number
776 emissions. *Journal of Geophysical Research Atmospheres* 124, 3384–3400,
777 <https://doi.org/10.1029/2018JD029155> (2019).
- 778 Bock, L. and U. Burkhardt, Reassessing properties and radiative forcing of contrail cirrus using a climate
779 model. *Journal of Geophysical Research Atmospheres* 121, 9717–9736,
780 <https://doi.org/10.1002/2016JD025112> (2016).
- 781 Boeing, Orders and Deliveries for January 2018, <http://www.boeing.com/commercial/#/orders-deliveries>
782 (2018).
- 783 Boucher, O. and M. S. Reddy, Climate trade-off between black carbon and carbon dioxide emissions.
784 *Energy Policy* 36, 193–200, <https://doi.org/10.1016/j.enpol.2007.08.039> (2008).
- 785 Boucher, O., D. Randall, P. Artaxo, C. Bretherton, G. Feingold, P. Forster, V.-M. Kerminen, Y. Kondo,
786 H. Liao, U. Lohmann, P. Rasch, S.K. Satheesh, S. Sherwood, B. Stevens, and X.Y. Zhang, 2013: Clouds
787 and aerosols. In *Climate Change 2013: The Physical Science Basis. Contribution of Working Group I to*
788 *the Fifth Assessment Report of the Intergovernmental Panel on Climate Change*. T.F. Stocker, D. Qin, G.-
789 K. Plattner, M. Tignor, S.K. Allen, J. Doschung, A. Nauels, Y. Xia, V. Bex, and P.M. Midgley, Eds.
790 Cambridge University Press, pp. 571-657, doi:10.1017/CBO9781107415324.016.
- 791 Brasseur, G. P., M. Gupta, B. E. Anderson, S. Balasubramanian, S. Barrett, D. Duda, G. Fleming, P. M.
792 Forster, J. Fuglestedt, et al., Impact of Aviation on Climate: FAA’s Aviation Climate Change Research
793 Initiative (ACCRI) Phase II. *Bulletin of the American Meteorological Society* 97, 561–583,
794 <https://doi.org/10.1175/BAMS-D-13-00089.1> (2016).
- 795 Burkhardt, U., B. Kärcher, U. Schumann, Global Modelling of the contrail and contrail cirrus climate
796 impact. *Bulletin of the American Meteorological Society* 91, 479-484,
797 <https://doi.org/10.1175/2009BAMS2656.1> (2010).
- 798 Burkhardt, U. and B. Kärcher, Global radiative forcing from contrail cirrus. *Nature Climate Change* 1,
799 54–58, <https://doi.org/10.1038/nclimate1068> (2011).
- 800 Burkhardt, U., L. Bock, A. Bier, Mitigating the contrail cirrus climate impact by reducing aircraft soot
801 number emissions. *npj Climate and Atmospheric Science* 1:37, [https://doi.org/10.1038/s41612-018-0046-](https://doi.org/10.1038/s41612-018-0046-4)
802 4 (2018).
- 803 Cain, M., J. Lynch, M. R. Allen, J. S. Fuglestedt, D. J. Frame, A. H. Macey, Improved calculation of
804 warming-equivalent emissions for short-lived climate pollutants. *npj Climate and Atmospheric Science*,
805 2:29, <https://doi.org/10.1038/s41612-019-0086-4> (2019).
- 806 Carlin, B., Q. Fu, U. Lohmann, G. Mace, K. Sassen, J. Comstock, High-cloud horizontal inhomogeneity
807 and solar albedo bias. *Journal of Climate* 15, 2321–2339, [https://doi.org/10.1175/1520-](https://doi.org/10.1175/1520-0442(2002)015<2321:HCHIAS>2.0.CO;2)
808 0442(2002)015<2321:HCHIAS>2.0.CO;2 (2002).
- 809 Chen, C.-C., A. Gettelman, C. Craig, P. Minnis, D. P. Duda, Global contrail coverage simulated by
810 CAM5 with the inventory of 2006 global aircraft emissions. *Journal of Advances in Modeling Earth*
811 *Systems* 4, 04003. <https://doi.org/10.1029/2011MS000105> (2012).
- 812 Chen, C.-C. and A. Gettelman, Simulated radiative forcing from contrails and contrail cirrus. *Atmospheric*
813 *Chemistry and Physics*, 13, 12525–12536, <https://doi.org/10.5194/acp-13-12525-2013> (2013).

- 814 Ciais, P., Sabine, C., Bala, G., Bopp, L., Brovkin, V., Canadell, J., Chhabra, A., DeFries, R., Galloway, J.,
 815 Heimann, M., Jones, C., Le Quéré, C., Myneni, R. B., Piao, S., and Thornton, P. Carbon and Other
 816 Biogeochemical Cycles, in: Climate Change 2013: The Physical Science Basis. Contribution of Working
 817 Group I to the Fifth Assessment Report of the Intergovernmental Panel on Climate Change, edited by:
 818 Stocker, T. F., Qin, D., Plattner, G.-K., Tignor, M., Allen, S. K., Boschung, J., Nauels, A., Xia, Y., Bex,
 819 V., and Midgley, P. M., Cambridge University Press, Cambridge, UK and New York, NY, USA (2013)
- 820 Clarke, L., J. Edmonds, H. Jacoby, H. Pitcher, J. Reilly, R. Richels, “Scenarios of Greenhouse Gas
 821 Emissions and Atmospheric Concentrations”. Sub-report 2.1A of Synthesis and Assessment Product 2.1
 822 by the U.S. Climate Change Science Program and the Subcommittee on Global Change Research
 823 (Department of Energy, Office of Biological & Environmental Research, Washington, 7 DC. 2007) pp.
 824 54, https://globalchange.mit.edu/sites/default/files/CCSP_SAP2-1a-FullReport.pdf.
- 825 Collins, W. J., D. J. Frame, J. S. Fuglestedt, K. P. Shine, Stable climate metrics for emissions of short
 826 and long-lived species – combining steps and pulses. *Environmental Research Letters* 15(2), 024018,
 827 <https://doi.org/10.1088/1748-9326/ab6039> (2019).
- 828 Dalsøren, S. B., C. L. Myhre, G. Myhre, A. J. Gomez-Pelaez, O. A. Søvde, I. S. A. Isaksen, R. F. Weiss,
 829 C. M. Harth, Atmospheric methane evolution the last 40 years. *Atmospheric Chemistry and Physics* 16,
 830 3099–3126, <https://doi.org/10.5194/acp-16-3099-2016> (2016).
- 831 DeMott, P. J., Y. Chen, S. M. Kreidenweis, D. C. Rogers, D. E. Sherman, Ice formation by black carbon
 832 particles. *Geophysical Research Letters* 26, 2429–2432, <https://doi.org/10.1029/1999GL900580> (1999).
- 833 Derwent, R. G., W. J. Collins, C. E. Johnson, D. S. Stevenson, Transient behaviour of tropospheric ozone
 834 precursors in a global 3-D CTM and their indirect greenhouse effects. *Climatic Change* 49, 463–487,
 835 <https://doi.org/10.1023/A:1010648913655> (2001).
- 836 Dstan 91-91 “Turbine fuel, kerosene type, Jat A-1. Ministry of Defence, Defence Standard 91-91”, Issue
 837 7, Amendment 3. Defence Equipment and Support (UK Defence Standardization, Glasgow, UK, 2015).
- 838 Ebbinghaus, A. and P. Wiesen, Aircraft fuels and their effects upon engine emissions. *Air and Space*
 839 *Europe* 3, 101-103, [https://doi.org/10.1016/S1290-0958\(01\)90026-7](https://doi.org/10.1016/S1290-0958(01)90026-7) (2001).
- 840 Etminan, M., G. Myhre, E. J. Highwood, K. P. Shine, Radiative forcing of carbon dioxide, methane, and
 841 nitrous oxide: A significant revision of the methane radiative forcing. *Geophysical Research Letters* 43,
 842 12,614–12,623 <https://doi.org/10.1002/2016GL071930> (2016).
- 843 Faber, J., D. Greenwood, D. S. Lee, M. Mann, P. M. de Leon, D. Nelissen, B. Owen, M. Ralph, J. Tilston,
 844 A. van Velzen, G. van de Vreede, “Lower NO_x at higher altitudes: policies to reduce the climate impact of
 845 aviation NO_x emissions”. (CE-Delft, 08.7536.32, Delft, The Netherlands, 2008).
- 846 Fleming, G. and U. Ziegler, Environmental trends in aviation to 2050. In ‘ICAO Environmental Report,
 847 2016’, International Civil Aviation Organization, Montreal. (2016) [https://www.icao.int/environmental-](https://www.icao.int/environmental-protection/Documents/EnvironmentalReports/2019/ENVReport2019_pg17-23.pdf)
 848 [protection/Documents/EnvironmentalReports/2019/ENVReport2019_pg17-23.pdf](https://www.icao.int/environmental-protection/Documents/EnvironmentalReports/2019/ENVReport2019_pg17-23.pdf)
- 849 Fleming, G. and I. de Lepinay, “Environmental trends in aviation to 2050”, in ICAO Environmental
 850 Report, 2019 Destination Green the Next Chapter, (ICAO Montreal, 2019),
 851 [https://www.icao.int/environmental-](https://www.icao.int/environmental-protection/Documents/EnvironmentalReports/2019/ENVReport2019_pg17-23.pdf)
 852 [protection/Documents/EnvironmentalReports/2019/ENVReport2019_pg17-23.pdf](https://www.icao.int/environmental-protection/Documents/EnvironmentalReports/2019/ENVReport2019_pg17-23.pdf) (2019)
- 853 Forster, P.M.d.F. and K. P. Shine, Radiative forcing and temperature trends from stratospheric ozone
 854 changes. *Journal of Geophysical Research* 102, 10841–10855, <https://doi.org/10.1029/96JD03510>
 855 (1997).

- 856 Forster, C., A. Stohl, P. James, V. Thouret, The residence times of aircraft emissions in the stratosphere
857 using a mean emission inventory and emissions along actual flight tracks. *Journal of Geophysical*
858 *Research Atmospheres* 108, 8524, <https://doi.org/10.1029/2002JD002515> (2003).
- 859 Freeman, S., D. S. Lee, L. L. Lim, A. Skowron, R. R. De León, Trading off aircraft fuel burn and NO_x
860 emissions for optimal climate policy. *Environmental Science and Technology* 52, 2498–2505,
861 <https://doi.org/10.1021/acs.est.7b05719> (2018).
- 862 Friedlingstein, P., P. Cox, R. Betts, L. Bopp, W. von Bloh, V. Brovkin, P. Cadule, S. Doney, M. Eby, I.
863 Fung, G. Bala, J. John, C. Jones, F. Joos, T. Kato, M. Kawamiya, W. Knorr, K. Lindsay, H. D. Matthews,
864 T. Raddatz, P. Rayner, C. Reick, E. Roeckner, K.-G. Schnitzler, R. Schnur, K. Strassmann, A. J. Weaver,
865 C. Yoshikawa and N. Zeng, Climate-carbon cycle feedback analysis: Results from the C⁴MIP model
866 intercomparison, *Journal of Climate* 19, 3337–3353, <https://doi.org/10.1175/JCLI3800.1> (2006)
- 867 Frömming, C., M. Ponater, K. Dahlmann, V. Grewe, D. S. Lee, R. Sausen, Aviation-induced radiative
868 forcing and surface temperature change in dependency of the emission altitude. *Journal of Geophysical*
869 *Research Atmospheres* 117, 9717–9736, <https://doi.org/10.1029/2012JD018204> (2012).
- 870 Fuglestad, J. S. and T. Berntsen, “A simple model for scenario studies of changes in climate, Version
871 1.0”, (CICERO, Oslo, Norway, 1999) pp. 59, <https://cicero.oslo.no/no/publications/internal/326>.
- 872 Fuglestad, J. S., T. K. Berntsen, I. S. A. Isaksen, H. T. Mao, X. Z. Liang, W. C. Wang, Climatic forcing
873 of nitrogen oxides through changes in tropospheric ozone and methane; global 3D model studies.
874 *Atmospheric Environment* 33, 961–977 (1999).
- 875 Fuglestad, J., T. Berntsen, G. Myhre, K. Rypdal, R. B. Skeie Climate forcing from the transport sectors.
876 *Proceedings of the National Academy of Sciences U.S.A.* 105(2), 454-458,
877 <https://doi.org/10.1073/pnas.0702958104> (2008).
- 878 Fuglestad, J. S., T. Berntsen, V. Eyring, I. Isaksen, D. S. Lee, R. Sausen, Shipping emissions: from
879 cooling to warming of climate—and reducing impacts on health. *Environmental Science and Technology*
880 43, 9057–9062, <https://doi.org/10.1021/es901944r> (2009).
- 881 Fuglestad, J. S., K. P. Shine, T. Berntsen, J. Cook, D. S. Lee, A. Stenke, R. B. Skeie, G. J. M. Velders,
882 I. A. Waitz, Transport impacts on atmosphere and climate: Metrics. *Atmospheric Environment* 44, 4648–
883 4677, <https://doi.org/10.1016/j.atmosenv.2009.04.044> (2010).
- 884 Gauss, M., I. S. A. Isaksen, S. Wong, W. C. Wang, Impact of H₂O emissions from cryoplanes and
885 kerosene aircraft on the atmosphere, *Journal of Geophysical Research Atmospheres* 108 (D10), 4304,
886 <https://doi.org/10.1029/2002JD002623> (2003).
- 887 Gasser, T., G. P. Peters, J. S. Fuglestad, W. J. Collins, D. T. Shindell and P. Ciais, Accounting for the
888 climate-carbon feedback in emission metrics. *Earth Syst. Dynam.* 8, 235–253, <https://doi.org/10.5194/esd-8-235-2017> (2017).
- 890 Gettelman, A. and C. Chen, The climate impact of aviation aerosols. *Geophysical Research Letters* 40,
891 2785–2789, <https://doi.org/10.1002/grl.50520> (2013).
- 892 Gounou, A. and R. J. Hogan, A sensitivity study of the effect of horizontal photon transport on the
893 radiative forcing of contrails. *Journal of the Atmospheric Sciences* 64, 1706–1716,
894 <https://doi.org/10.1175/JAS3915.1> (2007).
- 895 Gottschaldt, K., C. Voigt, P. Jöckel, M. Righi, R. Deckert, S. Dietmüller, Global sensitivity of aviation
896 NO_x effects to the HNO₃-forming channel of the HO₂ + NO reaction. *Atmospheric Chemistry and Physics*
897 13, 3003–3025, <https://doi.org/10.5194/acp-13-3003-2013> (2013).

- 898 Grewe, V., and A. Stenke, AirClim: an efficient tool for climate evaluation of aircraft technology.
899 *Atmospheric Chemistry and Physics* 8, 4621–4639, <https://doi.org/10.5194/acp-8-4621-2008> (2008).
- 900 Hansen, J., M. Sato, R. Ruedy, Radiative forcing and climate response. *Journal of Geophysical Research*
901 *Atmospheres* 102 (D6), 6831–6864, <https://doi.org/10.1029/96JD03436> (1997).
- 902 Hansen, J., and L. Nazarenko Soot climate forcing via snow and ice albedos. *Proceedings of the National*
903 *Academy of Sciences U.S.A.* 101, 423–428, <https://doi.org/10.1073/pnas.2237157100> (2004).
- 904 Hansen, J., M. Sato, R. Ruedy, L. Nazarenko, A. Lacis, G. A. Schmidt, G. Russell, I. Aleinov, M. Bauer,
905 S. Bauer, N. Bell, B. Cairns, V. Canuto, M. Chandler, Y. Cheng, A. Del Genio, G. Faluvegi, E. Fleming,
906 A. Friend, T. Hall, C. Jackman, M. Kelley, N. Kiang, D. Koch, J. Lean, J. Lerner, K. Lo, S. Menon, R.
907 Miller, P. Minnis, T. Novakov, V. Oinas, Ja. Perlwitz, Ju. Perlwitz, D. Rind, A. Romanou, D. Shindell, P.
908 Stone, S. Sun, N. Tausnev, D. Thresher, B. Wielicki, T. Wong, M. Yao, S. Zhang, Efficacy of climate
909 forcings. *Journal of Geophysical Research Atmospheres* 110, D18104.
910 <https://doi.org/10.1029/2005JD005776> (2005).
- 911 Hari, T. K., Z. Yaakob, N. Binitha, Aviation biofuel from renewable resources: routes, opportunities and
912 challenges. *Renewable and Sustainable Energy Reviews* 42, 1234–1244
913 <https://doi.org/10.1016/j.rser.2014.10.095> (2015).
- 914 Hasselmann K., S. Hasselmann, R. Giering, V. Ocana, H. von Storch, Sensitivity study of optimal CO₂
915 emission paths using a Simplified Structural Integrated Assessment Model (SIAM). *Climatic Change* 37,
916 345–386, <https://doi.org/10.1023/A:1005339625015> (1997).
- 917 Hendricks, J., B. Kärcher, U. Lohmann, Effects of ice nuclei on cirrus clouds in a global climate model.
918 *Journal of Geophysical Research Atmospheres* 116, 2156–2202, <https://doi.org/10.1029/2010JD015302>
919 (2011).
- 920 Hodnebrog, Ø., T. K. Berntsen, O. Dessens, M. Gauss, V. Grewe, I. S. A. Isaksen, B. Koffi, G. Myhre, D.
921 Olivié, M. J. Prather, J. A. Pyle, F. Stordal, S. Szopa, Q. Tang P. van Velthoven, J. E. Williams, K.
922 Ødemark, Future impact of non-land based traffic emissions on atmospheric ozone and OH – an
923 optimistic scenario and a possible mitigation strategy. *Atmospheric Chemistry and Physics* 11, 11,293–
924 11,317, <https://doi.org/10.5194/acp-11-11293-2011> (2011).
- 925 Hodnebrog, Ø., T. K. Berntsen, O. Dessens, M. Gauss, V. Grewe, I. S. A. Isaksen, B. Koffi, G. Myhre, D.
926 Olivié, M. J. Prather, F. Stordal, S. Szopa, Q. Tang, P. van Velthoven, J. E. Williams, Future impact of
927 traffic emissions on atmospheric ozone and OH based on two scenarios. *Atmospheric Chemistry and*
928 *Physics* 12, 12,211–12,225, <https://doi.org/10.5194/acp-12-12211-2012> (2012).
- 929 Holmes, C. D., Q. Tang, M. J. Prather, Uncertainties in climate assessment for the case of aviation
930 NO. *Proceedings of the National Academy of Science U.S.A.* 108(27), 10997–11002,
931 <https://doi.org/10.1073/pnas.1101458108> (2011).
- 932 Holmes, C. D., M. J. Prather, O. A. Søvde, G. Myhre, Future methane, hydroxyl, and their uncertainties:
933 key climate and emission parameters for future predictions. *Atmospheric Chemistry and Physics* 13, 285–
934 302, <https://doi.org/10.5194/acp-13-285-2013> (2013).
- 935 Hoor, P., J. Borken-Kleefeld, D. Caro, O. Dessens, O. Endresen, M. Gauss, V. Grewe, D. Hauglustaine, I.
936 S. A. Isaksen, P. Jöckel, J. Lelieveld, G. Myhre, E. Meijer, D. Olivié, M. Prather, C. Schnadt-Poberaj, K.
937 P. Shine, J. Staehelin, Q. Tang, J. van Aardenne, P. van Velthoven, R. Sausen, The impact of traffic
938 emissions on atmospheric ozone and OH: results from QUANTIFY. *Atmospheric Chemistry and Physics*
939 9, 3113–3136, <https://doi.org/10.5194/acp-9-3113-2009> (2009).

- 940 Hoose, C. and O. Möhler, Heterogeneous ice nucleation on atmospheric aerosols: a review of results from
 941 laboratory experiments. *Atmospheric Chemistry and Physics* 12, 9817–9854, [https://doi.org/10.5194/acp-](https://doi.org/10.5194/acp-12-9817-2012)
 942 12-9817-2012 (2012).
- 943 Hough, A. M., The development of a two-dimensional global tropospheric model – 1. The model
 944 transport. *Atmospheric Environment* 23, 1235–1261, [https://doi.org/10.1016/0004-6981\(89\)90150-9](https://doi.org/10.1016/0004-6981(89)90150-9)
 945 (1989).
- 946 Hough, A. M., Development of a two-dimensional global tropospheric model: model chemistry. *Journal*
 947 *of Geophysical Research Atmospheres* 96, 7325–7362, <https://doi.org/10.1029/90JD01327> (1991).
- 948 Irvine, E. A., B. J. Hoskins, K. P. Shine, A Lagrangian analysis of ice-supersaturated air over the North
 949 Atlantic. *Journal of Geophysical Research Atmospheres* 119, 90–100,
 950 <https://doi.org/10.1002/2013JD020251> (2013).
- 951 IATA, Economic Performance of the Airline Industry.
 952 [https://www.iata.org/contentassets/f88f0ceb28b64b7e9b46de44b917b98f/iata-economic-performance-of-](https://www.iata.org/contentassets/f88f0ceb28b64b7e9b46de44b917b98f/iata-economic-performance-of-the-industry-end-year-2018-report.pdf)
 953 [the-industry-end-year-2018-report.pdf](https://www.iata.org/contentassets/f88f0ceb28b64b7e9b46de44b917b98f/iata-economic-performance-of-the-industry-end-year-2018-report.pdf) (2019).
- 954 IATA, Outlook for air travel in the next 5 years, [https://www.iata.org/en/iata-](https://www.iata.org/en/iata-repository/publications/economic-reports/covid-19-outlook-for-air-travel-in-the-next-5-years/)
 955 [repository/publications/economic-reports/covid-19-outlook-for-air-travel-in-the-next-5-years/](https://www.iata.org/en/iata-repository/publications/economic-reports/covid-19-outlook-for-air-travel-in-the-next-5-years/) (2020)
- 956 ICAO (2018) ICAO Carbon Emissions Calculator Methodology, version 11, June 2018,
 957 ([https://www.icao.int/environmental-](https://www.icao.int/environmental-protection/CarbonOffset/Documents/Methodology%20ICAO%20Carbon%20Calculator_v11-2018.pdf)
 958 [protection/CarbonOffset/Documents/Methodology%20ICAO%20Carbon%20Calculator_v11-2018.pdf](https://www.icao.int/environmental-protection/CarbonOffset/Documents/Methodology%20ICAO%20Carbon%20Calculator_v11-2018.pdf))
 959 accessed 19-05-2020.
- 960 ICAO, ‘Destination Green the Next Chapter’, ICAO Environmental Report, Montreal,
 961 [https://www.icao.int/environmental-protection/Documents/ICAO-ENV-Report2019-F1-WEB%20\(1\).pdf](https://www.icao.int/environmental-protection/Documents/ICAO-ENV-Report2019-F1-WEB%20(1).pdf)
 962 (2019).
- 963 IEA, International Energy Agency. International Energy Agency Oil Information, 1960-2017. [data
 964 collection]. 12th Edition. UK Data Service. SN: 5187, <http://doi.org/10.5257/iea/oil/2019-1> (2019).
- 965 IPCC (1999), “*Aviation and the Global Atmosphere*”, Intergovernmental Panel on Climate Change
 966 Special Report, J. E. Penner, D. H. Lister, D. J. Griggs, D. J. Dokken, M. McFarland, Eds. (Cambridge
 967 University Press, Cambridge, UK, 1999) [https://www.ipcc.ch/report/aviation-and-the-global-atmosphere-](https://www.ipcc.ch/report/aviation-and-the-global-atmosphere-2/)
 968 [2/](https://www.ipcc.ch/report/aviation-and-the-global-atmosphere-2/).
- 969 IPCC (2001) “Climate Change 2001: The Scientific Basis. Contribution of Working Group I to the Third
 970 Assessment Report of the Intergovernmental Panel on Climate Change”. J.T. Houghton, Y. Ding, D.J.
 971 Griggs, M. Noguer, P.J. van der Linden, X. Dai, K. Maskell and C.A. Johnson (eds). Cambridge
 972 University Press, UK. https://www.ipcc.ch/site/assets/uploads/2018/07/WG1_TAR_FM.pdf
- 973 IPCC (2007), “Climate change 2007. “Mitigation of climate change”, in: Contribution of Working Group
 974 III to the Fourth Assessment Report of the Intergovernmental Panel on Climate Change”, B. Metz, O. R.
 975 Davidson, P. R. Bosch, R. Dave, L. A. Meyer, eds (Cambridge University Press, UK)
 976 <https://www.ipcc.ch/report/ar4/wg3/>
- 977 IPCC (2013) “Climate Change 2013: The Physical Science Basis, Contribution of Working Group I to the
 978 Fifth Assessment Report of the Intergovernmental Panel on Climate Change”, T. F. Stocker, D. Qin, G. -
 979 K. Plattner, M. Tignor, S. K. Allen, J. Boschung, A. Nauels, Y. Xia, V. Bex, P. M. Midgley, Eds.
 980 (Cambridge University Press, Cambridge, United Kingdom and New York, NY, USA, 2013).
 981 <https://www.ipcc.ch/report/ar5/wg1/>

- 982 IPCC (2018) “Global Warming of 1.5°C. An IPCC Special Report on the impacts of global warming of
 983 1.5°C above pre-industrial levels and related global greenhouse gas emission pathways, in the context of
 984 strengthening the global response to the threat of climate change, sustainable development, and efforts to
 985 eradicate poverty”, Masson-Delmotte, V., P. Zhai, H.-O. Pörtner, D. Roberts, J. Skea, P.R. Shukla, A.
 986 Pirani, W. Moufouma-Okia, C. Péan, R. Pidcock, S. Connors, J.B.R. Matthews, Y. Chen, X. Zhou, M.I.
 987 Gomis, E. Lonnoy, T. Maycock, M. Tignor, and T. Waterfield (eds), (2018).
 988 <https://www.ipcc.ch/sr15/download/>
- 989 Joos, F., M. Bruno, R. Fink, T. F. Stocker, U. Siegenthaler, C. LeQuéré, J. L. Sarmiento, J.L., An efficient
 990 and accurate representation of complex oceanic and biospheric models for anthropogenic carbon uptake.
 991 *Tellus* 48B, 397e417, <https://doi.org/10.1034/j.1600-0889.1996.t01-2-00006.x> (1996)
- 992 Joos, F., R. Roth, J. S. Fuglestedt, G. P. Peters, I. G. Enting, W. von Bloh, V. Brovkin, E. J. Burke, M.
 993 Eby, N. R. Edwards, T. Friedrich, T. L. Frolicher, P. R. Halloran, P. B. Holden, C. Jones, T. Kleinen, F. T.
 994 Mackenzie, K. Matsumoto, M. Meinshausen, G.-K. Plattner, A. Reisinger, J. Segschneider, G. Shaffer,
 995 M. Steinacher, K. Strassmann, K. Tanaka, A. Timmermann, A. J. Weaver, Carbon dioxide and climate
 996 impulse response functions for the computation of greenhouse gas metrics: a multi-model analysis.
 997 *Atmospheric Chemistry and Physics* 13, 2793–2825, <https://doi.org/10.5194/acp-13-2793-2013> (2013).
- 998 Kapadia, Z. Z., D. V. Spracklen, S. R. Arnold, D. J. Borman, G. W. Mann, K. J. Pringle, S. A. Monks, C.
 999 L. Reddington, F. Benduhn, A. Rap, C. E. Scott, E. W. Butt, M. Yoshioka, Impacts of aviation fuel sulfur
 1000 content on climate and human health. *Atmospheric Chemistry and Physics* 16, 10521–10541,
 1001 <https://doi.org/10.5194/acp-16-10521-2016> (2016).
- 1002 Kärcher, B., U. Burkhardt, A. Bier, L. Bock, I. J. Ford, The microphysical pathway to contrail formation.
 1003 *Journal of Geophysical Research Atmospheres* 120, 7893–7927, <https://doi.org/10.1002/2015JD023491>
 1004 (2015).
- 1005 Kärcher, B. Formation and radiative forcing of contrail cirrus. *Nature Communications* 9:1824,
 1006 <https://doi.org/10.1038/s41467-018-04068-0> (2018).
- 1007 Khodayari, A., D. J. Wuebbles, S. Olsen, J. S. Fuglestedt, T. Berntsen, M. T. Lund, I. Waitz, P. Wolfe,
 1008 P. M. Forster, M. Meinshausen, D. S. Lee, L. L. Lim, Intercomparison of the capabilities of simplified
 1009 climate models to project the effects of aviation CO₂ on climate. *Atmospheric Environment* 75, 321–328,
 1010 <https://doi.org/10.1016/j.atmosenv.2013.03.055> (2013).
- 1011 Khodayari, A., S. C. Olsen, D. J. Wuebbles, Evaluation of aviation NO_x-induced radiative forcings for
 1012 2005 and 2050. *Atmospheric Environment* 91, 95–103, <https://doi.org/10.1016/j.atmosenv.2014.03.044>
 1013 (2014a).
- 1014 Khodayari, A., S. Tilmes, S. C. Olsen, D. B. Phoenix, D. J. Wuebbles, J.-F. Lamarque, C.-C. Chen,
 1015 Aviation 2006 NO_x-induced effects on atmospheric ozone and HO_x in Community Earth System Model
 1016 (CESM). *Atmospheric Chemistry and Physics* 14, 9925–9939, <https://doi.org/10.5194/acp-14-9925-2014>
 1017 (2014b).
- 1018 Köhler, M. O., G. Rädcl, O. Dessens, K. P. Shine, H. L. Rogers, O. Wild, J. A. Pyle, Impact of
 1019 perturbation of nitrogen oxide emissions from global aviation *Journal of Geophysical Research*
 1020 *Atmospheres* 113, D11305, <https://doi.org/10.1029/2007JD009140> (2008).
- 1021 Köhler, M. O., G. Rädcl, K. P. Shine, H. L. Rogers, J. A. Pyle, Latitudinal variation of the effect of
 1022 aviation NO_x emissions on atmospheric ozone and methane and related climate metrics. *Atmospheric*
 1023 *Environment* 64, 1–9, <https://doi.org/10.1016/j.atmosenv.2012.09.013> (2013).
- 1024 Lamarque, J.-F., T. C. Bond, V. Eyring, C. Granier, A. Heil, Z. Klimont, D. Lee, C. Liou, A. Mieville,
 1025 B. Owen, M. G. Schultz, D. Shindell, S. J. Smith, E. Stehfest, J. van Aardenne, O. R. Cooper, M.

- 1026 Kainuma, N. Mahowald, J. R. McConnell, V. Naik, K. Riahi, D. P. van Vuuren, Historical (1850–2000)
1027 gridded anthropogenic and biomass burning emissions of reactive gases and aerosols: methodology and
1028 application. *Atmospheric Chemistry and Physics* 10, 7017–7039, [https://doi.org/10.5194/acp-10-7017-](https://doi.org/10.5194/acp-10-7017-2010)
1029 2010 (2010).
- 1030 Lamquin, N., C. J. Stubenrauch, K. Gierens, U. Burkhardt, H. Smit, A global climatology of upper
1031 tropospheric ice supersaturation occurrence inferred from the Atmospheric Infrared Sounder calibrated by
1032 MOZAIC. *Atmospheric Chemistry and Physics* 12, 381–405, <https://doi.org/10.5194/acp-12-381-2012>
1033 (2012).
- 1034 Lauder, A. R., I. G. Enting, J. O. Carter, N. Clisby, A. L. Cowie, B. K. Henry, M. R. Raupach, Offsetting
1035 methane emissions — An alternative to emission equivalence metrics. *International Journal of*
1036 *Greenhouse Gas Control* 12, 419–429, <https://doi.org/10.1016/j.ijggc.2012.11.028> (2012).
- 1037 Lee, D. S., D. Fahey, P. M. Forster, P. J. Newton, R. C. N. Wit, L. L. Lim, B. Owen, R. Sausen, Aviation
1038 and global climate change in the 21st century. *Atmospheric Environment* 43, 3520–3537
1039 <https://doi.org/10.1016/j.atmosenv.2009.04.024> (2009).
- 1040 Lee, D. S., G. Pitari, V. Grewe, K. Gierens, J. E. Penner, A. Petzold, M. Prather, U. Schumann, A. Bais,
1041 T. Berntsen, D. Iachetti, L. L. Lim, R. Sausen, Transport impacts on atmosphere and climate: Aviation.
1042 *Atmospheric Environment* 44, 4678–4734, <https://doi.org/10.1016/j.atmosenv.2009.06.005> (2010).
- 1043 Le Quéré, C. and 76 others, Global carbon budget 2018. *Earth System Science Data* 10, 2141–2194,
1044 <https://doi.org/10.5194/essd-10-2141-2018> (2018).
- 1045 Le Quéré, C., R. B. Jackson, M. W. Jones, A. J. P. Smith, S. Abernethy, R. M. Andrew, A. J. De-Goll, D.
1046 R. Willis, Y. Shan, J. G. Canadell, P. Friedlingstein, F. Creutzig and G. P. Peters, Temporary reduction in
1047 daily global CO₂ emissions during the COVID-19 forced confinement, *Nature Climate Change*,
1048 <https://doi.org/10.1038/s41558-020-0797-x> (2020).
- 1049 Lim, L. L., D. S. Lee, B. Owen, A. Skowron, S. Matthes, U. Burkhardt, S. Dietmuller, G. Pitari, G. Di
1050 Genova, D. Iachetti, I. Isaksen, O. A. Søvde, REACT4C: Simplified mitigation study. TAC-4
1051 Proceedings, June 22nd to 25th, 2015, Bad Kohlgrub, 181-185,
1052 https://www.pa.op.dlr.de/tac/2015/Proceedings_of_TAC4_conference_final.pdf (2015).
- 1053 Liou, K. N., Y. Takano, Q. Yue, P. Yang, On the radiative forcing of contrail cirrus contaminated by
1054 black carbon. *Geophysical Research Letters* 40, 778–784, <https://doi.org/10.1002/GRL.50110> (2013).
- 1055 Lund, M. T., B. Aamaas, T. Berntsen, L. Bock, U. Burkhardt, J. S. Fuglestedt, K. P. Shine, Emission
1056 metrics for quantifying regional climate impacts of aviation. *Earth System Dynamics* 8, 547–563,
1057 <https://doi.org/10.5194/esd-8-547-2017> (2017).
- 1058 Mahrt, F., K. Kilchhofer, C. Marcolli, P. Grönquist, R. O. David, M. Rösch, U. Lohmann, Z. A. Kanji,
1059 The impact of cloud processing on the ice nucleation abilities of soot particles at cirrus temperatures.
1060 *Journal of Geophysical Research* 125, e2019JD030922, <https://doi.org/10.1029/2019JD030922> (2020).
- 1061 Maier-Reimer, E. and K. Hasselmann, Transport and storage of CO₂ in the ocean—An inorganic ocean-
1062 circulation carbon cycle model. *Climate Dynamics* 2, 63–90, <https://doi.org/10.1007/BF01054491> (1987).
- 1063 Matthes, M., V. Grewe, K. Dahmann, C. Frömming, E. Irvine, L. Lim, F. Linke, B. Lührs, B. Owen, K.
1064 Shine, S. Stromatas, H. Yamashita, F. Yin, A concept for multi-criteria environmental assessment of
1065 aircraft trajectories. *Aerospace* 4 42, <https://doi.org/10.3390/aerospace4030042> (2017).
- 1066 Markowicz, K. M. and M. L. Witek, Simulations of contrail optical properties and radiative forcing for
1067 various crystal shapes. *Journal of Applied Meteorology and Climatology* 50, 1740–1755,
1068 <https://doi.org/10.1175/2011JAMC2618.1> (2011).

- 1069 Marquart, S., R. Sausen, M. Ponater, V. Grewe, Estimate of the climate impact of the cryoplanes,
1070 *Aerospace Science and Technology*, 5, 73-84, [https://doi.org/10.1016/S1270-9638\(00\)01084-1](https://doi.org/10.1016/S1270-9638(00)01084-1) (2001).
- 1071 Mastrandrea, M. D., K. J. Mach, G. K. Plattner, O. Edenhofer, T. F. Stocker, C. B. Field, K. L. Ebi, P. R.
1072 Matschoss, The IPCC AR5 guidance note on consistent treatment of uncertainties: a common approach
1073 across the working groups. *Climatic Change* 108, 675–691, <https://doi.org/10.1007/s10584-011-0178-6>
1074 (2011).
- 1075 Meinshausen, M., S. J. Smith, K. Calvin, J. S. Daniel, M. L. T. Kainuma, J. -F. Lamarque, K. Matsumoto,
1076 S. A. Montzka, S. C. B. Raper, K. Riahi, A. Thomson, G. J. M. Velders, D. P. P. van Vuuren, The RCP
1077 greenhouse gas concentrations and their extensions from 1765 to 2300. *Climatic Change* 109, 213–241,
1078 <https://doi.org/10.1007/s10584-011-0156-z> (2011).
- 1079 Millar, R. J., Z. R. Nicholls, P. Friedlingstein, M. R. Allen, A modified impulse-response representation
1080 of the global near-surface air temperature and atmospheric concentration response to carbon dioxide
1081 emissions. *Atmospheric Chemistry and Physics*. 17, 7213–7228, [https://doi.org/10.5194/acp-17-7213-](https://doi.org/10.5194/acp-17-7213-2017)
1082 2017 (2017).
- 1083 Miller, M., P. Brook and C. Eyers, Reduction of Sulphur limits in aviation fuel standards (SULPHUR).
1084 EASA research project EASA.2008/C11, European Aviation Safety Agency. (2010)
1085 [https://www.easa.europa.eu/sites/default/files/dfu/2009-SULPHUR-](https://www.easa.europa.eu/sites/default/files/dfu/2009-SULPHUR-Reduction%20of%20sulphur%20limits%20in%20aviation%20fuel%20standards-Final%20Report.pdf)
1086 [Reduction%20of%20sulphur%20limits%20in%20aviation%20fuel%20standards-Final%20Report.pdf](https://www.easa.europa.eu/sites/default/files/dfu/2009-SULPHUR-Reduction%20of%20sulphur%20limits%20in%20aviation%20fuel%20standards-Final%20Report.pdf)
- 1087 Minnis, P., S. T. Bedka, D. P. Duda, K. M. Bedka, T. Chee, J. K. Ayers, R. Palikonda, D. A.
1088 Spangenberg, K. V. Khlopenkov, R. Boeke, Linear contrail and contrail cirrus properties determined from
1089 satellite data. *Geophysical Research Letters*, 40, 3220–3226, <https://doi.org/10.1002/grl.50569> (2013).
- 1090 Möhler, O., S. Büttner, C. Linke, M. Schnaiter, H. Saathof, O. Stetzer, R. Wagner, M. Krämer, A.
1091 Mangold, V. Ebert, U. Schurath, Effect of sulfuric acid coating on heterogenous ice nucleation by soot
1092 aerosol particles. *Journal of Geophysical Research* 110 (D11), <https://doi.org/10.1029/2004JD005169>
1093 (2005).
- 1094 Montzka, S. A., C. M. Spivakovsky, J. H. Butler, J. W. Elkins, L. T. Lock, D. J. Mondeel, New
1095 observational constraints for atmospheric hydroxyl on global and hemispherical scales. *Science* 288, 500–
1096 503, <https://doi.org/10.1126/science.288.5465.500> (2000).
- 1097 Moore, R. H., K. L. Thornhill, B. Weinzierl, D. Sauer, E. D'Ascoli, J. Kim, et al., Biofuel blending
1098 reduces particle emissions from aircraft engines at cruise conditions. *Nature*, 543, 411–415,
1099 <https://doi.org/10.1038/nature21420> (2017)
- 1100 Myhre, G., J. S. Nilsen, L. Gulstad, K. P. Shine, B. Rognerud, I. S. A. Isaksen, Radiative forcing due to
1101 stratospheric water vapor from CH₄ oxidation. *Geophysical Research Letters* 34, L01807,
1102 <https://doi.org/10.1029/2006GL027472> (2007).
- 1103 Myhre, G., M. Kvalevåg, G. Rädcl, J. Cook, K. P. Shine, H. Clark, F. Karcher, K. Markowicz, A. Kardas,
1104 P. Wolkenberg, Y. Balkanski, M. Ponater, P. Forster, A. Rap, R. R. de Leon, Intercomparison of
1105 radiative forcing calculations of stratospheric water vapour and contrails. *Meteorologische Zeitschrift* 18,
1106 585–596, <https://doi.org/10.1127/0941-2948/2009/0411> (2009).
- 1107 Myhre, G., K. P. Shine, G. Rädcl, M. Gauss, I. S. A. Isaksen, Q. Tang, M. J. Prather, J. E. Williams, P.
1108 van Velthoven, O. Dessens, B. Koffi, S. Szopa, P. Hoor, V. Grewe, J. Borcken-Kleefeld, T. K. Berntsen, J.
1109 S. Fuglestedt, Radiative forcing due to changes in ozone and methane caused by the transport sector.
1110 *Atmospheric Environment* 45, 387–394, <https://doi.org/10.1016/j.atmosenv.2010.10.001> (2011).
- 1111 Myhre, G., D. Shindell, F. -M Breon, W. Collins, J. Fuglestedt, J. Huang, D. Koch, J. -F. Lamarque, D.
1112 Lee., B. Mendoza, T. Nakajima, A. Robock, G. Stephens, T. Takemura, H. Zhang, “Anthropogenic and

- 1113 Natural Radiative Forcing” in Climate Change 2013: the Physical Science Basis, Contribution of
 1114 Working Group I to the Fifth Assessment Report of the Intergovernmental Panel on Climate Change,
 1115 (Cambridge University Press, 2013). <https://www.ipcc.ch/report/ar5/wg1/>
- 1116 Newinger, C. and U. Burkhardt, Sensitivity of contrail cirrus radiative forcing to air traffic scheduling.
 1117 *Journal of Geophysical Research Atmospheres* 117, D10205, <https://doi.org/10.1029/2011JD016736>
 1118 (2012).
- 1119 OECD, Green growth and the future of aviation. Paper prepared for the 27th Round Table on Sustainable
 1120 Development held at OECD Headquarters 23-24 January 2012 (OECD 2012). [https://www.oecd.org/sd-](https://www.oecd.org/sd-roundtable/papersandpublications/49482790.pdf)
 1121 [roundtable/papersandpublications/49482790.pdf](https://www.oecd.org/sd-roundtable/papersandpublications/49482790.pdf)
- 1122 Olivié, D. J. L., D. Cariolle, H. Teyssède, D. Salas, A. Voldoire, H. Clark, D. Saint-Martin, M. Michou,
 1123 F. Karcher, Y. Balkanski, M. Gauss, O. Dessens, B. Koffi, R. Sausen, Modeling the climate impact of
 1124 road transport, maritime shipping and aviation over the period 1860–2100 with an AOGCM. *Atmospheric*
 1125 *Chemistry and Physics* 12, 1449–1480, <https://doi.org/10.5194/acp-12-1449-2012> (2012).
- 1126 Olsen, S. C., G. P. Brasseur, D. J. Wuebbles, S. R. H. Barrett, H. Dang, S. D. Eastham, M. Z. Jacobson,
 1127 A. Khodayari, H. Selkirk, A. Sokolov, N. Unger, Comparison of model estimates of the effects of
 1128 aviation emissions on atmospheric ozone and methane. *Geophysical Research Letters* 40, 6004–6009,
 1129 <https://doi.org/10.1002/2013GL057660> (2013).
- 1130 Penner, J.E., Y. Chen, M. Wang, and X. Liu, Possible influence of anthropogenic aerosols on cirrus
 1131 clouds and anthropogenic forcing. *Atmospheric Chemistry and Physics*, 9, 879–96,
 1132 <https://doi.org/10.5194/acp-9-879-2009> (2009).
- 1133 Penner, J. E., C. Zhou, A. Garnier, D. L. Mitchell, Anthropogenic aerosol indirect effects in cirrus clouds.
 1134 *Journal of Geophysical Research Atmospheres*, 123, 11,652–11,677,
 1135 <https://doi.org/10.1029/2018JD029204> (2018).
- 1136 Petzold, A., M. Gysel, X. Vancassel, R. Hitzenberger, H. Puxbaum, S. Vrochticky, E. Weingartner, U.
 1137 Baltensperger, P. Mirabel, On the effects of organic matter and sulphur-containing compounds on the
 1138 CCN activation of combustion particles. *Atmospheric Chemistry and Physics* 5, 3187–3203,
 1139 <https://doi.org/10.5194/acp-5-3187-2005> (2005).
- 1140 Pitari, G., D. Iachetti, G. Genova, N. De Luca, O. A. Søvde, Ø. Hodnebrog, D. S. Lee, L. L. Lim, Impact
 1141 of coupled NO_x/aerosol aircraft emissions on ozone photochemistry and radiative forcing. *Atmosphere* 6,
 1142 751–782, <https://doi.org/10.3390/atmos6060751> (2015).
- 1143 Pitari, G., I. Cionni, G. Di Genova, O. A. Søvde, L. Lim, Radiative forcing from aircraft emissions of
 1144 NO_x: model calculations with CH₄ surface flux boundary condition. *Meteorologische Zeitschrift* 26(6),
 1145 663-687, <https://doi.org/10.1127/metz/2016/0776> (2017).
- 1146 Pomroy, H. R. and J. A. Illingworth, Ice cloud inhomogeneity: Quantifying bias in emissivity from radar
 1147 observations. *Geophysical Research Letters* 27, 2101–2104, <https://doi.org/10.1029/1999GL011149>
 1148 (2000).
- 1149 Ponater, M., S. Marquart, R. Sausen, U. Schumann, On contrail climate sensitivity. *Geophysical Research*
 1150 *Letters* 32, L10706, <https://doi.org/10.1029/2005GL022580> (2005).
- 1151 Ponater, M., S. Pechtl, R. Sausen, U. Schumann, G. Hüttig, Potential of the cryoplane technology to
 1152 reduce aircraft climate impact: a state-of-the-art assessment. *Atmospheric Environment* 40, 6928-6944,
 1153 <https://doi.org/10.1016/j.atmosenv.2006.06.036> (2006).
- 1154 Ponater, M., M. Bickel, L. Bock, and U. Burkhardt, Towards determining the efficacy of contrail cirrus.
 1155 In Matthes, S. and A. Blum, Making Aviation Environmentally Sustainable, 3rd ECATS Conference,

- 1156 Book of Abstracts, Volume 1. ISBN 978-1-910029-58-9. 51-44 (2020). ([http://www.ecats-](http://www.ecats-network.eu/uploads/2020/06/ECATS_Main_BookOfAbstracts_Vol1_final.pdf)
1157 [network.eu/uploads/2020/06/ECATS_Main_BookOfAbstracts_Vol1_final.pdf](http://www.ecats-network.eu/uploads/2020/06/ECATS_Main_BookOfAbstracts_Vol1_final.pdf))
- 1158 Prather, M. J., Lifetimes and eigenstates in atmospheric chemistry. *Geophysical Research Letters* 21,
1159 801–804, <https://doi.org/10.1029/94GL00840> (1994).
- 1160 Prather, M., D. Ehhalt, F. Dentener, R. Derwent, E. Dlugokencky E, “Atmospheric chemistry and
1161 greenhouse gases”, in *Climate Change 2001: The Scientific Basis, Contribution of Working Group I to*
1162 *the Third Assessment Report of the Intergovernmental Panel on Climate Change*, J. T. Houghton ed.
1163 (Cambridge University Press, Cambridge, United Kingdom and New York, NY, USA, 2001) pp. 239–
1164 287. <https://www.ipcc.ch/site/assets/uploads/2018/03/TAR-04.pdf>
- 1165 Prather, M. J., C. D. Holmes, J. Hsu, Reactive greenhouse gas scenarios: Systematic exploration of
1166 uncertainties and the role of atmospheric chemistry, *Geophysical Research Letters*, 39, L09803,
1167 <https://doi.org/10.1029/2012GL051440> (2012).
- 1168 Rap, A., P. M. Forster, J. M. Haywood, A. Jones, O. Boucher, Estimating the climate impact of linear
1169 contrails using the UK Met Office climate model. *Geophysical Research Letters* 37, L20703,
1170 <https://doi.org/10.1029/2010GL045161> (2010).
- 1171 Revelle, R. and H. E. Suess, Carbon dioxide exchange between atmosphere and ocean and the question of
1172 an increase of atmospheric CO₂ during the past decades, *Tellus*, 9, 18–27, [https://doi.org/10.1111/j.2153-](https://doi.org/10.1111/j.2153-3490.1957.tb01849.x)
1173 [3490.1957.tb01849.x](https://doi.org/10.1111/j.2153-3490.1957.tb01849.x) (1957).
- 1174 Richardson, T. B., P.M. Forster, C. J. Smith, A. C. Maycock, T. Wood, T. Andrews, O. Boucher, G.
1175 Faluvegi, D. Fläschner, Ø. Hodnegrog, M. Kasoar, A. Kirkevåg, J.-F. Lamarque, J. Mülmenstädt, G.
1176 Myhre, D. Olivié, R. W. Portmann, B. H. Samset, D. Shawki, D. Shindell, P. Stier, T. Takemura, A.
1177 Voulgarakis, D. Watson-Parris, Efficacy of climate forcings in PDRMIP models. *Journal of Geophysical*
1178 *Research: Atmospheres* 124, <https://doi.org/10.1029/2019JD030581> (2019).
- 1179 Righi, M., J. Hendricks, R. Sausen, The global impact of the transport sectors on atmospheric aerosol:
1180 simulations for year 2000 emissions. *Atmospheric Chemistry and Physics* 13, 9939–9970,
1181 <https://doi.org/10.5194/acp-13-9939-2013> (2013).
- 1182 Sander, S. P., R. R. Friedl, A. R. Ravishankara, D. M. Golden, C. E. Kolb, M. J. Kurylo, M. J. Molina, G.
1183 K. Moortgat, B. J. Finlayson-Pitts, “Chemical Kinetics and Photochemical Data for Use in Atmospheric
1184 Studies”, (JPL Publ. 06-2, No. 15, 2006). https://jpldataeval.jpl.nasa.gov/pdf/JPL_02-25_rev02.pdf
- 1185 Sausen R. and U. Schumann, Estimates of the climate response to aircraft CO₂ and NO_x emissions
1186 scenarios. *Climatic Change* 44, 27–58 (2000).
- 1187 Sausen, R. I. Isaksen, V. Grewe, D. Hauglustaine, D. S. Lee, G. Myhre, M. O. Köhler, G. Pitari, U.
1188 Schumann, F. Stordal, C. Zerefos, Aviation radiative forcing in 2000: An update on IPCC (1999).
1189 *Meteorologische Zeitschrift* 14, 555–561, <https://doi.org/10.1127/0941-2948/2005/0049> (2005).
- 1190 Schumann, U., J. E. Penner, Y. Chen, C. Zhou, K. Graf, Dehydration effects from contrails in a coupled
1191 contrail-climate model. *Atmospheric Chemistry and Physics* 15, 11179–11199,
1192 <https://doi.org/10.5194/acp-15-11179-2015> (2015).
- 1193 Schumann, U., R. Baumann, D. Baumgardner, S. T. Bedka, D. P. Duda, V. Freudenthaler, J.-F. Gayet, A.
1194 J. Heymsfield, P. Minnis, M. Quante, E. Raschke, H. Schlager, M. Vázquez-Navarro, C. Voigt, Z. Wang,
1195 Properties of individual contrails: a compilation of observations and some comparisons. *Atmospheric*
1196 *Chemistry and Physics* 17, 403–438, <https://doi.org/10.5194/acp-17-403-2017> (2017).

- 1197 Shine, K. P., J.S. Fuglestedt, K. Hailemariam, N. Stuber, Alternatives to the global warming potential
1198 for comparing climate impacts of emissions of greenhouse gases. *Climatic Change* 68, 281–302,
1199 <https://doi.org/10.1007/s10584-005-1146-9> (2005).
- 1200 Skeie, R. B., J. Fuglestedt, T. Berntsen, G. P. Peters, R. Andrew, M. Allen, S. Kallbekken, Perspective
1201 has a strong effect on the calculation of historical contributions to global warming. *Environmental*
1202 *Research Letters* 12, 024022, <https://doi.org/10.1088/1748-9326/aa5b0a> (2017).
- 1203 Skowron, A., D. S. Lee, J. Hurley, “Aviation NO_x Global Warming Potential”, in 2nd International
1204 Conference on Transport, Atmosphere and Climate, 25-28 June 2009, Aachen/Maastricht,
1205 Germany/Netherlands, <https://www.pa.op.dlr.de/tac/2009/proceedings/FB2010-10.pdf> (2009).
- 1206 Skowron, A., D. S. Lee, R. R. de León, The assessment of the impact of aviation NO_x on ozone and other
1207 radiative forcing responses—The importance of representing cruise altitudes accurately. *Atmospheric*
1208 *Environment* 74, 159–168, <https://doi.org/10.1016/j.atmosenv.2013.03.034> (2013).
- 1209 Skowron, A., D. S. Lee, R. R. de León, Variation of radiative forcings and global warming potentials
1210 from regional aviation NO_x emissions. *Atmospheric Environment* 104, 69–78,
1211 <https://doi.org/10.1016/j.atmosenv.2014.12.043> (2015).
- 1212 Søvde, O. A., S. Matthes, A. Skowron, D. Iachetti, L. Lim, B. Owen, Ø. Hodnebrog, G. Di Genova, G.
1213 Pitari, D. S. Lee, G. Myhre, I. S. A. Isaksen, Aircraft emission mitigation by changing route altitude: A
1214 multi-model estimate of aircraft NO_x emission impact on O₃ photochemistry. *Atmospheric Environment*
1215 95, 468–479, <https://doi.org/10.1016/j.atmosenv.2014.06.049> (2014).
- 1216 Smith, C. J., R. J. Kramer, G. Myhre, P. M. Forster, B. J. Soden, T. Andrews, O. Boucher, G. Faluvegi,
1217 D. Fläschner, Ø. Hodnebrog, M. Kasoar, V. Kharin, A. Kirkevåg, J.-F. Lamarque, J. Mülmenstädt, D.
1218 Olivié, T. Richardson, B. H. Samset, D. Shindell, P. Stier, T. Takemura, A. Voulgarakis, D. Watson-
1219 Parris, Understanding rapid adjustments to diverse forcing agents. *Geophysical Research Letters* 45,
1220 doi:10.1029/2018GL079826 (2018)
- 1221 Stevenson, D. S., C. E. Johnson, W. J. Collins, R. G. Derwent, K. P. Shine, J. M. Edwards, Evolution of
1222 tropospheric ozone radiative forcing. *Geophysical Research Letters* 25, 3819–3822,
1223 <https://doi.org/10.1029/1998GL900037> (1998).
- 1224 Stevenson, D. S., R. M. Doherty, M. G. Sanderson, W. J. Collins, C. E. Johnson, R. G. Derwent,
1225 Radiative forcing from aircraft NO_x emissions: mechanisms and seasonal dependence *Journal of*
1226 *Geophysical Research Atmospheres* 109, D17307, <https://doi.org/10.1029/2004JD004759> (2004).
- 1227 Stordal, F., M. Gauss, G. Myhre, E. Mancini, D. A. Hauglustaine, M. O. Köhler, T. Berntsen, E. J. G.
1228 Stordal, D. Iachetti, G. Pitari, I. S. A. Isaksen, TRADEOFFs in climate effects through aircraft routing:
1229 forcing due to radiatively active gases. *Atmospheric Chemistry and Physics Discussions* 6, 10733–10771
1230 (2006).
- 1231 Stuber, N., M. Ponater, R. Sausen, Why radiative forcing might fail as a predictor of climate change.
1232 *Climate Dynamics* 24, 497–510 doi:10.1007/s00382-004-0497-7 (2005).
- 1233 Stuber, N., P. Forster, G. Rädcl, K. Shine, The importance of the diurnal and annual cycle of air traffic for
1234 contrail radiative forcing. *Nature* 441, 864–867, <https://doi.org/10.1038/nature04877> (2006).
- 1235 Teoh, R., M. E. J. Stettler, A. Majumdar, U. Schumann, B. Graves, A. M. Boies, A methodology to relate
1236 black carbon particle number and mass emissions. *Journal of Aerosol Science* 132, 44–59,
1237 <https://doi.org/10.1016/j.jaerosci.2019.03.006> (2019).

- 1238 Teoh, R., Schumann, U., Majumdar A., Stettler, M. E. J., Mitigating the climate forcing of aircraft
1239 contrails by small-scale diversions and technology adoption. *Environmental Science and Technology*, 54
1240 2941–2950, doi: 10.1021/acs.est.9b05608 (2020).
- 1241 Tesche, M., P. Achtert, P. Glantz, K. J. Noone, Aviation effects on already-existing cirrus clouds. *Nature*
1242 *Communications* 7, 12016, <https://doi.org/10.1038/ncomms12016> (2016).
- 1243 UKDS (2016) http://stats.ukdataservice.ac.uk/index.aspx?r=349678&DataSetCode=IEA_COAL_BA,
1244 2016.
- 1245 UNFCCC, <https://unfccc.int/nationally-determined-contributions-ndcs>
- 1246 Unger, N., T. C. Bond, J. S. Wang, D. M. Koch, S. Menon, D. T. Shindell, S. Bauer, Attribution of
1247 climate forcing to economic sectors. *Proceedings of the National Academy of Sciences U.S.A.* 107, 3382–
1248 3387, <https://doi.org/10.1073/pnas.0906548107> (2010).
- 1249 Unger, N., Global climate impact of civil aviation for standard and desulfurized jet fuel. *Geophysical*
1250 *Research Letters* 38, 1–6, <https://doi.org/10.1029/2011GL049289> (2011).
- 1251 Unger, N., Y. Zhao, H. Dang, Mid-21st century chemical forcing of climate by the civil aviation sector.
1252 *Geophysical Research Letters* 40, 641–645, <https://doi.org/10.1002/grl.50161> (2013).
- 1253 Unterstrasser, S., Large-eddy simulation study of contrail microphysics and geometry during the vortex
1254 phase and consequences on contrail-to-cirrus transition. *Journal of Geophysical Research Atmospheres*
1255 119, 7537–7555, <https://doi.org/10.1002/2013JD021418> (2014).
- 1256 Voulgarakis, A., V. Naik, J.-F. Lamarque, D. T. Shindell, P. J. Young, M. J. Prather, O. Wild, R. D. Field,
1257 D. Bergmann, P. Cameron-Smith, I. Cionni, W. J. Collins, S. B. Dalsøren, R. M. Doherty, V. Eyring, G.
1258 Faluvegi, G. A. Folberth, L. W. Horowitz, B. Josse, I. A. McKenzie, T. Nagashima, D. A. Plummer, M.
1259 Righi, S. T. Rumbold, D. S. Stevenson, S. A. Strode, K. Sudo, S. Szopa, G. Zeng, Analysis of present-day
1260 and future OH and methane lifetime in the ACCMIP simulations. *Atmospheric Chemistry and Physics* 13,
1261 2563–2587, <https://doi.org/10.5194/acp-13-2563-2013> (2013).
- 1262 Wilcox, L., K. P. Shine, B. J. Hoskins, Radiative forcing due to aviation water vapour emissions.
1263 *Atmospheric Environment* 63, 1–13, <https://doi.org/10.1016/j.atmosenv.2012.08.072> (2012).
- 1264 Wild, O., M. J. Prather, H. Akimoto, Indirect long-term global radiative cooling from NO_x emissions.
1265 *Geophysical Research Letters* 28, 1719–1722, <https://doi.org/10.1029/2000GL012573> (2001).
- 1266 Xie B., H. Zhang, Z. Wang, S. Zhao, Q. Fu, A modelling study of effective radiative forcing and climate
1267 response due to tropospheric ozone. *Advances in Atmospheric Sciences* 33, 819–828 doi: 10.1007/s00376-
1268 016-5193-0 (2016).
- 1269 Yin, F., V. Grewe, C. Frömming, H. Yamashita, Impact on flight trajectory characteristics when avoiding
1270 the formation of persistent contrails for transatlantic routes. *Transportation Research Part D: Transport*
1271 *and Environment* 65, 466–484, <https://doi.org/10.1016/j.trd.2018.09.017> (2018).
- 1272 Zhou, C. and J. E. Penner, Aircraft soot indirect effect on large-scale cirrus clouds: Is the indirect forcing
1273 by aircraft soot positive or negative? *Journal of Geophysical Research Atmospheres* 119, 11,303–11,320,
1274 <https://doi.org/10.1002/2014JD021914> (2014).
- 1275

1276 **Table 1.** Emission indices used in ERF and RF calculations

Emission	Emission index	Reference	Notes
CO ₂	3.16 kg/kg fuel	ICAO (2018)	
NO _x	15.14 g/kg fuel	Fleming and Ziegler (2016)	2018, 2011
	14.12 g/kg fuel	Barrett et al. (2010)	2005
Water vapor	1.231 kg/kg fuel	Barrett et al. (2010)	
Soot	0.03 g/kg fuel	Barrett et al. (2010)	
	2×10 ¹⁴ particles/kg fuel ^a		
Sulphur (SO ₂)	1.2 g/kg fuel	Miller et al. (2010)	Assumed S content of 600 ppm

1277 ^a Assumes mean particle size in the range of 11–79 nm diameter.

1278

1279
1280
1281**Table 2.** Best estimates and high/low limits of the 90% likelihood ranges for aviation ERF components derived in this study

ERF (mW m ⁻²)	2018 ^a	2011 ^a	2005 ^a	Sensitivity to emissions	ERF/RF
Contrail cirrus	57.4 (17, 98)	44.1 (13, 75)	34.8 (10, 59)	$9.36 \times 10^{-10} \text{ mW m}^{-2} \text{ km}^{-1}$	0.42
CO ₂	34.3 (28, 40)	29.0 (24, 34)	25.0 (21, 29)		1.0
Short-term O ₃ increase	49.3 (32, 76)	37.3 (24, 58)	33.0 (21, 51)	$34.4 \pm 9.9 \text{ mW m}^{-2} (\text{Tg (N) yr}^{-1})^{-1}$	1.37
Long-term O ₃ decrease	-10.6 (-20, -7.4)	-7.9 (-15, -5.5)	-6.7 (-13, -4.7)	$-9.3 \pm 3.4 \text{ mW m}^{-2} (\text{Tg (N) yr}^{-1})^{-1}$	1.18
CH ₄ decrease	-21.2 (-40, -15)	-15.8 (-30, -11)	-13.4 (-25, -9.4)	$-18.7 \pm 6.9 \text{ mW m}^{-2} (\text{Tg (N) yr}^{-1})^{-1}$	1.18
Stratospheric water vapor decrease	-3.2 (-6.0, -2.2)	-2.4 (-4.4, -1.7)	-2.0 (-3.8, -1.4)	$-2.8 \pm 1.0 \text{ mW m}^{-2} (\text{Tg (N) yr}^{-1})^{-1}$	1.18
Net NO _x	17.5 (0.6, 29)	13.6 (0.9, 22)	12.9 (1.9, 20)	$5.5 \pm 8.1 \text{ mW m}^{-2} (\text{Tg (N) yr}^{-1})^{-1}$	
Stratospheric H ₂ O increase	2.0 (0.8, 3.2)	1.5 (0.6, 2.4)	1.4 (0.6, 2.3)	$0.0052 \pm 0.0026 \text{ mW m}^{-2} (\text{Tg (H}_2\text{O) yr}^{-1})^{-1}$	---
Soot (aerosol-radiation)	0.94 (0.1, 4.0)	0.71 (0.1, 3.0)	0.67 (0.1, 2.8)	$100.7 \pm 165.5 \text{ mW m}^{-2} (\text{Tg (BC) yr}^{-1})^{-1}$	---
Sulfate (aerosol-radiation)	-7.4 (-19, -2.6)	-5.6 (-14, -1.9)	-5.3 (-13, -1.8)	$-19.9 \pm 16.0 \text{ mW m}^{-2} (\text{Tg (SO}_2\text{) yr}^{-1})^{-1}$	---
Sulfate and soot (aerosol-cloud)	---	---	---	---	---
Net ERF (only non-CO ₂ terms)	66.6 (21, 111)	51.4 (16, 85)	41.9 (14, 69)	---	---
Net aviation ERF	100.9 (55, 145)	80.4 (45, 114)	66.9 (38, 95)	---	---
Net anthropogenic ERF in 2011	---	2290 (1130, 3330) ^b	---	---	---

1282 ^a The uncertainty distributions for all forcing terms are lognormal except for CO₂ and contrail cirrus (normal) and Net
1283 NO_x (discrete pdf).

1284 ^b Boucher et al., 2013. IPCC also separately estimated the contrail cirrus term for 2011 as 50 (20, 150) mW m⁻².

1285

1286 **Table 3.** Best estimates and low/high limits of the 95% likelihood ranges for aviation RF components
 1287 derived in this study ^a

RF (mW m ⁻²)	2018 ^b	2011 ^b	2005 ^b	L09 2005 values	Sensitivity to emissions (this work)
Contrail cirrus	111.4 (33, 189)	85.6 (25, 146)	67.5 (20, 115)	(11.8 ^c)	1.82 x 10 ⁻⁹ mW m ⁻² km ⁻¹
CO ₂	34.3 (31, 38)	29.0 (26, 32)	25.0 (23, 27)	28.0	
Short-term O ₃ increase	36.0 (23, 56)	27.3 (17, 42)	24.0 (15, 37)	26.3	25.1 ± 7.3 mW m ⁻² (Tg (N) yr ⁻¹) ⁻¹
Long-term O ₃ decrease	-9.0 (-17, -6.3)	-6.7 (-13, -4.7)	-5.7 (-11, -4.0)	----	-7.9 ± 2.9 mW m ⁻² (Tg (N) yr ⁻¹) ⁻¹
CH ₄ decrease	-17.9 (-34, -13)	-13.4 (-25, -9.3)	-11.4 (-21, -7.9)	-12.5	-15.8 ± 5.9 mW m ⁻² (Tg (N) yr ⁻¹) ⁻¹
Stratospheric water vapor decrease	-2.7 (-5.0 -1.9)	-2.0 (-3.8, -1.4)	-1.7 (-3.2, -1.2)	----	-2.4 ± 0.9 mW m ⁻² (Tg (N) yr ⁻¹) ⁻¹
Net NO _x	8.2 (-4.8, 16)	6.5 (-3.3, 12)	6.6 (1.9, 12)	13.8 ^d	1.0 ± 6.6 mW m ⁻² (Tg (N) yr ⁻¹) ⁻¹
Stratospheric H ₂ O increase	2.0 (0.8, 3.2)	1.5 (0.6, 2.4)	1.4 (0.6, 2.3)	2.8	0.0052 ± 0.0026 mW m ⁻² (Tg (H ₂ O) yr ⁻¹) ⁻¹
Soot (aerosol-radiation)	0.94 (0.1, 4.0)	0.71 (0.1, 3.0)	0.67 (0.1, 2.8)	3.4	100.7 ± 165.5 mW m ⁻² (Tg (BC) yr ⁻¹) ⁻¹
Sulfate (aerosol-radiation)	-7.4 (-19, -2.6)	-5.6 (-14, -1.9)	-5.3 (-13, -1.8)	-4.8	-19.9 ± 16.0 mW m ⁻² (Tg (SO ₂) yr ⁻¹) ⁻¹
Sulfate and soot (aerosol-cloud)	----	----	----	----	----
Net RF (only non-CO ₂ terms)	114.8 (35, 194)	88.4 (27, 149)	70.3 (22, 119)	----	----
Net aviation RF	149.1 (70, 229)	117.4 (56, 179)	95.2 (47, 144)	78.0	----

1288 ^a ERF values are shown in **Table 2**.

1289 ^b The uncertainty distributions for all forcing terms are lognormal except for CO₂ and contrail cirrus (normal) and Net
 1290 NO_x (discrete pdf).

1291 ^c Linear contrails only; excludes the increase in cirrus cloudiness due to aged spreading contrails.

1292 ^d Excludes updated CH₄ RF evaluation of Etmann et al. (2016) and equilibrium-to-transient correction.

1293

1294 **Table 4a.** Confidence levels for the ERF estimates in **Figure 3**

Terms	Evidence	Agreement	Conf. level	Basis for uncertainty estimates	Understanding change since L09
Contrail cirrus formation in high-humidity regions	Limited	Medium	Low*	Robust evidence for the phenomenon. Large remaining uncertainties in magnitude in part due to incomplete representation of key processes	The inclusion of contrail cirrus processes in global climate models.
Carbon dioxide (CO₂) emissions	Robust	Medium	High**	Trends in aviation CO ₂ emissions and differences between simplified C-cycle models	Better assessment of uncertainties from multiple models
Short-term ozone increase	Medium	Medium	Medium*	Observed trends of tropospheric ozone and laboratory studies of chemical kinetics, reliance on a large number of model results for aviation emissions	Elevated owing to many more studies
Long-term ozone decrease	Limited	Medium	Low*	Reliance on chemical modelling studies	Not provided previously
Methane decrease	Medium	Medium	Medium*	Observed trends of tropospheric methane and laboratory studies of chemical kinetics, reliance on a large number of model results for aviation emissions	Elevated owing to many more studies
Stratospheric water vapour decrease	Limited	Medium	Low*	Reliance on chemical modelling studies	Not provided previously
Net NO_x	Medium	Limited	Low*	Associated uncertainties with combining above effects	Elevated owing to more studies but lowered in total owing to additional terms and methodological constraints
Water vapor emissions in the stratosphere	Medium	Medium	Medium	Limited studies of perturbation of water vapor budget of UT/LS	Elevated owing to more studies
Aerosol-radiation interactions					
From soot emissions	Limited	Medium	Low	Limited studies and uncertain emission index	More studies
From sulfur emissions	Limited	Medium	Low	Limited studies and uncertain emission index	More studies
Aerosol-cloud interactions					
From sulfur emissions	Limited	Low	Very low	None available; few studies, probably a negative ERF	Not provided previously
From soot emissions	Limited	Low	Very low	None available; few studies, varying in sign and magnitude of ERF constrained by poor understanding of processes	Not provided previously

1295 * This term has the additional uncertainty of the derivation of an effective radiative forcing from a radiative forcing.

1296 ** This term differs from 'Very High' level in IPCC (2013) because additional uncertainties are introduced by the
1297 assessment of marginal aviation CO₂ emissions and their resultant concentrations in the atmosphere from simplified
1298 carbon cycle models.

1299

1300

1301

1302 **Table 4b.** Basis for confidence levels in **Table 4a**^a

Medium	High	Very High
<i>High agreement</i>	<i>High agreement</i>	<i>High agreement</i>
<i>Limited evidence</i>	<i>Medium evidence</i>	<i>Robust evidence</i>
Low	Medium	High
<i>Medium agreement</i>	<i>Medium agreement</i>	<i>Medium agreement</i>
<i>Limited evidence</i>	<i>Medium evidence</i>	<i>Robust evidence</i>
Very Low	Low	Medium
<i>Low agreement</i>	<i>Low agreement</i>	<i>Low agreement</i>
<i>Limited evidence</i>	<i>Medium evidence</i>	<i>Robust evidence</i>

1303 ^a The basis for the confidence level is given as a combination of evidence
 1304 (limited, medium, robust) and agreement (low, medium and high) based
 1305 on guidance given by Mastrandrea et al. (2011).

1306

1307 **Table 5.** Emission metrics and corresponding CO₂-equivalent emissions for the ERF components of 2018
 1308 aviation emissions and cloudiness

1309 **Metrics**

ERF term	GWP ₂₀	GWP ₅₀	GWP ₁₀₀	GTP ₂₀	GTP ₅₀	GTP ₁₀₀
CO ₂	1	1	1	1	1	1
Contrail cirrus (Tg CO ₂ basis)	2.32	1.09	0.63	0.67	0.11	0.09
Contrail cirrus (km basis)	39	18	11	11	1.8	1.5
Net NO _x	619	205	114	-222	-69	13
Aerosol-radiation						
Soot emissions	4288	2018	1166	1245	195	161
SO ₂ emissions	-832	-392	-226	-241	-38	-31
Water vapor emissions	0.22	0.10	0.06	0.07	0.01	0.008

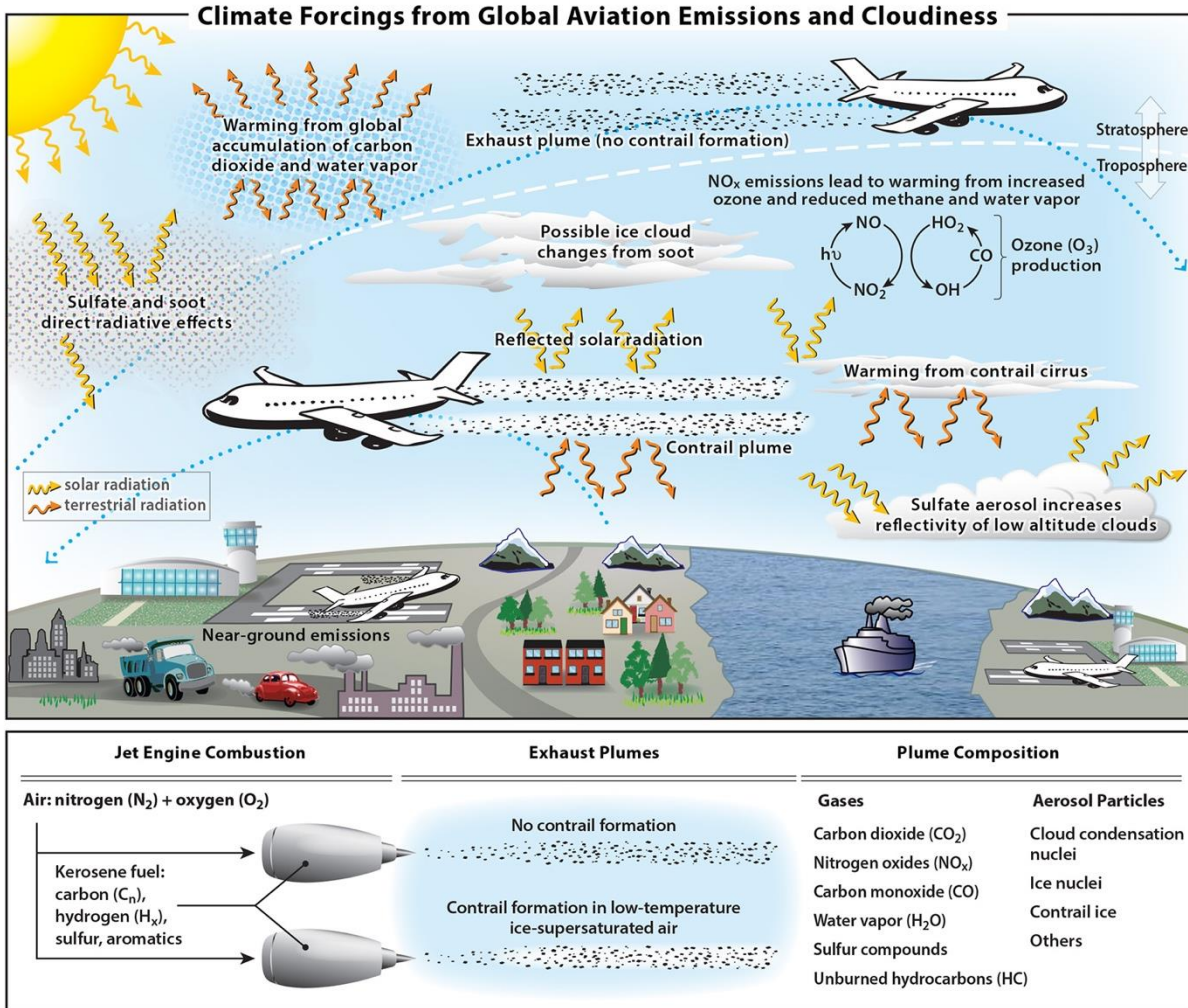
1310

1311 **CO₂-eq emissions (Tg CO₂ yr⁻¹) for 2018**

ERF term	GWP ₂₀	GWP ₅₀	GWP ₁₀₀	GTP ₂₀	GTP ₅₀	GTP ₁₀₀	GWP* ₁₀₀ (E ⁺ CO _{2e})
CO ₂	1034	1034	1034	1034	1034	1034	1034
Contrail cirrus (Tg CO ₂ basis)	2399	1129	652	695	109	90	1834
Contrail cirrus (km basis)	2395	1127	651	694	109	90	1834
Net NO _x	887	293	163	-318	-99	19	339
Aerosol-radiation							
Soot emissions	40	19	11	12	2	2	20
SO ₂ emissions	-310	-146	-84	-90	-14	-12	-158
Water vapor emissions	83	39	23	27	4	3	42
Total CO ₂ -eq (using km basis)	4128	2366	1797	1358	1035	1135	3111
Total CO ₂ -eq / CO ₂	4.0	2.3	1.7	1.3	1.0	1.1	3.0

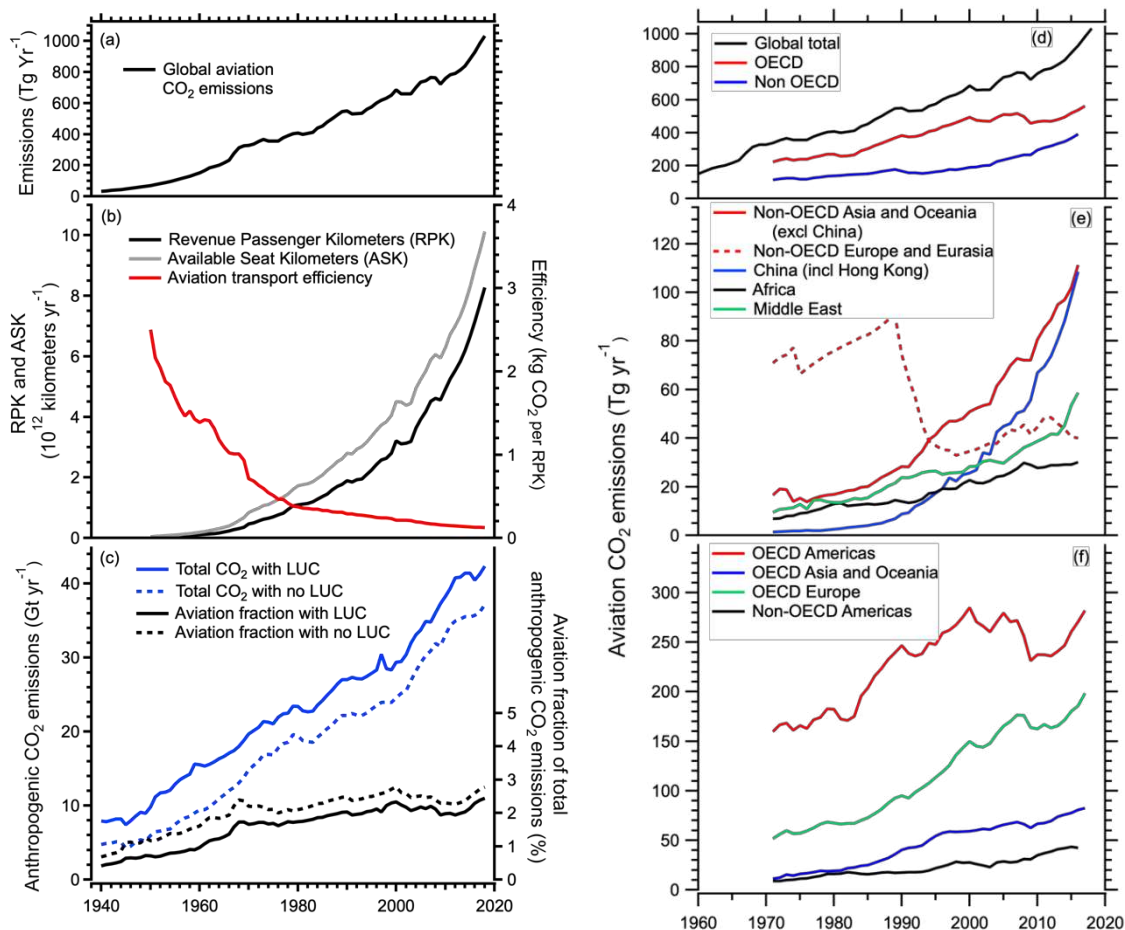
1312

1313
1314



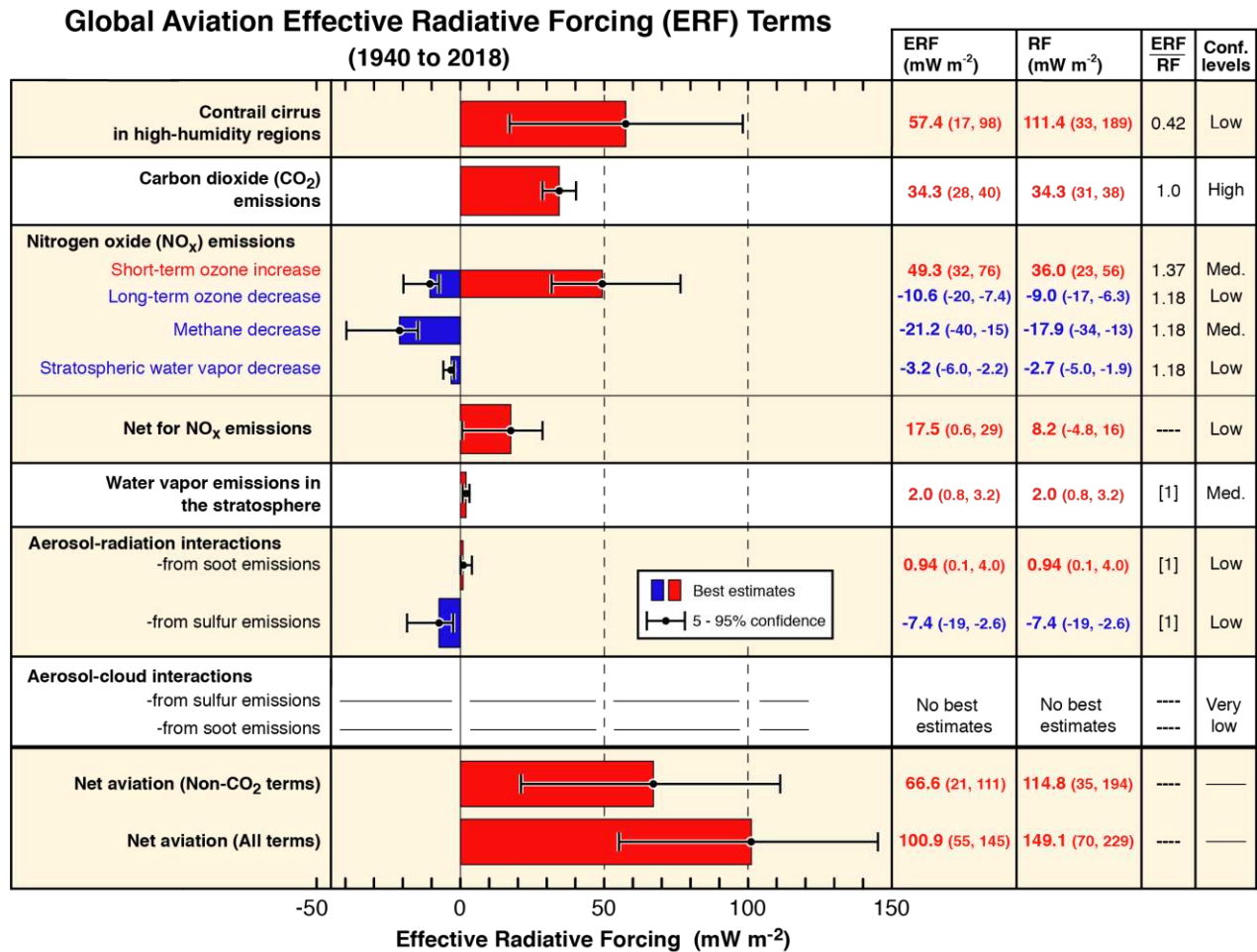
1315 **Figure 1.** Schematic overview of the processes by which aviation emissions and increased cirrus
 1316 cloudiness affect the climate system. Net positive RF (warming) contributions arise from CO₂, water
 1317 vapor, NO_x, and soot emissions, and from contrail cirrus (consisting of linear contrails and the cirrus
 1318 cloudiness arising from them). Negative RF (cooling) contributions arise from sulfate aerosol production.
 1319 Net warming from NO_x emissions is a sum over warming (short-term ozone increase) and cooling
 1320 (decreases in methane and stratospheric water vapor, and a long-term decrease in ozone) terms. Net
 1321 warming from contrail cirrus is a sum over the day/night cycle. These contributions involve a large number
 1322 of chemical, microphysical, transport and, radiative processes in the global atmosphere. The quantitative
 1323 ERF values associated with these processes are shown in **Figure 3** for 2018.

1324

1325
1326

1327 **Figure 2.** Data related to the growth of aviation traffic and CO₂ emissions from 1940 to 2018. Panel (a):
 1328 Global aviation CO₂ emissions. Underlying fuel usage data for 1940 to 1970 are derived from Sausen and
 1329 Schumann (2000) and for 1970–2016 from International Energy Agency (UKDS, 2016) data, which
 1330 include international bunker fuels. For 2017/18, the values are scaled from information from the
 1331 International Air Transport Association (see Appendix A). The average annual increase of global
 1332 emissions from 1960 to 2018 is 15 Tg CO₂ yr⁻¹ and the corresponding decadal average growth rates are 8.0,
 1333 2.2, 3.0, 2.3 and 1.1% yr⁻¹, yielding an overall average of 3.3% yr⁻¹. Panel (b): Global aviation traffic in
 1334 RPK and ASK from airlines.org (<http://airlines.org/dataset/world-airlines-traffic-and-capacity/>), and the
 1335 transport efficiency of global aviation in kg CO₂ per RPK. The passenger load factor defined as RPK/ASK
 1336 increased from about 60% in 1960 to 82% in 2018. Panel (c): Total anthropogenic CO₂ emissions and the
 1337 aviation fractions of this total with and without the inclusion of CO₂ emissions from land use change
 1338 (LUC) from the Global Carbon Budget 2018 (Le Quéré et al., 2018). Panel (d)–(f): Additional aviation
 1339 emissions data by region and year. The yearly sums of OECD and non-OECD values in (d) equal the
 1340 respective global total values. The regional values in (e) and (f) also sum to equal the yearly global total
 1341 values. Note different vertical scales. (<http://www.oecd.org/about/membersandpartners/>) (UKDS, 2016)
 1342 (Country listings in SD Spreadsheet).

1343
1344
1345

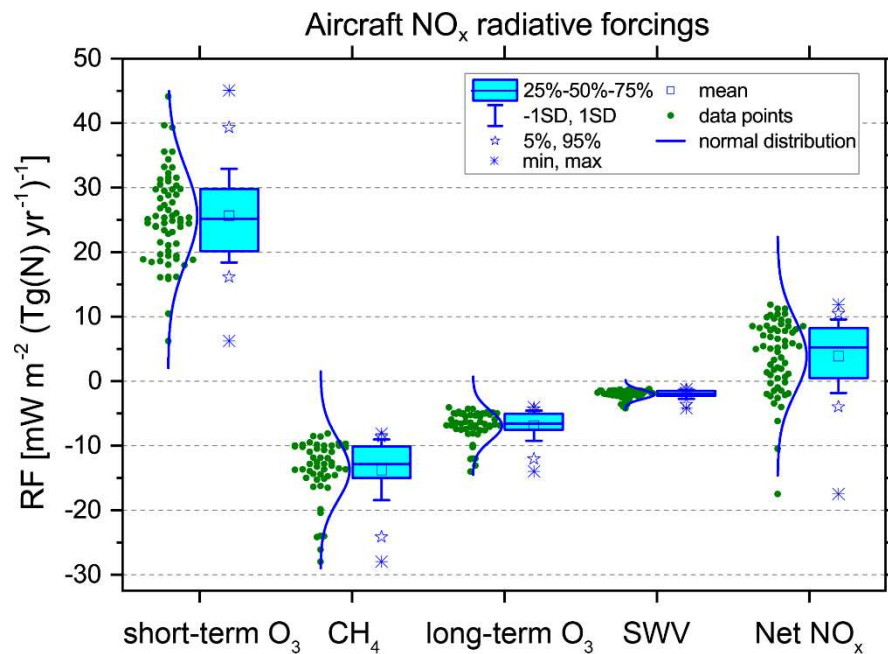


1346

1347 **Figure 3.** Best-estimates for climate forcing terms from global aviation from 1940 to 2018. The bars and
 1348 whiskers show ERF best estimates and the 5–95% confidence intervals, respectively. Red bars indicate
 1349 warming terms and blue bars indicate cooling terms. Numerical ERF and RF values are given in the
 1350 columns with 5–95% confidence intervals along with ERF/RF ratios and confidence levels. ERF and RF
 1351 values are shown for other years in **Tables 2 and 3, Figure 6** and the SD spreadsheet. RF values are
 1352 multiplied by the respective ERF/RF ratio to yield ERF values. ERF/RF values designated as [1] indicate
 1353 that no estimate is available yet. The basis for confidence levels is presented in **Table 4**.

1354

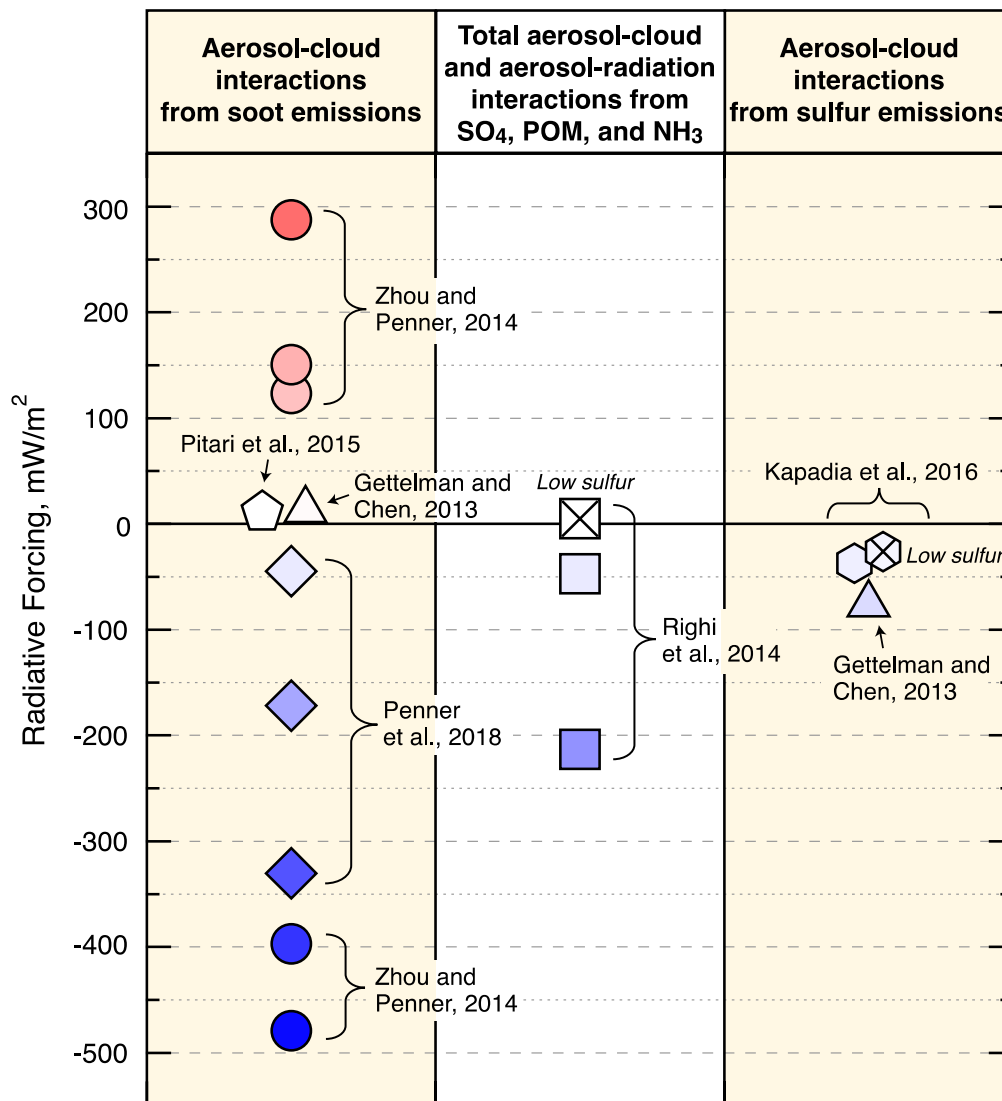
1355



1356 **Figure 4.** Results from an ensemble of 18 models from 20 studies for aviation NO_x impacts: short-term O₃
 1357 increases; CH₄ reductions, CH₄-induced long-term reductions of O₃, CH₄-induced reductions of
 1358 stratospheric water vapor (SWV) and Net NO_x. Each data point represents a value of RF per unit emission
 1359 ($\text{mW m}^{-2} (\text{Tg N yr}^{-1})^{-1}$) as normalized from a published study (see SD). CH₄-induced O₃ and SWV are
 1360 calculated using standardized methodology (see text for details). Note that the displayed values do not
 1361 include correction factors to account for the non-steady-state CH₄ responses to NO_x emissions and the new
 1362 CH₄ RF parameterization. These adjustments are applied in forming the best estimates as discussed in
 1363 Appendix D.

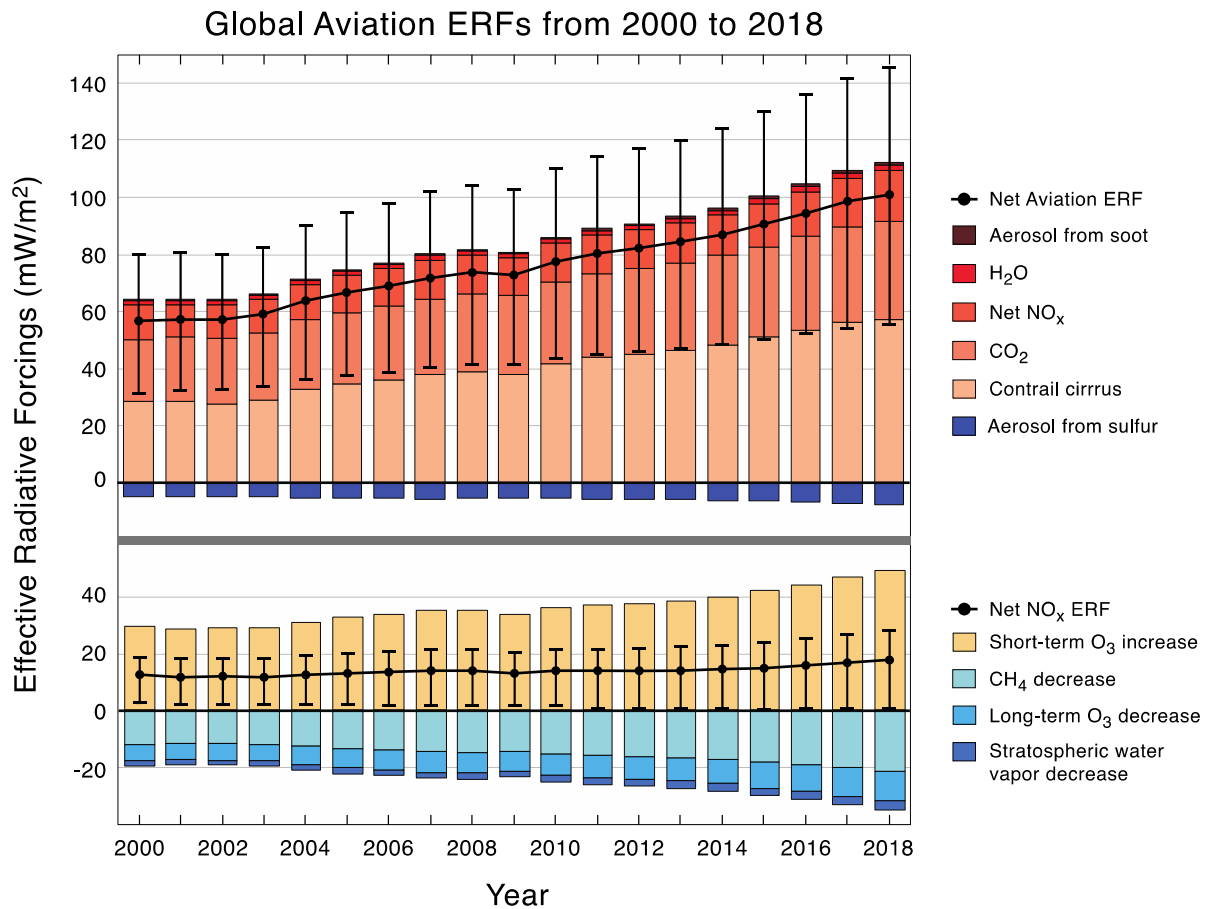
1364

RF Estimates for Aerosol-Cloud Interactions



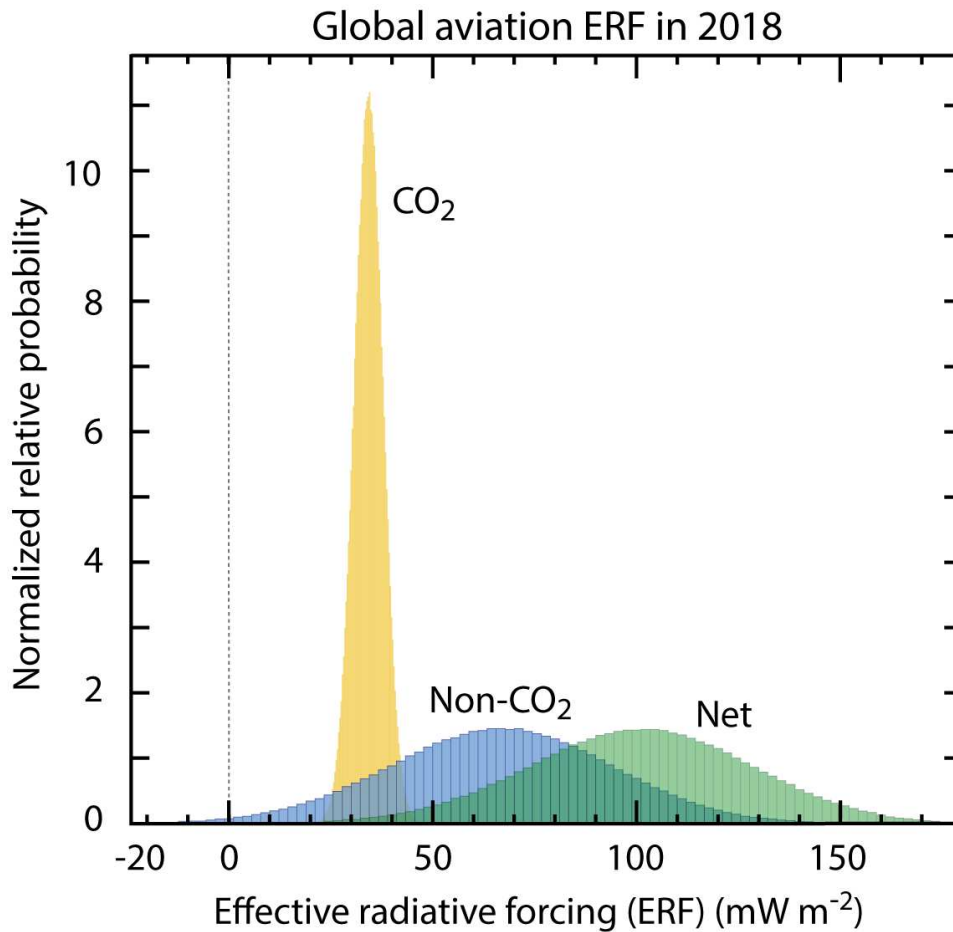
1365

1366 **Figure 5.** Summary of RF estimates for aerosol-cloud interactions for aviation aerosol as calculated in the
 1367 SD spreadsheet for a variety of published results normalized to 2018 air traffic and 600 ppm fuel sulfur.
 1368 The results are shown for soot; total particulate organic matter (POM), sulfate and ammonia (NH₃); and
 1369 sulfate aerosol from the indicated studies. The color shading gradient in the symbols indicates increasing
 1370 positive or negative magnitudes. No best estimate was derived in the present study for any aerosol-cloud
 1371 effect due to the large uncertainties. In previous studies, the estimates for the soot aerosol-cloud effect are
 1372 associated with particularly large uncertainty in magnitude and uncertainty in the sign of the effect (Penner
 1373 et al., 2009; Zhou and Penner, 2014; Penner et al., 2018). As part of the present study, an author (JEP) re-
 1374 evaluated these earlier studies and concluded that the Penner et al. (2018) results supersede the earlier
 1375 Penner et al. (2009) and Zhou and Penner (2014) results because of assumptions regarding updraft
 1376 velocities during cloud formation. In addition, a bounding sensitivity case in which all aviation soot acts as
 1377 an IN in Penner et al. (2018) is not included here.



1378
 1379 **Figure 6.** Timeseries of calculated ERF values and confidence intervals for annual aviation forcing terms
 1380 from 2000 to 2018. The top panel shows all ERF terms and the bottom panel shows only the NO_x terms
 1381 and net NO_x ERF. All values are available in the SD spreadsheet, in Tables 2 and 3, and in **Figure 3** for
 1382 2018 values. The net values are not arithmetic sums of the annual values because the net ERF, as shown in
 1383 **Figure 3** for 2018, requires a Monte Carlo analysis that properly includes uncertainty distributions and
 1384 correlations (see text).

1385



1386

1387 **Figure 7.** Probability distribution functions (PDFs) for aviation ERFs in 2018 based on the results in
 1388 **Figure 3** and **Table 2**. PDFs are shown for separately for CO₂, the sum of non-CO₂ terms, and the net
 1389 aviation ERF. Since the area of each distribution is normalized to the same value, relative probabilities can
 1390 be intercompared. Uncertainties are expressed by a distribution about the best-estimate value that is normal
 1391 for CO₂ and contrail cirrus, and lognormal for all other components. A one-million-point Monte Carlo
 1392 simulation run was used to calculate all PDFs.

1393

1394 **Appendices**1395 **A. Trends in aviation CO₂ emissions**

1396 Global aviation CO₂ emissions for 1940–1970 were taken from Sausen and Schumann (2000) and for the
 1397 years 1971–2016 were calculated from International Energy Agency (IEA) data on usage of JET-A and
 1398 aviation gasoline, largely from annual ‘Oil Information’ digests (e.g., [https://webstore.iea.org/oil-](https://webstore.iea.org/oil-information-2019)
 1399 [information-2019](https://webstore.iea.org/oil-information-2019)). The regional data are from the same source but accessed online from the IEA Oil
 1400 Information (1960–2017) held at the UK Data Service (IEA, 2019). Note that these data are proprietary
 1401 and must be purchased from IEA. Data were unavailable for 2017 and 2018, so incremental annual
 1402 percentage increases in global aviation fuel usage and, therefore CO₂ emissions, for those years were taken
 1403 from reports of the International Air Transport Association (IATA, 2019). Some uncertainties exist from
 1404 the annual fuel estimations and to a much smaller extent, the emission factors. The IEA does not give
 1405 uncertainties for annual kerosene fuel sales or usage. Sausen and Schumann (2000), from which the 1940
 1406 to 1970 data are based here, estimated that the uncertainty in cumulative fuel consumption from 1940 to
 1407 1995 (their dataset) is 20%. There is a known discrepancy of IEA estimates of aviation fuel usage being
 1408 greater by about 10% than that derived from bottom-up global civil aviation inventories. Actual fuel usage
 1409 is likely to be somewhere between the two estimates: aviation emissions inventories are known to be
 1410 incomplete, with only scheduled traffic being available from some air traffic regions, and fuel usage
 1411 potentially being underestimated from flight routing and cruise altitudes; IEA data on the other hand
 1412 includes military aviation fuel (not included in civil aviation inventories) and a small fraction of kerosene
 1413 not used in aviation, but sold for that purpose (L09). The CO₂ emission factors for aviation fuel on the
 1414 other hand are well determined, and the uncertainty is likely within 1%.

1415 **B. Aviation CO₂ radiative forcings**1416 **Calculation of CO₂ concentrations from emissions—LinClim SCM**

1417 The response of CO₂ concentrations, C(t), to a CO₂ aviation emissions rate, E(t), is modelled using the
 1418 method described in Hasselmann et al., (1997) and is expressed as:

$$\Delta C(t) = \int_{t_0}^t G_C(t-t')E(t')dt' \quad (\text{B.1})$$

1419
 1420 where

$$G_C(t) = \sum_{j=0}^5 \alpha_j e^{-t/\tau_j} \quad (\text{B.2})$$

1422 and τ_j is the e-folding time of mode j and the equilibrium response of mode j to a unit emissions of $\alpha_j \tau_j$.

1423 The mode parameters used in this study are presented in Sausen and Schumann (2000) and approximate
 1424 the carbon-cycle model in Meier-Reimer and Hasselmann (1987). The applicability of these parameters in
 1425 the context of aviation response was tested in a model intercomparison exercise (Khodayari et al., 2013).
 1426 For the time horizon of 50-60 years into the future, these were found to compare well with other more
 1427 sophisticated carbon-cycle models such as MAGICC 6.0, which is widely used in the IPCC Fourth
 1428 Assessment Report (IPCC, 2007). Beyond this horizon, aviation CO₂ concentrations begin to have an
 1429 impact on the ocean and biosphere uptake of CO₂ and the non-linearities of the system must be accounted
 1430 for.

1431 **Calculation of CO₂ concentrations from emissions—CICERO-2 SCM**

1432 The CICERO-2 SCM (Fuglestad and Berntsen, 1999; Skeie et al., 2017) uses interconnected process-
 1433 specific IRFs with explicit treatment of air-sea and air-biosphere exchange of CO₂ (Joos et al., 1996;
 1434 Alfsen and Berntsen, 1999) that forms a nonlinear carbon cycle. The ocean and biosphere IRFs in

1435 CICERO-2 express how the CO₂ impulse decays within each reservoir. The CO₂ partial pressure in each
 1436 reservoir is calculated as a function of the carbon in that reservoir, and the CO₂ partial pressure in each
 1437 reservoir is related to the CO₂ partial pressure in the atmosphere by explicitly solving for the
 1438 atmosphere/ocean/biosphere CO₂ mass transfer. Therefore, the CICERO-2 carbon cycle takes into account
 1439 the nonlinearity in ocean chemistry and biosphere uptake at high CO₂ partial pressures since it represents
 1440 the atmospheric change in CO₂ as a function of total background.

1441 **Calculation of CO₂ concentrations from emissions—FaIR SCM**

1442 The FaIR SCM is described by Millar et al. (2017) and summarized as follows. FaIR is a modified version
 1443 of the IPCC AR5 four time-constant impulse response function (IRF) model, which represents the
 1444 evolution of atmospheric CO₂ by partitioning emissions of anthropogenic CO₂ between four reservoirs of
 1445 an atmospheric CO₂ concentrations change, following a pulse emission (see Myhre et al., 2013 for more
 1446 details). In more comprehensive models, ocean uptake efficiency declines with accumulated CO₂ in ocean
 1447 sinks (Revelle and Suess, 1957) and uptake of carbon into both terrestrial and marine sinks are reduced by
 1448 warming (Friedlingstein et al., 2006). FAIR captures some of these dynamics within the simple IRF
 1449 structure, mimicking the behaviour of Earth System Models/Earth System Models of Intermediate
 1450 Complexity in response to finite-amplitude CO₂ injections; this is achieved by introducing a state-
 1451 dependent carbon uptake with a single scaling factor, α , to all four of the time constants in the carbon cycle
 1452 of the IPCC AR5 impulse response model used for the calculation of CO₂-equivalence metrics. This
 1453 approach is described in more detail by Millar et al. (2017).

1454 **C. Radiative forcing, efficacy and effective radiative forcing (ERF)**

1455 Radiative forcing (RF) has been introduced as a predictor for the expected equilibrium global mean of the
 1456 (near) surface temperature change ΔT_s that results from the introduction of climate forcers, such as
 1457 additional atmospheric CO₂ or a change in the solar irradiation (e.g., IPCC, 2007):

$$1458 \quad \Delta T_s = \lambda \text{ RF} \quad (\text{C.1})$$

1459 where λ is the climate sensitivity parameter ($\text{K} (\text{W m}^{-2})^{-1}$). Several definitions of RF exist. According to
 1460 the simplest one, the instantaneous RF is the change in the total irradiation (incoming short-wave solar
 1461 radiation minus the outgoing long-wave terrestrial radiation) at the top of the atmosphere over the
 1462 industrial era. However, for most of the climate forcers a better definition (with respect to the linearity of
 1463 Eq. (C.1)) is the stratosphere-adjusted RF at the tropopause. Here, after the introduction of the new climate
 1464 forcer, the temperature of the stratosphere is allowed to reach a new radiative equilibrium, while all other
 1465 atmospheric state variables are kept constant. The stratosphere-adjusted RF at the tropopause was used in
 1466 many of the earlier IPCC reports (IPCC, 1999) and in earlier assessments of aviation climate impacts
 1467 (Sausen et al., 2005; L09).

1468 While Eq. (C.1) is a fairly good approximation for many nearly spatially homogeneously distributed
 1469 climate forcers, such as global increases of CO₂ or CH₄, Eq. (C.1) fails to some extent for many forcers
 1470 that are heterogeneously distributed either horizontally or vertically; such is the case for aviation-induced
 1471 ozone perturbations and contrail cirrus (e.g., Hansen et al., 1997, 2005; Forster and Shine, 1997; Stuber et
 1472 al., 2005). To overcome this problem Hansen and Nazarenko (2004) introduced the efficacy, r_i , into Eq.
 1473 (C.1):

$$1474 \quad \Delta T_s = r_i \lambda_{\text{CO}_2} \text{ RF} = \lambda_i \text{ RF with } \lambda_i = r_i \lambda_{\text{CO}_2} \quad (\text{C.2})$$

1475 Here λ_{CO_2} is the climate sensitivity parameter for a CO₂ perturbation. While λ in (C.1) is considered a
 1476 universal constant, which can only be determined by climate models and hence is model dependent, λ_i
 1477 depends on the type of forcing, as does r_i . (While r_{CO_2} is 1 by definition, $r_{\text{linear contrails}}$ is <1 (Ponater, et al.,
 1478 2005; Rap et al., 2010)). Eq. (C.2) can also be expressed differently:

$$1479 \quad T_s = \lambda_{\text{CO}_2} \text{ RF}_i^* \text{ with } \text{RF}_i^* = r_i \text{ RF} \quad (\text{C.3})$$

1480 Here RF_i^* is the forcing modified by the efficacy, which yields a better approximation for the surface
 1481 temperature change than RF. However, the calculation of the RF_i^* is computationally much more
 1482 expensive than the calculation of RF, as it requires the determination of the equilibrium temperature
 1483 change, ΔT_s , with a comprehensive climate model.

1484 As an alternative, the effective radiative forcing (ERF) has been introduced as a more practical indicator of
 1485 the eventual global mean temperature response (IPCC, 2013). While RF_i^* assumes equilibrium climate
 1486 change, ERF only includes all 'fast' atmospheric responses to a given climate forcer. For example, rapid
 1487 adjustments in cloud cover, such as from aerosols, or in properties that respond to changes in water vapor,
 1488 can either increase or decrease the initial RF. In contrast, the instantaneous, stratosphere-adjusted, and
 1489 effective RFs for well-mixed greenhouse gases are nearly equal. In practice, ERF is determined with a
 1490 comprehensive climate model, which calculates a new equilibrium radiative imbalance, while the sea
 1491 surface temperature and/or the global surface temperature is kept constant. As a consequence, an ERF
 1492 value is expected to be somewhere between RF and RF_i^* values and closer to RF_i^* values.

1493 **D. Aviation NO_x radiative forcings**

1494 **Impacts of NO_x emissions on ozone, methane and stratospheric water vapor**

1495 *Model studies.* In this ensemble analysis of the climate forcing from aviation NO_x emissions, the results of
 1496 20 studies published since the IPCC (1999) aviation report were considered: IPCC (1999), Sausen et al.
 1497 (2005), Stordal et al. (2006), Köhler et al. (2008), Hoor et al. (2009), Myhre et al. (2011), Frömming et al.
 1498 (2012), Olivié et al. (2012), Gottschaldt et al. (2013), Köhler et al. (2013), Olsen et al. (2013), Skowron et
 1499 al. (2013), Khodayari et al. (2014a), Khodayari et al. (2014b), Søvde et al. (2014), Skowron et al. (2015),
 1500 Pitari et al. (2015), Kapadia et al. (2016), Pitari et al. (2017), Lund et al. (2017). Three studies that reported
 1501 results from a 100-year integration of a pulse NO_x emission (Wild et al. 2001, Derwent et al. 2001,
 1502 Stevenson et al. 2004) were not included in this analysis, nor has as Unger et al. (2010) which uses a
 1503 different methodology to the aforementioned.

1504 This model ensemble represents various methodologies in calculating and treating the long-term effects; in
 1505 order to avoid gaps and additional uncertainties, standardized RFs for reductions in CH_4 -induced O_3 and
 1506 SWV were adopted, except for one study that calculates the 'real' long-term effects from their 50-yr
 1507 integrations (Pitari et al., 2017):

- 1508 • All analyzed short-term O_3 RFs account for a stratospheric adjustment: Assuming that it reduces the
 1509 instantaneous RF by ~20% (Myhre et al., 2013, Stevenson et al., 1998), a factor of 0.8 was applied to
 1510 any O_3 RF that is an instantaneous RF (e.g., in the cases of Khodayari et al. (2014a,b) and Olsen et al.
 1511 (2013)).

- 1512 • Reductions in CH_4 -induced O_3 and SWV are defined as 50% (Myhre et al., 2013) and 15% (Myhre et
 1513 al., 2007) of reported CH_4 RFs, respectively. This is applicable for studies that either originally did not
 1514 provide CH_4 -induced O_3 and SWV estimates (e.g., IPCC, 1999, Sausen et al., 2005, Olsen et al., 2013)
 1515 or derived these RFs using another assumptions (e.g., Stordal et al., 2006, Köhler et al., 2008, Hoor et
 1516 al., 2009, Gottschaldt et al., 2013, Köhler et al., 2013, Skowron et al., 2013, Khodayari et al., 2014a).

1517 Further assumptions regarding data treatment are:

- 1518 • Frömming et al. (2012), Olivié et al. (2012), Khodayari et al. (2014b) and Kapadia et al. (2016)
 1519 provide the short-term O_3 RFs only and p-TOMCAT in Stordal et al. (2006) calculates just the long-
 1520 term effects; thus, these numbers are included in the respective NO_x variable analysis but do not
 1521 contribute to the net NO_x estimate.

- 1522 • Whenever the same estimate appears repetitively in subsequent studies, it is treated as a single entry:
 1523 this is the case for CAM4 short-term O_3 RF that appears in Khodayari et al. (2014a; b) and Olsen et al.

1524 (2013), CAM5 short-term O₃ RF that can be found in Khodayari et al. (2014a; b) and NASA ModelE2
1525 short-term O₃ and CH₄ RFs presented by Unger et al. (2013) and Olsen et al. (2013).

1526 In addition, the ERF estimates for the CH₄ term include shortwave RF (Etminan et al., 2016). The
1527 inclusion of shortwave forcing in the simplified expression increases CH₄ RF from aviation NO_x emissions
1528 by 23% (based on MOZART-3 CTM runs driven for all the aircraft emission inventories represented in the
1529 model ensemble) (**Table D.1**).

1530 **Ensemble values.** This ensemble analysis covers a period of almost two decades; however, none of the RF
1531 per unit of emitted N estimates show any trends over time of publication and the spread in RF per unit of
1532 emitted N values has not changed. The short-term O₃ RF varies from 6.2 to 45.1 mW m⁻² (Tg (N) yr⁻¹)⁻¹,
1533 where these values come from the NASA ModelE2 (Olsen et al., 2013) and p-TOMCAT (Hoor et al.,
1534 2009) models, respectively. The long-term CH₄ RF varies from -27.9 to -8.1 mW m⁻² (Tg (N) yr⁻¹)⁻¹, from
1535 the p-TOMCAT (Köhler et al., 2008) and MOZART3 (Skowron et al., 2015) models, respectively. The
1536 spread of other CH₄-induced long-term effects follows that of CH₄. The net-NO_x RF varies from -17.5 to
1537 11.9 mW m⁻² (Tg (N) yr⁻¹)⁻¹ from ECHAM/MESSy (Gottschaldt et al., 2013) and CAM4 (Khodayari et al.,
1538 2014a), respectively. The results from the mid-1990s CTMs are within the envelope of RFs generated
1539 more recently (**Figure 3**). The numbers from IPCC (1999) and related studies, Sausen et al. (2005) and
1540 L09, where the non-CO₂ effects were originally calibrated to the results from IPCC (1999), do not alter the
1541 best NO_x RF values and their uncertainties (**Table D.2**).

1542 **Correlations.** The correlations between the NO_x RF components are shown in **Figure D.1**. In addition to
1543 the significant negative correlations between the short-term and the long-term aviation RF components,
1544 correlations between the net-NO_x effect and its components are also apparent, especially for the short-term
1545 O₃ and net-NO_x components; however, their strength is around half. The high correlations (p=1, R²=1)
1546 across the long-term effects is expected since CH₄-induced O₃ and SWV are all derived based on CH₄ RFs.
1547 In units of mW m⁻² (Tg(N) yr⁻¹)⁻¹, 49% of this ensemble short-term O₃ RF is concentrated between 20 and
1548 35, 43% of CH₄ RFs is found between -14 and -10, 41% of CH₄-induced O₃ RFs is between -7 and -5 and
1549 45% of SWV RFs vary from -2.5 to -1.5. Of the normalized net-NO_x RFs resulting from this ensemble,
1550 44% are observed between 5 and 10 mW m⁻² (Tg(N) yr⁻¹)⁻¹.

1551 **Transient vs. equilibrium.** In calculating the CH₄ RF response to aviation NO_x emissions, the lack of steady-
1552 state conditions is an important consideration. Since methane (CH₄) has a lifetime of the order 8–12 years
1553 (largely model-dependent) any NO_x perturbation takes on the order ~40 years to come within 2% of the
1554 steady state solution. Moreover, the timescale of removal of CH₄ from the atmosphere is made longer
1555 through a positive chemical feedback (Prather, 1994). In order to overcome the necessity to run a global
1556 chemical transport model (CTM) with full chemistry for such long integrations, a parameterization to
1557 account for this perturbation was originally developed by Fuglestedt et al. (1999) and has been widely
1558 adopted since then. However, with the significant annual increases in aviation NO_x emissions over the last
1559 several decades (**Figure D.2a**) the CH₄ response does not reach its steady-state value in any given year of
1560 emissions, so the steady-state solution generally overstates the CH₄ response in a particular year from
1561 historical time-evolving emissions. Similar considerations apply to other sectors with substantial NO_x
1562 emissions such as shipping (Myhre et al., 2011). If steady-state conditions are utilized, there is a
1563 conceptual and quantitative mismatch when comparing the NO_x RF from aviation with other RF terms,
1564 since RF represents a particular condition at a point in time, not the steady-state conditions. To remedy this
1565 mismatch, Myhre et al. (2011) suggested that a factor accounting for the non-steady-state condition of CH₄
1566 be introduced, thereby modifying the CH₄ impact for a given year of interest, and further suggested that for
1567 the aviation RF in the year 2000 the CH₄ term be reduced by approximately 35% for aircraft emissions
1568 using a simplified estimation derived from Grewe and Stenke (2008).

1569 Here, we present an updated methodology to calculate the non-steady-state aviation-NO_x-induced CH₄
1570 perturbation for the specific year of 2018. The method relies on transient and steady-state runs of the

1571 TROPOS 2D CTM. The results of the steady-state runs using constant emissions for a given year are
 1572 compared with those of transient runs using background historical surface emissions from anthropogenic
 1573 activities and the corresponding aviation NO_x emissions. The latter requires full implementation of time-
 1574 varying CH_4 emissions into the model simulation, a requirement that is not a standard set-up for many of
 1575 the CTM/GCMs currently in use where CH_4 conditions are defined from observations as fixed
 1576 concentrations with relaxation terms introduced to accommodate perturbations to these concentrations. The
 1577 use of CTM runs explicitly accounts for changing background atmospheric conditions over the integration
 1578 period as well as the change in emission rate dependence of the O_3 and CH_4 responses.

1579 *Method.* In order to compare these two methods, two types of experiments were performed:

- 1580 • Transient experiment: a long-term simulation with anthropogenic (surface and aviation) emissions
 1581 evolving over time covering the period 1950–2050, using historical data up to 2000 and the RCP-4.5
 1582 scenario after 2000 (**Figure D.2a**),
- 1583 • Steady-state experiment: a 100-year simulation with constant anthropogenic (surface and aviation)
 1584 emissions representing the year 2000, 2018 or 2050 (**Figure D.2a**); the steady-state CH_4 response starts
 1585 to be observed 60–70 years into the run.

1586 Each of these experiments was run twice, with and without aviation emissions, and the difference between
 1587 these two results defined as the aircraft response (e.g., **Figure D.2d-f**). The initial concentrations of CH_4
 1588 were set using the observations from NOAA surface stations (Montzka et al., 2000) for 1950 and 2000; for
 1589 the year 2050 the CH_4 concentrations are taken from projections of the MAGICC model (Meinshausen et
 1590 al., 2011). The background anthropogenic emissions of CO , CH_4 , NO_x , N_2O , and non-methane volatile
 1591 organic carbon (NMVOC) compounds, as well as aircraft NO_x emissions, evolve during the period 1950-
 1592 2050 (Lamarque et al., 2010; Clarke et al., 2007) (**Figure D.2a**). The natural emissions from soils and
 1593 oceans were kept constant and represent the year 2000 (Prather et al., 2001).

1594 The TROPOS CTM is a latitudinally-averaged, two-dimensional Eulerian global tropospheric chemistry
 1595 model extensively evaluated by Hough (1989; 1991). The model's domain extends from pole-to-pole (24
 1596 latitudinal grid cells) and from the surface to an altitude of 24 km (12 vertical layers). TROPOS is driven
 1597 by chemistry, emissions, transport, removal processes and upper boundary conditions. There are 56
 1598 chemical species in the chemical mechanism of the model, which consists of 91 thermal reactions, 27
 1599 photolytic reactions and 7 more reactions, which include night-time NO_3 chemistry. The reaction rates and
 1600 cross sections were updated to the evaluation of Sander et al. (2006) (see Skowron et. al, 2009). There are
 1601 no fixed concentrations within the model domain other than the upper boundary conditions, which are
 1602 specified for long-lived species and for gases that have stratospheric sources. This 2D CTM has the
 1603 disadvantage of zonal symmetry but has the advantage of an adequate chemical scheme and computational
 1604 efficiency, such that long-term integrations can be reasonably performed. Owing to the aforementioned
 1605 reasons, the O_3 response in TROPOS is overestimated by a factor of ~2 by comparison with a range of up-
 1606 to-date 3D models. As a consequence, the CH_4 results in **Figures. D.2d-f** were reduced accordingly. This
 1607 modification of the original TROPOS responses does not affect the core result of this study, which is the
 1608 *relative* difference of CH_4 responses between transient and equilibrium methods.

1609 *Results.* **Figure D.2b** shows the evolution of the global CH_4 burden over the period 1950–2050 in the
 1610 transient TROPOS simulation. There is a steady growth in the atmospheric CH_4 burden, with a small
 1611 decline over the period 1997–2007 in response to the decrease in CH_4 emissions over the period 1990–
 1612 2000. The steady-state simulations for the year 2000 and 2050 agree well (within 1%) with transient CH_4
 1613 responses for the respective years. A similar agreement is observed for modelled transient and steady-state
 1614 CH_4 lifetimes in **Figure D.2c**. Most of the CH_4 loss in the atmosphere is driven by OH and the oxidative
 1615 capacity of the atmosphere changes over time (thus CH_4 lifetime as well), influenced by emissions of CO ,
 1616 NO_x , NMVOC or CH_4 .

1617 **Figure D.2c** shows the evolution of global CH₄ lifetime (LT) over the period 1950–2050: there is a
 1618 decrease in the CH₄ lifetime between 1950 and 2000 (until around 2007), whilst under the RCP-4.5
 1619 scenario the opposite is observed, with the CH₄ lifetime increasing by 3.5% by the end of 2050 compared
 1620 with 2000. The TROPOS CH₄ lifetimes agree relatively well with other studies (e.g., Holmes et al., 2013;
 1621 Voulgarakis et al.; 2013, Dalsøren et al., 2016) not only in terms of absolute numbers but also the rate of
 1622 changes; a detailed comparison is presented in **Table D.3**. The perturbation lifetime of CH₄ in TROPOS is
 1623 37% longer than its global lifetime and the sensitivity coefficient $s = \partial \ln(\text{LT}) / \partial \ln(\text{CH}_4)$ is 0.27, placing
 1624 these estimates in the middle of model ranges (e.g., Prather 2001, Holmes et al. 2011). These terms were
 1625 calculated using a 5% increase of CH₄ global levels for the year 2000. There is no need to apply the
 1626 feedback factor (1.37) to the TROPOS CH₄ estimates as it is already included in the observed responses;
 1627 TROPOS does not have a fixed boundary conditions, so CH₄ and OH can *freely* interact.

1628 Aircraft NO_x emissions, via the chemical coupling to OH and HO₂, enhance OH, which reduces the global
 1629 CH₄ lifetime. **Figure D.2d** shows the evolution of the CH₄ lifetime reduction in the transient 1950–2050
 1630 simulation and in steady-state runs for conditions representing the years 2000 and 2050. In the transient
 1631 run, there is a steady decrease of global CH₄ lifetime as a consequence of a constant increase of aviation
 1632 NO_x emissions during the period 1950–2050. The agreement in 2000 and 2050 between the transient and
 1633 steady-state CH₄ lifetime reductions is within 6% (on a global scale) (see **Table D.3**). These relatively
 1634 small differences in CH₄ lifetime lead to much more pronounced differences in the associated global CH₄
 1635 burdens as shown in **Figure D.2e**. In contrast to the lifetime results, the CH₄ burden response in the
 1636 transient run lags behind the steady-state CH₄ response with differences of 27% in the year 2000 and 20%
 1637 in the year 2050. Similarly, the calculations for 2018 emissions yield a multiplicative correction factor of
 1638 0.79 (**Figure D.2f**), which has been incorporated into the ERF values of CH₄, long-term O₃ and SWV
 1639 shown in **Figure 5**.

1640 The CH₄ results contrast with O₃ changes from aircraft NO_x emissions, which agree within 3% between
 1641 transient and steady-state experiments with aircraft O₃ burdens of 10.3 and 10.6 Tg (O₃), respectively, in
 1642 the year 2000. These TROPOS O₃ magnitudes are at the upper limit of model ranges, as present-day
 1643 aircraft O₃ perturbations found in the literature vary from 3 to 11 Tg (O₃) (e.g., Hoor et al., 2009; Holmes
 1644 et al., 2011; Khodayari et al., 2014a). The aircraft O₃ burden increases by 41% in 2050, reaching 17.2 and
 1645 18.0 Tg(O₃) for transient and steady-state experiments, respectively. This agrees with other studies (e.g.,
 1646 Olsen et al., 2013) that report a multi-model average increase of 44% in O₃ burden from future aircraft
 1647 NO_x emissions under the RCP-4.5 scenario.

1648 The present approach is in general agreement with that presented by Grewe and Stenke (2008), which
 1649 accounts for CH₄ concentrations not being in steady-state with OH changes in the year of simulation. The
 1650 present CTM results further demonstrate the importance of explicitly calculating CH₄ changes in response
 1651 to time-dependent aviation NO_x emissions rather than assuming constant emissions. The difference
 1652 between transient and steady-state CH₄ for the year 2000 found with TROPOS is smaller than that
 1653 resulting from the Grewe and Stenke (2008) approach (Myhre et al., 2011) (27% and 35%, respectively).
 1654 **Table D.4** presents a further comparison of CH₄ correction factors derived in this study. The systematic
 1655 differences are likely due to the Grewe and Stenke (2008) values being based on a simplified
 1656 chemistry/climate model (AirClim) and the present TROPOS simulations having a different experimental
 1657 setup (all our emissions (surface + aircraft) are time-varying) and a full chemical reaction scheme with
 1658 explicit calculations performed on time-varying emissions. Indeed, if TROPOS is run with constant
 1659 background emissions representing the year 2000 in a similar manner using Grewe and Stenke (2008)
 1660 methodology, the difference between transient and steady-state CH₄ for the year 2000 increases from 27%
 1661 to 31%. This change shows that background emissions modify the CH₄ correction factor and further
 1662 emphasizes the need to have surface and aircraft emissions that simultaneously follow historical pathways.
 1663 In other studies using the Grewe and Stenke (2008) methodology, CH₄ correction factors vary from 0.74 to
 1664 1.15 depending on the investigated year (2025 or 2050) and aircraft emission scenario (SRES A1B, B1 and

1665 B1 ACARE) (the factor can be larger than 1 if the aircraft emissions are assumed to decrease in the
1666 preceding years) (Hodnebrog et al., 2011; 2012).

1667 Uncertainties in the CH₄ correction factor are associated mainly with inter-model differences and the
1668 applied emission scenarios; the correction factor is sensitive, within ~10%, to inter-model differences
1669 (based on two models, TROPOS and AirClim) and it can vary by another ± 10% depending on emission
1670 scenario (based on a range of RCP projections up to 2050). Given that the uncertainties of the CH₄
1671 correction factor on the net-NO_x RF are rather small, especially when compared with overall uncertainties,
1672 we do not include in the estimated uncertainty of the net-NO_x RF value a separate uncertainty due to the
1673 correction factor.

1674 **E. Contrail cirrus**

1675 The global contrail cirrus RF is calculated by homogenizing existing estimates through the use of specific
1676 scaling factors. The factors relate to the choice of air traffic inventory and its basis year; the use of the full
1677 3D flight distance; the use of hourly air traffic data; the feedback of natural clouds; and correcting for
1678 weaknesses in the radiative transfer calculations. The corrections and scaling actions are:

1679 • The estimate of Chen and Gettelman (2013) was corrected by redoing the CAM simulation using a
1680 lower ice crystal radius of 7 μm and a larger contrail cross-sectional area of 0.09 km² for the
1681 initialization of contrails at an age of about 15–20 minutes, in agreement with observations (Schumann
1682 et al., 2017). The resulting change in cirrus cloudiness including the adjustment in cloudiness due to the
1683 presence of contrail cirrus leads to a radiative forcing of 57 mW m⁻².

1684 • A scaling S₁ of 1.4 is applied for estimates based on the AERO2k inventory for the year 2002 instead
1685 of the AEDT inventory for the year 2006 (Bock and Burkhardt, 2016);

1686 • A scaling S₂ of 1.14 is applied to estimates that are based on track distance instead of slant distance
1687 (Bock and Burkhardt, 2016). The ‘slant’ air traffic distance is the full flight distance and not the ground
1688 projected ‘track’ distance.

1689 • A scaling S₃ of 0.87 is applied to estimates that used monthly instead of hourly resolved air traffic
1690 data. This scaling is based on an estimate for the impact of the temporal resolution of the air traffic data
1691 of -25% to -30% within CAM (Chen et al., 2012) and one of no significant change in ECHAM4-
1692 CCMod.

1693 • A scaling S₄ of 1.15 is applied to account for the underestimation of RF in radiative transfer
1694 calculations that use frequency bands instead of line by line calculations (Myhre et al. 2009).

1695 The study details and scaling results are shown in **Table E.1**. Weighting each estimate equally, the best
1696 estimate of global contrail cirrus RF is approximately 66 mW m⁻². As noted in the main text, the Chen and
1697 Gettelman (2013) calculation is interpreted as being closer to an ERF than an RF, so was excluded from
1698 this averaging. This mean RF estimate does not include the RF due to contrails forming within natural
1699 cirrus. Uncertainty due to scalings S₃–S₄ is included in the uncertainty discussion below, whereas
1700 uncertainty in scalings S₁–S₂, namely updating the ECHAM4-CCMod estimates using sensitivities from
1701 ECHAM5-CCMod, is neglected.

1702 The statistical uncertainty of global contrail cirrus RF cannot be estimated from the small number of
1703 available studies. Uncertainties affecting our contrail cirrus estimates are, on the one hand, due to (A)
1704 uncertainties in the radiative response to the presence of contrail cirrus and, on the other hand, (B)
1705 uncertainties in the upper tropospheric water budget and the contrail cirrus scheme. In most cases, we can
1706 only infer very rough estimates for the uncertainties related to specific processes.

1707 (A) Uncertainties associated with the radiative response to contrail cirrus are:

- 1708 A1. Uncertainty related to the model's radiative transfer scheme of approximately 35% (Myhre et al.,
1709 2009).
- 1710 A2. Uncertainty in the inhomogeneity of ice clouds within a grid box of a climate model (Carlin et al.,
1711 2002; Pomroy and Illingworth, 2000), the vertical cloud overlap, and the use of plane parallel geometry
1712 as compared to full 3D radiative transfer (Gounou and Hogan, 2007), which together amount to
1713 approximately 35%.
- 1714 A3. Uncertainty estimating radiative transfer in a global climate model in the presence of very small ice
1715 crystals within young contrails, which may amount to about 10% (Bock and Burkhardt, 2016). The
1716 uncertainty is dependent on the contrail cirrus ice water content.
- 1717 A4. Uncertainty due to the ice crystal habit is approximately 20% according to Markowicz and Witek
1718 (2011).
- 1719 A5. Uncertainty in the radiative transfer due to soot cores within the contrail cirrus ice crystals is
1720 thought to be large, as the change in the shortwave (SW) albedo is large (Liou et al., 2013). The soot
1721 impact on contrail cirrus RF has not yet been quantified.
- 1722 Overall, uncertainty in the radiative response to contrail cirrus (excluding A3) is estimated to be about
1723 55%, assuming independence of different uncertainties and excluding the impact of ice crystal soot cores.
1724 The uncertainty A3 is included in the uncertainty estimate under (B) because A3 and B2 are dependent
1725 uncertainties.
- 1726 (B) Uncertainty in contrail cirrus RF associated with the upper-tropospheric water budget and the contrail
1727 cirrus scheme are:
- 1728 B1. Uncertainty in contrail cirrus RF associated with the uncertainty in upper-tropospheric ice
1729 supersaturation. This results from a lack of knowledge in ambient conditions due to the low vertical
1730 resolution of satellite instruments (Lamquin et al., 2012) and to the ability of models to reproduce the
1731 observed statistics of ice supersaturation. This contributes about 20% to uncertainty.
- 1732 B2. There is uncertainty related to ice crystal number densities within young contrails. Ice nucleation
1733 within the plume can vary drastically depending on the water supersaturation reached within the plume
1734 and on the soot emissions (Kärcher et al., 2015; 2018). This dependency on the atmospheric state leads
1735 to a reduction in the number of nucleated ice crystals in particular in the tropics and at lower flight
1736 levels (Bier and Burkhardt, 2019) leading to a large uncertainty in the impact of tropical and subtropical
1737 air traffic. Depending on the atmospheric state and ice crystal numbers, a varying fraction of ice crystals
1738 can be lost in the contrail vortex phase (Unterstrasser, 2014). We assume an uncertainty in average
1739 contrail ice crystal numbers after the vortex phase of about 50% leading to an uncertainty in contrail
1740 cirrus RF of about 20%. This estimate of the sensitivity of contrail cirrus RF to ice crystal numbers in
1741 newly formed contrails is based on simulations with ECHAM5-CCMod (Burkhardt et al., 2018).
- 1742 B3. The uncertainty in the lifetime of contrail cirrus, affecting the day-/night-time contrail cover, has
1743 only a small impact on the estimated contrail cirrus RF (Chen and Gettelman, 2013; Newinger and
1744 Burkhardt, 2012). We estimate the associated uncertainty to be 5–10%.
- 1745 B4. From the sensitivity of the contrail cirrus RF to the temporal resolution in the air traffic dataset in
1746 ECHAM5 and CAM, we deduce an uncertainty of about 10%.
- 1747 B5. The estimate of the feedback of natural clouds, due to contrail cirrus changing the water and heat
1748 budget of the upper troposphere, is very uncertain and has not been properly quantified yet (Burkhardt
1749 and Kärcher, 2011; Schumann et al., 2015). We assume here the uncertainty related to this estimate to
1750 be only slightly smaller than the estimate itself, or about 15%.

1751 B6. Uncertainty in the RF estimate of Chen and Gettelman (2013) to assumptions in the initial ice-
1752 crystal radii and contrail cross-sectional areas is about 33%.

1753 We assume independence of the uncertainties except for the dependence of A3 and B3 on the uncertainty
1754 in B2. The overall uncertainty due to the water budget and the contrail cirrus scheme (including
1755 uncertainty A3) is about 40% and more than 50% in the case of the Chen and Gettelman (2013). From the
1756 two different sources of uncertainty (list A, radiative, and list B, contrail cirrus properties, above) we
1757 calculate an overall contrail cirrus RF uncertainty of about 70%, assuming independence of the overall
1758 uncertainties described in A and B.

1759 Note that we do not attempt to infer an estimate for the uncertainty of the factor ERF/RF. When
1760 calculating the contrail cirrus ERF, the error range given refers to the error range of contrail cirrus RF and
1761 not ERF.

1762 F. Emission metrics calculations

1763 We calculate the AGWP and AGTP, and corresponding GWPs and GTPs, for aviation CO₂, NO_x (which
1764 encompasses the ERF of short-term O₃, CH₄, CH₄-induced O₃ and SWV), soot, SO₂, and contrail cirrus.
1765 The methodology and analytical expressions for the emissions metrics are described in detail in previous
1766 literature (e.g., Fuglestedt et al. 2010; Myhre et al. 2013). The impulse response function (IRF) that
1767 describes the atmospheric decay of CO₂ upon emission is taken from Joos et al. (2013). For the other
1768 species, the atmospheric decay is given by a constant e-folding time taken as the ‘perturbation lifetime’.
1769 The lifetimes used here are broadly consistent with Fuglestedt et al. (2010). The radiative efficiency (RE)
1770 for CO₂ is calculated using year 2018 background concentrations of 407 ppm (annual mean, from monthly
1771 mean observed concentrations from NOAA GMD -
1772 ftp://aftp.cmdl.noaa.gov/products/trends/co2/co2_mm_gl.txt). This yields a RE of $1.68 \times 10^{-15} \text{ W m}^{-2} \text{ kg}^{-1}$,
1773 4% lower than used in the IPCC Fifth Assessment report (AR5) (Myhre et al., 2013). The climate response
1774 IRF is taken from Boucher and Reddy (2008). The latter has an inherent equilibrium climate sensitivity
1775 (ECS) of $1.06\text{K} (\text{W m}^{-2})^{-1}$, equivalent to a 3.9K equilibrium response to a doubling of CO₂.

1776 For the calculation of the average rate of CO₂-warming-equivalent emissions for aviation non-CO₂ forcings
1777 ($E_{\text{CO}_2\text{e}^*}$) under the GWP* metric in **Table 5**, we use the relationship between recent changes in effective
1778 RF and CO₂-equivalent emissions from Allen et al. (2018) (or Equation (1) with $\alpha = 0$),

$$1779 \quad E_{\text{CO}_2\text{e}^*} = [\Delta F / \Delta t] \times [H / \text{AGWP}_{\text{H}(\text{CO}_2)}] \quad (\text{F.1})$$

1780 where ΔF is the change in ERF over the recent period, Δt , and $\text{AGWP}_{\text{H}(\text{CO}_2)}$ is the absolute global warming
1781 potential of CO₂ at time horizon H. We use updated $\text{AGWP}_{\text{H}(\text{CO}_2)}$ values incorporating the updated
1782 radiative efficiency of CO₂ as described in the previous paragraph. Allen et al. (2018) used a backward-
1783 looking period of 20 years as Δt , whereas here we use a backward-looking 18-yr period as our time series
1784 of ERF components only extends back to 2000.

1785 G. List of Acronyms and abbreviations used in tables and figures of the Appendices

1786 ACARE—Advisory Council for Aeronautical Research in Europe
1787 ACCMIP—Atmospheric Chemistry and Climate Model Intercomparison Project
1788 AEDT—Aviation Environmental Design Tool
1789 AEM—Advanced Emission Model
1790 AERO2K—Global aircraft emissions data project for climate impacts evaluation
1791 AGAGE—Advanced Global Atmospheric Gases Experiment
1792 CAM—Community Atmosphere Model
1793 CCMoD—Contrail Cirrus Module
1794 CH₃CCl₃—Methyl chloroform
1795 COCIP—Contrail Cirrus Prediction Tool

1796	CTM—Chemical Transport Model
1797	ECHAM—European Centre/Hamburg Model
1798	IPCC—Intergovernmental Panel on Climate Change
1799	MAGICC—Model for the Assessment of Greenhouse Gas Induced Climate Change
1800	MOZART—Model for OZone And Related chemical Tracers
1801	NOAA—National Oceanic and Atmospheric Administration
1802	QUANTIFY—Quantifying the Climate Impact of Global and European Transport System
1803	REACT4C—Reducing Emissions from Aviation by Changing Trajectories for the benefit of Climate
1804	RCP—Representative Concentration Pathway
1805	SRES—Special Report on Emission Scenarios
1806	TAR—Third Assessment Report
1807	TRADEOFF—Aircraft emissions: contribution of different climate components to changes in radiative
1808	forcing—tradeoff to reduce atmospheric impact
1809	TROPOS—2D global TROPOSpheric model
1810	WDCGG—World Data Centre for Greenhouse Gases

1811 **Table D.1.** The CH₄ RFs derived for all the aircraft emission
 1812 inventories that are present in the model ensemble.^a

Inventories	CH ₄ RF, mW m ⁻²	
	Old	New
AEDT	-6.67	-8.22
AEM	-6.82	-8.41
AERO2K	-7.09	-8.74
REACT4C	-6.97	-8.59
QUANTIFY	-6.96	-8.58
TRADEOFF	-7.11	-8.76

1813 ^a Values are those represented in the model ensemble based on MOZART-3
 1814 CTM simulations (Old) and recalculated values using a revised simplified
 1815 expression for the CH₄ RF (New) as presented by Etminan et al. (2016). The
 1816 NO_x emissions of each inventory are normalized so that all RFs are scaled to
 1817 the same global total emissions (0.71 Tg(N) yr⁻¹) as in the REACT4C model.

1818

1819 **Table D.2.** The best NO_x RFs per unit emission derived for datasets that include and exclude late 1990s
 1820 numbers and related estimates, see text for details.

Components	Value	Uncertainty*	Value	Uncertainty*
	(mW m ⁻² (Tg (N) yr ⁻¹) ⁻¹)			
	with IPCC (1999)		without IPCC (1999)	
Short-term O ₃	25.6	±7.3	25.1	±7.2
CH ₄	-13.8	±4.7	-13.4	±4.5
CH ₄ -induced O ₃	-6.9	±2.3	-6.7	±2.3
SWV	-2.1	±0.7	-2.0	±0.7
Net NO _x	3.9	±5.7	4.0	±5.8

1821 *Stated uncertainties are one standard deviation (68% confidence interval).

1822

1823 **Table D.3.** Methane response in TROPOS and other studies

Variable	Year	2D CTM, TROPOS		Study	Literature		Variable estimate/change
		Transient	Steady-state ^a		Ref	Model/Years	
CH ₄ burden, Tg	2000	4770.8	4785.1	IPCC TAR	1998	4850 Tg	
				Voulgarakis et al 2013	ACCMIP	4750 ^d Tg	
				Dalsøren et al 2016	Oslo CTM3	4560 ^d Tg	
				Dalsøren et al 2016	1970–2012	+15 %	
				This study ^c		+13 %	
	2050	5051.6	5081.4	Voulgarakis et al 2013	ACCMIP	5000 ^d Tg	
			Voulgarakis et al 2013		+5.3 ^d %		
			This study ^c	2000–2050	+5.9 %		
CH ₄ abundance, ppb	2000	1784.2	1787.5	Observations	NOAA AGAGE WDCGG	1773 ppb 1774 ppb 1783 ppb	
	2050	1886.2	1897.6	Meinshausen et al 2011	MAGICC	1833 ppb	
CH ₄ lifetime (T _{CH4+OH}) ^b , yr	2000	10.6	10.5	Prather et al 2012	CH ₃ CCl ₃ -based	11.2 ± 1.3 yr	
				Voulgarakis et al 2013	ACCMIP	9.8 ± 1.6 yr	
				Holmes et al 2013	1980/85–2000/05	-2.2 ± 1.8 %	
				This study ^c		-2.06 %	
				Voulgarakis et al 2013	1980–2000	-4 %	
	This study ^c		-2 %				
2050	11.0	11.0	Voulgarakis et al 2013	2000–2050	+1.0 ^d %		
			This study ^c		+3.5 %		
aircraft CH ₄ lifetime (T _{CH4+OH}), yr	2000	-0.137	-0.145	Hoor et al 2009	AERO2K	-1.55 % Tg(N) ⁻¹	
				Myhre et al 2011	QUANTIFY	-1.46 % Tg(N) ⁻¹	
				Holmes et al 2011	Model ensemble	-1.77 % Tg(N) ⁻¹	
				Søvde et al 2014	REACT4C	-1.36 % Tg(N) ⁻¹	
				This study ^c	d _{ENOX} =QUANTIFY	-1.48 % Tg(N) ⁻¹	
	2050	-0.293	-0.311	Hodnebrog et al 2011	SRES B1	-1.61 % Tg(N) ⁻¹	
					B1 ACARE	-1.48 % Tg(N) ⁻¹	
				Hodnebrog et al 2012	SRES A1B	-1.22 % Tg(N) ⁻¹	
				Khodayari et al 2014a	AEDT Scenario1	-1.88 % Tg(N) ⁻¹	
				This study ^c	AEDT Baseline	-1.59 % Tg(N) ⁻¹	
			RCP45	-1.36 % Tg(N) ⁻¹			

^a this is an average of the last 10 years of simulations

1826 ^b the chemical (T_{CH_4+OH}) lifetime is around 7% greater than the total CH_4 lifetime, as modelled by TROPOS
 1827 ^c numbers are based on transient simulation
 1828 ^d numbers might not be very accurate as they are read directly from the graphs found in the respective papers
 1829

1830 **Table D.4.** Calculated CH_4 correction factors

Aviation emissions year	CH_4 correction factors	
	This study	Grewe and Stenke (2008) methodology
2000	0.73	0.65
2005	0.75	0.73
2011	0.78	0.81
2018	0.79	0.86

1831

1832 **Table E.1.** Scaling of contrail cirrus RF and ERF results ^a

Model	Inventory	Representation of flight distance	RF (mW/m^2)	Scalings	Scaled RF (mW/m^2) ^b	Reference
ECHAM4-CCMod	AERO2K 2002	track	38	S ₁ , S ₂ , S ₄	70	Burkhardt and Kärcher (2011)
ECHAM5-CCMod	AEDT 2006	slant	56	S ₃ , S ₄	56	Bock and Burkhardt (2016)
COCIP	AEDT 2006	flight vectors	63	S ₄	72	Schumann et al. (2015)
CAM5	AEDT 2006	slant	13 [57] ^c	S ₃ , S ₄	57	Chen and Gettelman (2013)
Best estimate					66 ^d	

1833 ^a Adapted from Table 1 of Bock and Burkhardt (2016).1834 ^b RF that would be expected in 2006 when using slant distance from the AEDT inventory with hourly resolution.1835 ^c An updated simulation (see text) yielded 57 $mW m^{-2}$.1836 ^d The best estimate is of RFs, and excludes the Chen and Gettelman (2013) results since this is closer to an ERF
 1837 (see main text).
 1838
 1839
 1840

1841 **Table F.1a.** Emission metrics and corresponding CO₂-equivalent emissions for the ERF components of
 1842 2018 aviation emissions and cloudiness using CO₂ IRF without C-cycle feedbacks from Gasser et al.
 1843 (2017), and climate IRF from Boucher and Reddy (2008).

1844 **Metrics**

ERF term	GWP ₂₀	GWP ₅₀	GWP ₁₀₀	GTP ₂₀	GTP ₅₀	GTP ₁₀₀
CO ₂	1	1	1	1	1	1
Contrail cirrus (Tg CO ₂ basis)	2.39	1.15	0.68	0.70	0.11	0.10
Contrail cirrus (km basis)	40	19	11	12	1.9	1.6
Net NO _x	637	216	122	-231	-75	14
Aerosol-radiation						
Soot emissions	4409	2125	1252	1295	210	177
SO ₂ emissions	-856	-412	-243	-251	-41	-34
Water vapor emissions	0.22	0.11	0.06	0.07	0.01	0.009

1845

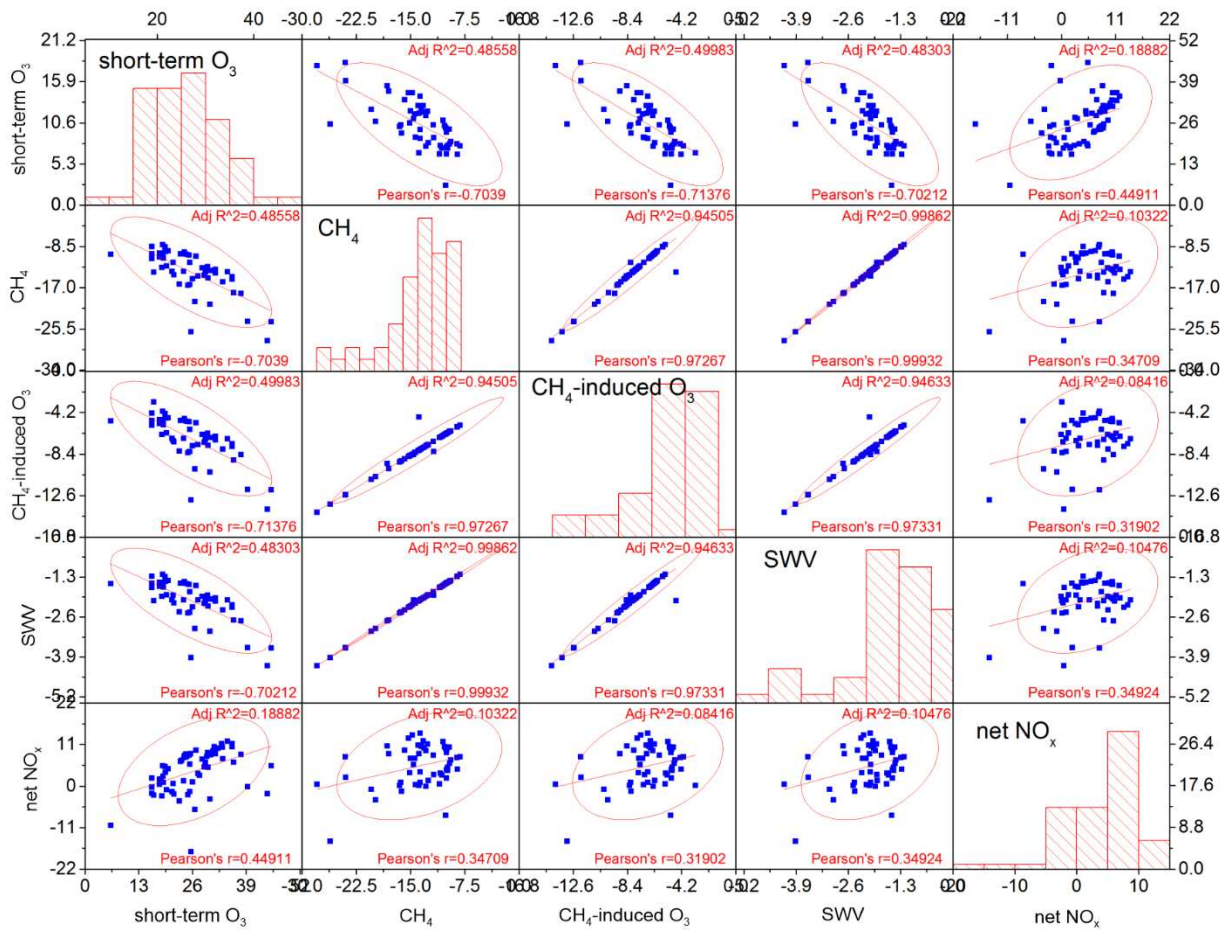
1846 **Table F.1b.** Emission metrics and corresponding CO₂-equivalent emissions for the ERF components of
 1847 2018 aviation emissions and cloudiness using CO₂ IRF without C-cycle feedbacks, and climate IRF from
 1848 Gasser et al. (2017).

1849 **Metrics**

ERF term	GWP ₂₀	GWP ₅₀	GWP ₁₀₀	GTP ₂₀	GTP ₅₀	GTP ₁₀₀
CO ₂	1	1	1	1	1	1
Contrail cirrus (Tg CO ₂ basis)	2.39	1.15	0.68	0.3	0.19	0.15
Contrail cirrus (km basis)	40	19	11	4	3.3	2.6
Net NO _x	637	216	122	-420	-18	22
Aerosol-radiation						
Soot emissions	4409	2125	1252	466	360	284
SO ₂ emissions	-856	-412	-243	-90	-70	-55
Water vapor emissions	0.22	0.11	0.06	0.03	0.018	0.014

1850

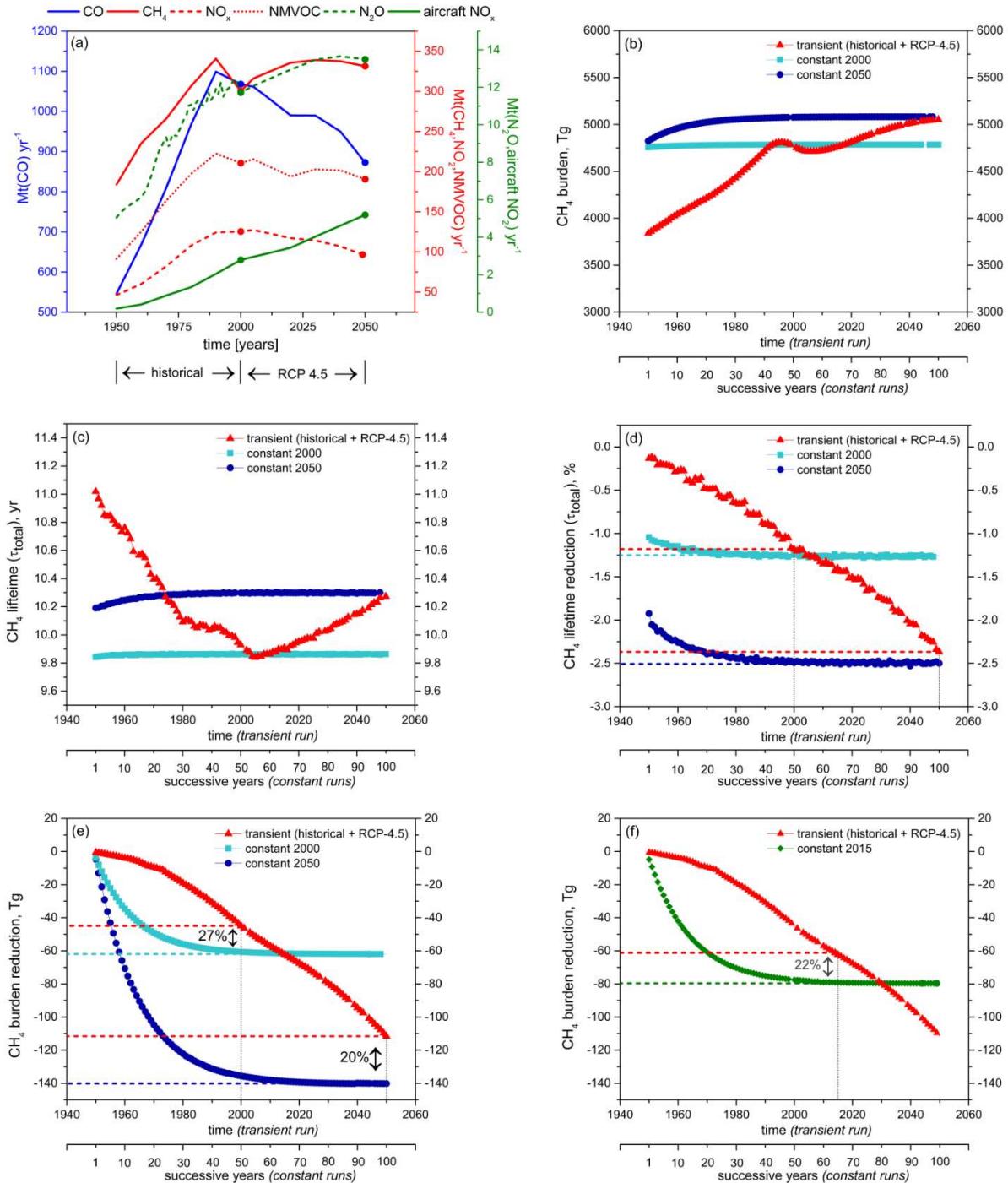
1851



1852

1853 **Figure D.1.** Matrix of pair-wise scatter plots of RF values from NO_x terms: short-term O₃, CH₄, CH₄-
 1854 induced O₃, SWV and net NO_x (i.e., the sum of all 4 components), all represented as normalized RFs
 1855 (mW m⁻² (Tg(N)yr⁻¹)⁻¹) from the ensemble studies (see details in text). The red line is the linear fit, the
 1856 ellipse shows the 95% confidence level and histograms present frequencies.

1857



1858

1859 **Figure D.2.** (a) Past and future anthropogenic emissions of CO, CH₄, NO_x, NMVOC, N₂O and aircraft NO_x
 1860 (IIASA RCP Database: <http://www.iiasa.ac.at/web-apps/tnt/RcpDb/>). Dots represent conditions for ‘constant
 1861 2000’ and ‘constant 2050’ simulations.

1862 (b) Evolution of the global CH₄ burden in TROPOS for transient aircraft NO_x emissions combining
 1863 historical emissions (1950–2000) and RCP-4.5 emissions (2000–2050); and constant emissions for the
 1864 years 2000 and 2050.

1865 (c) Global CH₄ lifetime due to aircraft NO_x emissions in TROPOS for transient emissions combining
1866 historical emissions (1950–2000) and RCP-4.5 emissions (2000–2050); and constant emissions for the
1867 years 2000 and 2050.

1868 (d) Global CH₄ lifetime reduction due to aircraft NO_x emissions in TROPOS for transient emissions
1869 combining historical emissions (1950–2000) and RCP-4.5 emissions (2000–2050); and constant
1870 emissions for the years 2000 and 2050. The dashed lines represent 2000 and 2050 equilibrium values
1871 (light and dark blue) and 2000 and 2050 transient values (red).

1872 (e) Global CH₄ burden reduction due to aircraft NO_x emissions in TROPOS for transient emissions
1873 combining historical emissions (1950–2000) and RCP-4.5 emissions (2000–2050); and constant
1874 emissions for the years 2000 and 2050. The dashed lines represent 2000 and 2050 equilibrium values
1875 (light and dark blue) and 2000 and 2050 transient values (red).

1876 (f) Global CH₄ burden reduction due to aircraft NO_x emissions in TROPOS for transient emissions
1877 combining historical emissions (1950–2000) and RCP-4.5 emissions (2000–2050); and constant
1878 emissions for the year 2018. The dashed lines represent 2018 equilibrium (green) and transient values
1879 (red).

1880